Seismic Risk Assessment of Energy Pipelines under Permanent Ground Deformation due to Fault Rupture

by

Sandip Dey

B.E., Indian Institute of Engineering Science and Technology Shibpur, 2012
M.A.Sc., Concordia University Montreal, 2014

A THESIS SUBMITTED IN PARTIAL FULFILLMENT OF
THE REQUIREMENTS FOR THE DEGREE OF

DOCTOR OF PHILOSOPHY

in

The College of Graduate Studies

(Civil Engineering)

THE UNIVERSITY OF BRITISH COLUMBIA

(Okanagan)

November 2021

The following individuals certify that they have read, and recommend to the College of Graduate Studies for acceptance, a thesis/dissertation entitled:

Seismic Risk Assessment of Energy Pipelines under Permanent Ground Deformation due to Fault Rupture

submitted by Sandip Dey in partial fulfilment of the requirements of the degree of Doctor of Philosophy

Solomon Tesfamariam, School of Engineering
Supervisor

Katsuichiro Goda, Western University
Supervisory Committee Member

Abbas Milani, School of Engineering
Supervisory Committee Member

Dimitry Sediako
University Examiner

Ian Moore
External Examiner

Abstract

This thesis entails developing analysis methods for evaluating seismic risk to oil and gas pipelines due to permanent ground deformation resulting from fault rupture. To address this, three modules are identified as core part of this research. Firstly, a finite element (FE) model for oil and gas pipeline crossing a seismic induced fault line is developed. Subsequently, uncertainty in input parameters is introduced in the developed FE model and analyzed in a multi-fidelity approach. Finally, probabilistic regional ground deformation due to fault rupture is assessed and integrated with the pipe-soil structural model.

A detailed FE analysis technique to study the behavior of buried continuous pipelines crossing fault movements is developed and established with appropriate evaluations. A non-linear sand constitutive model is adopted and implemented in commercial FE package ABAQUS. The adopted material model is first evaluated using available tri-axial test results. This material model is thereafter suitably calibrated for a large-scale test based on direct shear soil test data for that experiment. The pipe-soil FE model is then evaluated against full-scale experimental results.

Subsequently, structural response of a buried continuous steel pipeline undergoing fault rupture deformation is studied in a systematic manner. A detailed and efficient analysis framework for design of buried continuous steel pipelines crossing faults is proposed and explained with a case study using Taguchi method for design of experiments.

Further to this, uncertainty in input parameters, such as pipe diameter, pipe wall thickness, young's modulus, yield strength, ultimate strength, sand confining pressure, sand relative density, operating temperature and operating pressure is considered using a multi-fidelity approach which relies on analyses results from a small number of detailed structural analyses and large numbers of simplified structural analyses. The approach efficiently relies on both types of results to predict structural performance accurately considering uncertainty and variability in geometrical and material properties. Significant computational cost savings is achieved where by 500 analyses are completed using 15 minutes computational time low-fidelity (LF)

models instead of 48 hours computational time high-fidelity (HF) models with a 3.20GHz eight-core processor with 32 GB RAM for 500 analyses.

Finally, extension of the structural analysis framework to a regional scale is completed. This is done by calculating fault rupture induced regional ground displacements from available analytical techniques using probabilistic approaches and thereafter integrating it with the developed structural analysis uncertainty quantification framework.

Lay Summary

Buried continuous energy pipelines traversing seismically active regions are vulnerable to failure due to permanent ground deformation resulting from fault rupture. Hence, it is important to develop efficient and reliable methods to characterise seismic risks to these pipelines arising from permanent ground deformations due to fault ruptures. To address this, an experimentally evaluated FE pipe-soil model to study pipeline response due to ground deformation loads with consideration to associated uncertainties in influencing geometric and material factors have been developed. To ensure efficiency of the developed method, a multi-fidelity approach using Gaussian processes is introduced. A multi-fidelity approach relies on the accuracy of detailed HF models and the efficiency of simplified LF models to predict reasonably accurate results in an efficient manner. Finally, this developed method is integrated with available probabilistic regional ground deformation assessment approaches for regional seismic risk assessment of a pipeline network.

Preface

I, Sandip Dey, prepared all the seven chapters of this dissertation under the supervision of Professor Solomon Tesfamariam. This dissertation is prepared based on a compilation of four published peer-reviewed journal papers (Chapters 3, 4), one submitted journal paper (Chapter 6) and one paper under preparation (Chapter 5). The author of this dissertation conducted the literature review, performed all analyses, prepared surrogate and numerical models of the studied pipelines, processed the data, interpreted the results, and wrote all the chapters (manuscripts). Professors Solomon Tesfamariam, Katsuichiro Goda and Souvik Chakraborty offered technical assistance, reviewed the manuscripts and provided critical feedback to improve the manuscripts. Professor Solomon Tesfamariam facilitated the partial funding for this research.

Published papers

1. S. Dey, S. Chakraborty, S. Tesfamariam, Multi-fidelity approach for uncertainty quantification of buried pipeline response undergoing fault rupture displacements in sand, Computers and Geotechnics 136 (2021) 104197.

2. S. Dey, S. Chakraborty, S. Tesfamariam, Structural performance of buried pipeline undergoing strike-slip fault rupture in 3D using a non-linear sand model, Soil Dynamics and Earthquake Engineering 135 (November 2019) (2020) 106180.

Papers submitted

1. S. Dey, S. Tesfamariam, Design of buried pipeline undergoing fault rupture in sand using Taguchi design of experiments, Soil Dynamics and Earthquake Engineering.

Papers under preparation

1. Regional probabilistic seismic risk analysis of buried pipelines due to permanent ground deformation hazard for Victoria, British Columbia, Canada.

Table of Contents

List of Tables

List of Figures

Acknowledgements

I would like to express my sincere gratitude and appreciation to Dr. Solomon Tesfamariam for his guidance throughout the course of my doctoral studies. I also acknowledge the financial support facilitated by Dr. Tesfamariam through the Natural Sciences an Engineering Research Council of Canada (RGPIN-2019–05584) under the Discovery Grant program.

I would also like to thank Dr. Katsuichiro Goda for his help and guidance in regards to probabilistic regional ground deformation assessment. The probabilistic ground deformation approach used in this thesis has been provided by Dr. Katsuichiro Goda. I would also like to thank Dr. Souvik Chakraborty for his help and guidance in regards to uncertainty quantification. The initial conceptualization of this multi-fidelity uncertainty quantification work has been suggested by Dr. Souvik Chakraborty. I would also like to thank Dr. Abbas Milani for his valuable comments on enriching various parts of the thesis. Additionally, I would like to thank Dr. Dimitry Sediako and Dr. Ian Moore for their comments on enhancing various parts of the thesis.

I would also like to thank Dr. Tesfamariam research group members Sourav Das and Kostas Skandalos for having discussions on various technical aspects of my research.

Dedication

Dedicated to my parents.

Chapter 1

Introduction

1.1 Motivation

Buried continuous energy pipelines are important structures transporting oil, gas and other petroleum byproducts over large distances. Energy pipelines can be classified primarily into major transmission pipelines and secondary distribution networks. These pipelines are generally designed for their operating condition loads, such as operating temperature and internal pressure. However, in addition to these loads, these pipelines are also faced with the risk of failure due to seismic activity in seismically active regions. Buried continuous pipelines are especially vulnerable to failure due to fault rupture induced permanent ground deformations during earthquakes.

A review of literature indicates that for buried pipelines, seismic hazards are primarily due to wave propagation and permanent ground deformation. Damage due to permanent ground deformations are found typically in localized areas with high tendency and degree of damage whereas, damage due to seismic wave propagation are found to be distributed over much wider zones with substantially lower chances and degree of damage [5]. In general, continuous welded pipelines are more vulnerable to permanent ground deformation hazard in comparison to wave propagation hazard. Majority of research works in earthquake engineering has been on the behaviour of structures under seismic wave propagation, where as, significantly less attention has been paid on the behavior of structures under permanent ground deformation due to tectonic fault rupture. The reason being, this hazard is observed in relatively localized areas and poses a threat when the rupture propagates to the surface.

Traditionally, seismic risk assessment of buried pipeline system has involved estimation of damage in the pipelines using empirical correlations between observed damage to seismic wave propagation and permanent ground deformation data. These empirical correlations have been derived by a number of authors based on historically collected data. These data collected from historical seismic events range in various locations and time. Permanent ground deformations can be localized, such as due to a fault movement

or spatially extended; for example, due to soil liquefaction over a region. A number of empirical relationships exist in literature to quantify fault displacements based on the earthquake moment magnitude derived from historical seismic data. Additionally, numerous empirical relationships are available to predict magnitude and extent of extended permanent ground deformations, such as landslides, liquefaction and settlement.

Buried pipelines can be subjected to both transient ground deformations and permanent ground deformations in the event of an earthquake. Transient ground deformations are caused by passage of seismic waves whereas, permanent ground deformations are a result of surface rupture or effects, such as liquefaction and landslides. The impact of earthquake on buried infrastructure can vary. Damages due to transient effects are felt over wide geographical areas and damages tend to be widespread. On the other hand, surface ruptures coinciding with buried pipelines result in significantly high pipeline damages but in localised areas. The response of buried pipelines vary from above ground structures due to the soil support available to balance the inertia forces in contrast to above ground structures where the structure must bear the loads. Damages in continuous steel pipeline due to transient ground deformations has been reported for the Michoacan earthquake in 1985 [6]. Damages to continuous steel pipelines due to permanent ground deformation on numerous occasions have been reported for the San Fernando earthquake in 1971 [7]. Numerous pipeline failures are observed in the 1971 San Fernando earthquake, such as flexural failure and shear failure. Buckling failure are observed mostly in pipelines crossing faults. Extensive damage in buried pipelines due to landslides are observed in the 1964 Alaska earthquake. Large numbers of damages to buried pipelines due to earthquakes in Japan with magnitude greater than 7 since 1920 has been attributed to direct seismic shaking [8].

Several methods to assess seismic risk to buried pipelines due to ground shaking have been proposed in the past by [9–16]. Seismic risk analysis approaches for buried pipelines faced with fault rupture hazard has been proposed by [17–19]. However, there are some major limitations of these works. Firstly, simplified pipe-soil models are used which are not capable of predicting the true behavior of the pipeline. Additionally, probabilistic ground deformation hazard is computed using available regression models. Moreover, the methods use empirical fragility functions for pipeline damage to characterize seismic risk. Finally, these approaches are suitable for single pipeline fault crossing sites and not for large regions.

Earthquakes result due to release of accumulated stress at tectonic plate boundaries. Fault rupture is associated with release of excess stress and

strain energy when the rock can no-more resist them. Faults can be primarily classified as 'strike-slip' and 'dip-slip'. 'Strike-slip' fault rupture involves primarily movement in the horizontal direction. 'Dip-slip' fault rupture involves movement along the dip of the fault-plane. Under 'dip-slip' movement, when the horizontal movement is compression, it is called 'reverse faulting' whereas, when the horizontal movement is tensile, it is called 'normal faulting'. The pipeline structural response to surface rupture is dependent on the orientation of the pipeline in respect to the rupture. Failure mode due to axial compression may include buckling and failure mode due to axial tension may result in rupture. 'Strike-slip' faulting leads to symmetrical loading on both sides of the pipeline, whereas, 'dip-slip' faulting leads to unsymmetrical loading on both sides of the pipeline. Generally, 'dip-slip' faulting is more damaging than 'strike-slip' ones because the bearing load on a buried structure moving downward in soil is greater than the load to move it in the lateral direction.

1.2 Research Objectives

Literature review suggests that, there is lack in availability of clear guidelines and methodologies for assessing risk to buried continuous pipelines due to permanent ground deformations arising from fault ruptures. This broad problem covers methods for appropriately modelling pipe-soil structural model to evaluate pipeline structural response including implementation of suitable soil constitutive models, consideration to associated uncertainties in the structural model inputs, considerations to efficiency with respect to computational time and effort to make the process usable for realistic purposes and integration of the pipeline behavior with state of the art probabilistic methods for evaluating ground deformations arising due to fault rupture over a region.

The overall objective of this research is to develop an improved and robust method for seismic risk assessment of buried continuous energy pipelines subjected to fault rupture permanent ground deformations, considering uncertainty at various levels. The specific objectives of this research are as follows:

1. Develop an experimentally evaluated model for soil non-linear material property. This includes modifying the elastic-perfectly plastic Mohr-Coulomb model in ABAQUS and introducing suitable constitutive relations for mobilized friction angle and dilation angle with varying plastic shear strain. Thereafter, the objective is to evaluate the modified Mohr-Coulomb

model with a sand triaxial test.

Develop an experimentally evaluated detailed 3D FE model of pipeline undergoing fault rupture deformations. This includes generating suitable sand constitutive relations with respect to the large scale test and developing a detailed FE model to simulate large scale experimental arrangement and evaluating the model with experimental results.

2. Develop a multi-fidelity-based uncertainty quantification approach for buried pipeline undergoing fault rupture deformations.

3. Develop a method for determination of target strain envelope curves and perform sensitivity analysis using Taguchi design of experiments for pipelines undergoing permanent ground deformations.

4. To estimate probabilistic ground deformation hazard due to fault rupture at a given region using available state of the art techniques and integrate it with a pipeline response uncertainty quantification framework to determine pipeline seismic risk as a result of permanent ground deformation.

1.3 Overview

Firstly, nonlinear structural response of a buried continuous pipeline undergoing strike-slip fault rupture, i.e., where soil masses get displaced in the horizontal plane along a fault line, is studied in a detailed manner. A detailed analysis technique employing ABAQUS/Standard with implicit formulation to study the behavior of buried continuous pipelines crossing fault movements is proposed and established with suitable evaluations. A three-dimensional nonlinear FE model including both material and geometric non-linearity is used for this study. Firstly, a non-linear sand constitutive model is adopted and implemented in commercial FE package ABAQUS. The adopted material model is evaluated with available experimental triaxial test results. This material model is thereafter suitably calibrated for a large-scale test based on direct shear soil test data for that experiment. The study identified important soil strength parameters from direct shear soil tests conducted for the large-scale test program and converted them suitably with respect to the adopted sand constitutive model. The FE model is then evaluated against full-scale experimental results.

Subsequently, nonlinear structural response of buried continuous steel pipeline undergoing fault rupture deformation is studied in a systematic manner. A detailed and efficient analysis framework for design of buried continuous steel pipelines crossing faults is proposed and illustrated with a case study. This analysis framework considers a number of levels for each

of the factors (input parameters) thereby allowing to predict peak strain expected as a function of fault displacement for a range of variation of the input parameters. A three-dimensional nonlinear FE model including both material and geometric non-linearity previously developed and evaluated is used for this study. Taguchi method for design of experiments is then employed to evaluate the structural performance of buried pipelines. It is also used to identify the influence of different parameters on the structural behavior of buried pipelines. A case study involving NPS 24 steel pipeline with a realistic maximum operating internal pressure of 9.1 MPa is also carried out. Various realistic steel grades are selected for the study, such as Gr 290, Gr 386 and Gr 483. The method presented here is suitable for pipeline strain hazard analysis, applicable for a single site.

A further extension to the above deterministic analysis approach is to include uncertainty in the input parameters. One of the simplest methods for uncertainty quantification and propagation is the Monte Carlo simulation (MCS). The general process involves identifying sets of random and fixed variables, generating realizations corresponding to the random variables and then analysing each case using deterministic FE method. The results obtained from the multiple runs of the FE solver are used for computing the probability distribution and statistical moments of the stochastic output. A large number of FE runs are needed for this method to converge making it infeasible for solving actual problems. An alternative to the simulation based approaches discussed above are the surrogate based approaches. The primary idea here is to train a machine learning model to act as a surrogate to the computationally expensive FE solver. MCS is then performed by using the trained surrogate model. However, even the most efficient surrogate models require hundreds of FE runs for generating the necessary training data. This is problematic for cases, such as the 3D pipe soil interaction problem undergoing fault displacement as the nonlinear 3D FE solver is extremely expensive.

Given the limitations with the simulation based and surrogate based approaches discussed above, a special type of surrogate model, referred to as the multi-fidelity (MF) surrogate for uncertainty quantification of buried pipeline undergoing strike slip fault rupture in sand is proposed. In MF surrogate models, the training data is generated from two solvers – a computationally expensive HF solver that yields highly accurate results and a computationally efficient LF solver that yields results of reasonable accuracy. The idea is to have a small number of training samples from the HF solver (in the order of tens) and significant number of training samples from the LF solver (in the order of hundreds). Since the LF solver is relatively

efficient, the data generating process in this case is relatively efficient. As the LF solver, the beam element pipe along with bi-linear soil springs model have been used. The 3D model developed in the authors' previous study is used as the HF solver. Among different MF surrogates available in the literature, we have used the MF Gaussian process (MF-GP) also known as co-Kriging for the current study.

A novel method to estimate regional seismic risk to buried continuous pipelines probabilistically, due to earthquake-induced permanent ground deformations is proposed. The seismic risk assessment method is illustrated for buried gas pipelines in the City of Victoria considering seismic risk from the Leech River Valley Fault Zone (LRVFZ). The method considers uncertainty on earthquake rupture, soil properties, pipe geometry as well as operating conditions. It utilizes experimentally evaluated complex pipe-soil numerical models in an efficient manner. Major improvements of this method over existing studies are highlighted here. Firstly, stochastic source modelling and analytical Okada solutions are used in this study to generate regional ground deformation, probabilistically. Previous studies used regression equations to define probabilistic ground deformations along a fault. Secondly, in the current study complex experimentally evaluated pipe-soil FE models are employed including non-linear soil constitutive relations. Earlier investigations used simple soil spring – beam element pipe models to evaluate pipeline response. Finally, the current approach uses multi-fidelity Gaussian processes to ensure efficiency and limit required computational resource. This is required since a large number of runs are necessary for uncertainty quantification exercises. It is also necessary due to the computationally expensive nature of complex pipe-soil FE models used.

1.4 Thesis Organisation

The thesis is written based on manuscripts published/submitted in various journals. In chapter 1, introduction provides the research objectives and a brief background of the problem addressed here. A detailed literature review on various aspects of the research has been presented in chapter 2. Details on the developed pipe-soil FE model to study pipeline behavior under ground deformation loads are presented in chapter 3. A multi-fidelity based approach for uncertainty quantification on the above problem and development of associated fragility curves is presented in chapter 4. Integration of the developed uncertainty quantification model with regional probabilistic ground deformation approaches is presented in chapter 5. A

Taguchi design of experiments based sensitivity analysis and strain envelope curve development approach on the above problem is presented in chapter 6. Concluding remarks are made in chapter 7.

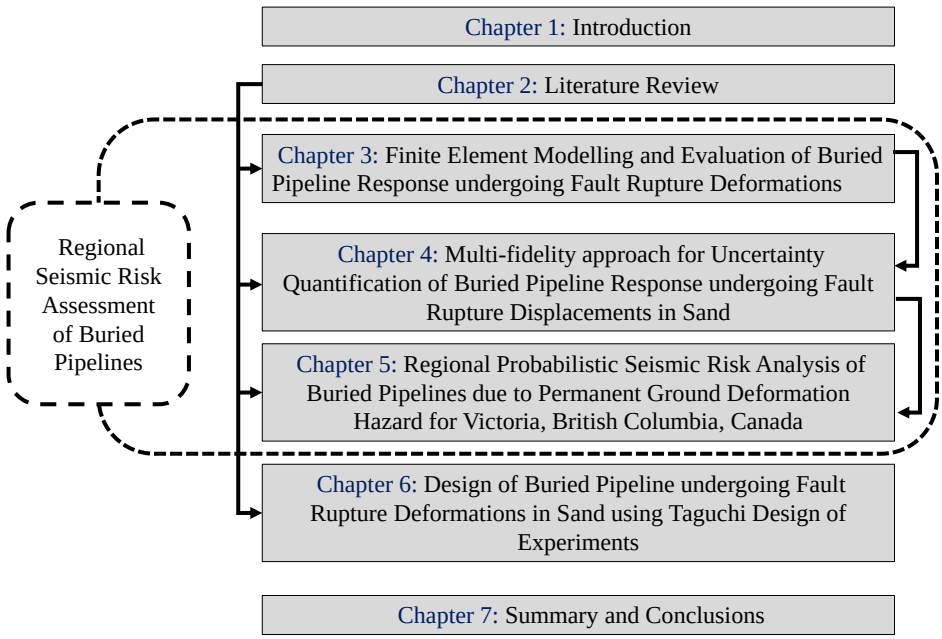

Figure 1.1: Thesis chapters flowchart

Chapter 2

Literature Review

2.1 Introduction

The literature review conducted can be classified as shown in Figure 2.1. The objective of the literature survey conducted is to address the above subject under a number of different modules. The areas covered in the literature review include methods to analyze the structural performance of a buried pipeline undergoing fault rupture deformations, experimental tests to study pipeline behavior under fault rupture, soil (sand) constitutive relations to appropriately model non-linear behavior, available approaches for uncertainty quantification, multi-fidelity methods for uncertainty quantification and probabilistic approaches to estimate ground deformation due to fault rupture on a regional scale.

2.2 Pipeline-fault rupture analysis

Energy pipelines are an important element of oil and gas infrastructure which comprise of major transmission pipelines and distribution pipeline network. Energy pipelines play a vital role in regional, national and international economy linking geopolitical matters and matters of global security [20]. Oil and gas pipelines are linear structures of high importance and failure in high pressure oil and gas pipeline can lead to severe consequences, such as contents spill leading to ecological disaster, explosion leading to fire, severe economic losses and loss of lives [21]. Buried energy pipelines travelling across seismically active regions are faced with an inherent risk due to seismic activity. This make seismic risk assessment of buried pipelines important to safeguard against possible seismic hazard. International design codes and available guidelines for energy pipelines, such as [22], [23], [24], [25], [26], [27] provide pipeline strain limits; however, they do not provide clear and detailed guidelines on predicting the strain demands for pipelines. Numerical modelling is recommended in some guidelines but only in a very generic sense. Additionally, none of these guidelines provide methods to re-

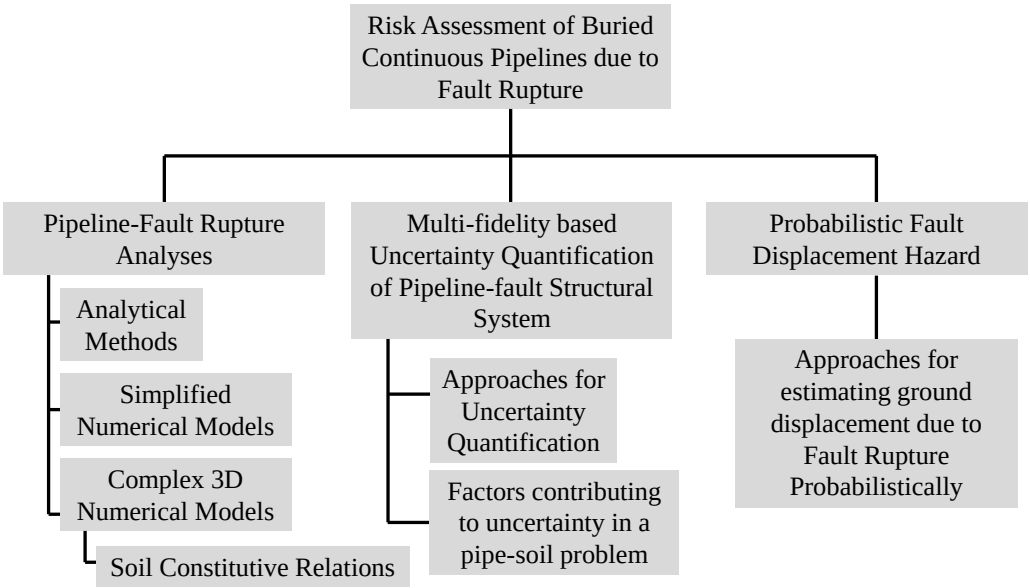

Figure 2.1: Literature Review Flowchart

liably use available soil constitutive relations and apply to site specific soil data to complete a detailed fault rupture-pipeline FE analysis. A representative summary of different studies on this topic are provided in Table 2.1.

Earthquakes are associated with fault ruptures, such as normal faulting, strike-slip faulting and reverse faulting as a result of bedrock thrusting. These ruptures propagate towards ground surface resulting in surface ruptures. These surface ruptures pose a serious threat towards the structural integrity of buried pipelines, along with other infrastructure. The response of buried pipelines to surface rupture has been studied extensively in numerous research investigations. Based on the method adopted, the available studies can be broadly classified into three categories – analytical and/or semi-analytical studies, experimental studies and numerical studies. In analytical and/or semi-analytical methods, simplified models are utilized to analyze the problem at hand ([28], [29]). The analytical and semi-analytical models-based approaches are generally based on beam on elastic foundation theory employing bi-linear steel material which are an approximate representation of the materials involved. These methods consider the pipe to be under tension and bending which covers only a partial loading scenario of the problem and are not accurate enough partly, due to their inability

to capture ovalities or local buckling. Attempts to improve the simplified models can also be found in the literature ([30], [31], [32], [33], [34]).

Experimental studies to identify the effect of fault ruptures on buried pipelines can also be found in literature. [35] carried out centrifuge tests to investigate the effect of moisture content, strain rate, burial depth and pipe diameter on the pipeline. [36] studied effect of normal and strike-slip faulting and the effect of fault crossing angle on the generated pipeline strains. [37] conducted centrifuge tests to examine one positive pipe-fault crossing angle and another negative pipe-fault crossing angle. [38] performed centrifuge tests to study the effect of burial depth and pipe diameter. Full-scale studies for identifying the behavior of buried pipelines can also be found in literature ([39], [40], [41], [42], [43], [44]).

[45] carried out numerical studies where the beam element is used to model the pipe and bi-linear springs are used to model the soil. This model is used to simulate a pipeline damage due to faulting observed in Izmit (Turkey). Use of similar simple numerical models is also reported in [46] and [17]. Another analytical approach to model pipe-soil interaction include that of by [47] where a shell pipe supported by spring elements simulating the soil is considered. Unfortunately, numerical models considering the pipe as a beam and surrounding soil as bi-linear springs supporting the pipe in three mutually perpendicular directions are incapable of capturing the true three-dimensional nature of this problem due to its simplistic nature [26]. Therefore, researchers now-a-days are inclined towards using more detailed three-dimensional continuum pipe-soil interaction models for this problem [1, 48–55]. The simplified beam element pipeline model supported by soil springs in three mutually perpendicular directions, is computationally inexpensive due to the absence of contact simulation, due to the involvement of much lesser number of elements and simplified formulations. However, the soil springs can only approximately model the soil response due to its spring stiffnesses acting in three mutually perpendicular directions. These stiffnesses have been obtained for axial, lateral, vertically up and vertically down movements of a pipeline and are not applicable for the complex pipe-soil movement that takes place during a fault rupture. There do exist beam element with additional degree of freedom for capturing complex phenomenon, such as ovalization. However, even such advanced beam elements can only be associated with soil springs and hence, the above-mentioned problem persists.

A 3D continuum soil and shell element pipeline model, on the other hand, is capable to simulating the true nature of pipe-soil interaction along with associated local buckling and ovalization of the pipeline. However, one

must bear in mind that the computational cost associated with such model is significantly more as compared to the beam-element based models. One of the primary challenges associated with three-dimensional pipe-soil interaction model is development of material model for soil. The most popular material model for sand is the Mohr-Coulomb criteria. In this model, the stress-strain relation is represented by using two parameters namely, cohesion and internal friction angles. The stress-strain behavior of dense sand can be grossly defined as elastic zone, pre-peak plastic zone ([56]), ranging from the initial yield surface up to the failure surface and the post peak softening zone, ranging from failure to higher deformations. Some of the most comprehensive and simple to use equations to define this behavior are provided by [57] and [58] among others. [58] conducted a series of triaxial tests of sands with varying relative densities and varying confining pressures to propose these equations. [59] and [60] provide expressions to estimate elastic modulus of soils. [61] proposed a closed-form relation between the peak and critical internal angle of friction. Other works on sand constitutive model includes that of by [62], [63], [64], [65], [66] and [67].

In regards to the current study, [1], [53] and [55] had analyzed pipeline responses under fault movements using 3D soil continuum model but only with linear variation of friction angle and dilation angle as a function of plastic deviatoric strain. [53] considered an idealized dense sand for their study. [68] had successfully used non-linear soil strength with varying plastic shear strain to analyze 2D pipe-soil problems.

2.3 Uncertainty quantification and uncertainty propagation of buried pipeline response

An important aspect associated with the problem of pipelines under fault movement is the presence of uncertainties. For example, there is an inherent variability in the pipeline geometry and material strength due to the details involved in the production process. Additionally, soil properties are characterised by significant variability over location and time. The operating conditions in the pipeline, such as internal pressure and temperature also varies over time. All these variability leads to significant uncertainties in the prediction of structural performance of a pipeline. To account for these uncertainties, design engineers generally use a safety factor over a deterministic analysis design. However, considering a safety factor may result in unsafe design or in some cases over conservative design, resulting in higher costs. Therefore, for a safe and economical design, it is important to track

Table 2.1: Representative summary of different studies on buried pipeline undergoing fault rupture.

Reference	Study Type				Variation of Important Parameters Studied						
	Analytical	Experimental	Numerical		Fault Type	Crossing Angle	Pipe Cross-section	Soil Type	Internal Pressure	Temperature	Pipe Material and Grade
			1D	3D							
[28]	*										
[29]	*										
[30]	*										
[31]	*					*					
[32]	*					*					
[33]	*					*					
[34]	*		*	*		*	*	*			
[35]		*					*	*			
[36]		*			*	*					
[37]		*				*					
[38]		*					*				
[39]		*				*	*		*		*
[41]		*		*			*				
[40]		*				*	*		*		*
[42]		*					*				
[43]	*	*		*			*	*			
[44]		*		*							
[45]			*					*			
[46]			*			*	*	*			*
[17]			*			*	*				
[48]				*		*	*	*	*		*
[49]				*		*					
[50]				*			*	*	*		*
[1]				*		*		*			*
[52]				*							
[53]				*			*				
[54]				*		*					
[55]		*		*		*			*		*

the propagation of uncertainties from the input variables to the output.

The literature on uncertainty quantification and uncertainty propagation in buried pipelines is quite sparse; this is primarily because of the computational cost associated with solving an uncertainty propagation problem. [69] considered variability of input parameters and used the response surface methodology to perform reliability analysis of a pipe-soil problem. [70] studied pipeline upheaval buckling using random variables for initial imperfection and pipe-soil interactions. Effect of spatial variability in pipe embedment depth, which in turn results in variable lateral resistance in sub-sea pipelines is studied by [71]. Reliability analysis of buried pipeline based on variability of traffic load is conducted by [72]. Upheaval buckling studies of pipeline considering variability in inputs using artificial neural network approaches is conducted by [73]. Studies which focused on studying variability of soil properties in pipe-soil interaction problems include that of by [74], [75] and [76]. Other probabilistic pipe-soil studies include [77], [78], [79], [80] and [81]. However, none of the studies discussed above deal with buried pipelines undergoing fault rupture displacements.

The only work in this domain is conducted by [18]. This work considers

uncertainties in defining the fault displacement hazard but is faced with a number of limitations, such as a simple approximate beam type pipe model supported by soil springs for structural analysis. Additionally, the study did not consider uncertainties with respect to important influencing parameters, such as pipeline geometric and material properties, soil material properties, operating conditions and pipeline-fault crossing angle. The objective of the current study is to address the limitations discussed above by conducting a thorough study to investigate the effect of input uncertainties on the response.

The simplest method for uncertainty quantification and propagation is the Monte Carlo simulation (MCS) ([82] and [83]). The general process involves identifying sets of random and fixed variables, generating realizations corresponds to the random variables and then analysing each case using deterministic FE method. The results obtained from the multiple runs of the FE solver are used for computing the probability distribution and statistical moments of the stochastic output. By post-processing the results, probability of failure of the system can also be calculated. Although MCS is simple to implement, the convergence rate of this method is extremely slow. Large numbers of FE runs are needed for this method to converge making it infeasible for solving actual problems. As an improvement to the classical MCS method, approaches, such as stratified sampling ([84] and [85]) and importance sampling ([86], [87] and [88]) have been proposed by researchers. However, even these methods often suffer from the curse of dimensionality. An alternative to the simulation based approaches discussed above are the surrogate based approaches. The primary idea here is to train a machine learning model to act as a surrogate to the computationally expensive FE solver. MCS is then performed by using the trained surrogate model. Popular surrogate models available in the literature include polynomial chaos expansion ([89] and [90]), neural networks ([73] and [91]), radial basis functions ([92] and [93]), analysis of variance decomposition ([94] and [95]) and Kriging ([93] and [96]). However, even the most efficient surrogate models require hundreds of FE runs for generating the training data. This is problematic for cases, such as the 3D pipe-soil interaction problem undergoing fault displacement as the nonlinear 3D FE solver is highly expensive.

Fragility curves provide a relation between the probability of exceeding a certain state of damage for a structure with that of the intensity of load acting on that structure. In regards to buried continuous pipelines there are a number of studies that have dealt with producing fragility functions of such systems, such as [97–105]. Most of these work however dealt with studying the effect of transient seismic ground deformations on continuous

pipelines. Study by [102] involved probabilistic risk assessment of a buried continuous pipeline under transverse permanent ground deformation due to landslide and there by leading to the generation of fragility curves. Work by [104] covers damage due to both seismic wave propagation as well as permanent ground deformation. A part of the current scope has been to utilize the developed multi-fidelity model to develop fragility curves for the considered pipeline-fault problem.

Design of experiments are rational ways of investigating all possibilities in a test involving several factors and their respective ranges [106]. Design of experiments in the past have been used for a range of purposes, such as agriculture, chemical industries, pharmaceutical industries, manufacturing industries, product development and various other fields [106]. The standard orthogonal arrays by Taguchi [107] are extensions of the initial works by [108] and [109]. The fundamental basis for fractional factorial arrays and orthogonal arrays is proposed by [108]. Methods to derive mixed-level orthogonal arrays from difference matrices are proposed by [109].

2.4 Multi-fidelity models

Uncertainty quantification exercises require a number of scenarios to be analyzed. Advanced numerical models capable of predicting the true behavior of a process require significant computational resources. In regards to the current research, the experimentally evaluated geotechnical numerical models are computationally quite expensive. An uncertainty quantification exercise which preserves the complexity and accuracy of a process requires advanced numerical models. Fitting a surrogate model with such models, also called HF models require large numbers of analyses to be completed. On the contrary, LF models or approximate models although computationally cheap are not able to capture the complexity of a process and certainly not accurate.

Multi-fidelity approaches leverage the accuracy and complexity of HF models with the efficiency of LF models to predict nearly accurate results in an efficient manner. Multi-fidelity surrogates are surrogate models, that fit information between input variables and output parameters. [110] identifies the primarily three methods to combine fidelities namely, adaptation, fusion and filtering. Adaptation works to improve the LF prediction based on HF behaviour. Fusion on the other hand, simply integrates the LF and HF response. Filtering uses LF response to evaluate HF response at specific points. [111] categorizes multi-fidelity surrogate modelling under several

types, such as multiplicative correction, additive correction and comprehensive correction. Multiplicative and additive correction methods modify the lower fidelity model with multiplicative or additive parameter. Comprehensive corrections introduce both multiplicative and additive corrections in the same surrogate.

A model $g : x \rightarrow y$ is a functional relationship between inputs x and outputs y. Considering that the uncertainty in inputs is defined by stochastic variable X, uncertainty propagation characterizes the statistics of $g(X)$, such as the model expectancy and variance. Variance reduction techniques use correlations between $g(X)$ and a supplementary random parameter whose statistical characteristics are obtained from the lower-fidelity models. [112] and [110] employed the control variate method as the multi-fidelity estimator. Given the limitation in computational resources, the objective here is to minimize the mean square error of the multi-fidelity estimator. [110] assumed a HF model g^1 and LF surrogate models $g^1, g^2, g^3, ..., g^k$ and considered the same input for all these models. The objective of the process is to evaluate the estimator:

$$t = E[g^1(\mathbb{Z}))] \tag{2.1}$$

corresponding to the HF model g^1 from input random variable $\mathbb{Z}$. The k scenarios of the random variable $\mathbb{Z}$ are denoted as $z_1, z_2, z_3, ...z_{mk}$. Model g^i is evaluated for $i = 1, 2, 3, ..., k$ at $z_1, z_2, z_3, ...z_{mi}$ resulting in $g^i(z_1), ...g^i(z_{mi})$. m_i of m represents the number of assessments for model g^i for $i = 1, 2, 3, ...k$. The Monte Carlo estimator is then expressed as:

$$y_m^{-i} = (1/m) \sum_{j=1}^{m} g^i(z_j) \tag{2.2}$$

which estimates $E[g^1(\mathbb{Z}))]$ by sampling $z_1, z_2, z_3, ...z_m$ of random variable $\mathbb{Z}$ where, $i = 1, 2, 3, ...k$. First the method estimates y_m^{-i} from m_i model evaluations $g^i(z_1), ...g^i(z_{mi})$ for $i = 1, 2, 3, ..., k$. Thereafter, it estimates Monte Carlo estimate y_{m-1}^{-i} from evaluations $g^i(z_1), ...g^i(z_{mi-1})$ with $i = 2, 3, ..., k$. The Multi-fidelity Monte-Carlo estimate is expressed as:

$$\hat{t} = y_m^{-1} + \sum_{i=2}^{k} \epsilon_i (y_{mi}^{-i} - y_{mi-1}^{-i}) \tag{2.3}$$

The coefficients $\epsilon_2, \epsilon_3, ...\epsilon_k$ control the respective weights of $(y_{mi}^{-i} - y_{mi-1}^{-i})$. The framework for the multi-fidelity Monte Carlo estimator modifies the estimated HF quantities with a sum of estimates of differences of lower-fidelity

quantities, there by fusing the outputs from both the high and LF models to predict the statistics of the HF model. The estimator is a function of the coefficients $\epsilon_2, \epsilon_3, ...\epsilon_k$ and the number of model evaluations $m_0, m_1, ...m_k$ and hence, these parameters are chosen in such a way to minimize the mean square error of the estimator for a given computational budget.

The work by [113] considers HF model $P_{high}(x, u)$ and LF model $P_{low}(x, u)$ with the input vectors defined by the design variables x and model parameters u. u is a random sample from random vector $U(\omega)$. The output from the HF model $P_{high}(x, U(\omega))$ is expressed as random variable $A(x, \omega)$. The statistic (mean and variance) of the HF model output is denoted as $s_A(x)$. The estimation of the mean for the HF model is considered as $s_A = E[A(\omega)]$. The estimator corresponding to s_A is $\hat{s_A}$. Considering constant values for design variables x_k, the HF model is $P_{high}(x_k, U(\omega))$ and the output is $A(\omega)$. Considering constant values for design variables x_k, the LF model is $P_{low}(x_k, U(\omega))$ and the output is $B(\omega)$. If independent and identically distributed random samples $(u_i, i = 1, 2, 3...)$ are drawn from $U(\omega)$, the HF and LF models $P_{high}(x_k, U(\omega))$ and $P_{low}(x_k, U(\omega))$ are evaluated to derive a_i and b_i. The control variate multi-fidelity estimator is then given as:

$$\widehat{s}_A = \frac{1}{n}\sum_{i=1}^{n} a_i + \epsilon(s_B - \frac{1}{n}\sum_{i=1}^{n} b_i) \tag{2.4}$$

ϵ is the control parameter and statistic $s_B = E[B(\omega)]$. The s_B can be approximated as: $\bar{b_m} = \frac{1}{m}\sum_{i=1}^{m} b_i$ when $m > n$. The multi-fidelity estimator thus becomes:

$$\hat{s_A} = \bar{a_n} + \epsilon(\bar{b_m} - \bar{b_n}) \tag{2.5}$$

The basic idea here is to enhance the original estimator $\bar{a_n}$ by $(\bar{b_m} - \bar{b_n})$ using a large number of evaluations m from the LF model. The variance of the multi-fidelity estimator is given as:

$$Var[s_{\hat{A},p}] = Var[\bar{a_n}] + \epsilon^2 Var[\bar{b_m}] + \epsilon^2 Var[\bar{b_n}] + 2\epsilon Cov[\bar{a_n}, \bar{b_m}] - 2\epsilon Cov[\bar{a_n}, \bar{b_n}] - 2\epsilon^2 Cov[\bar{b_m}, \bar{b_n}] \tag{2.6}$$

$$= \frac{\varsigma_A^2}{n} + \epsilon^2\frac{\varsigma_B^2}{m} + \epsilon^2\frac{\varsigma_B^2}{n} + 2\epsilon\frac{1}{nm}\sum_{i=1}^{n}\sum_{j=1}^{m} Cov[a_i, b_j] - 2\epsilon\frac{\varpi_{AB}\varsigma_A\varsigma_B}{n} - 2\epsilon^2\frac{1}{nm}\sum_{i=1}^{m}\sum_{j=1}^{n} Cov[b_i, b_j] \tag{2.7}$$

$$= \frac{\varsigma_A^2}{n} + \epsilon^2 \frac{\varsigma_B^2}{m} + \epsilon^2 \frac{\varsigma_B^2}{n} + 2\epsilon \frac{1}{nm} \sum_{i=1}^{n} Cov[a_i, b_i] - 2\epsilon \frac{\varpi_{AB}\varsigma_A\varsigma_B}{n} - 2\epsilon^2 \frac{1}{nm} \sum_{j=1}^{n} Cov[b_j, b_j] \tag{2.8}$$

$$= \frac{1}{n}(\varsigma_A^2 + \epsilon^2\varsigma_B^2 - 2\epsilon\varpi_{AB}\varsigma_A\varsigma_B) - \frac{1}{m}(\epsilon^2\varsigma_B^2 - 2\epsilon\varpi_{AB}\varsigma_A\varsigma_B) \tag{2.9}$$

where, $\varsigma_B^2 = Var[B(\omega)]; \varpi_{AB} = Corr[A(\omega), B(\omega)]$

This variance can be minimized in terms of ϵ and r, where $r = m/n$ to obtain the optimum value of $Var[s_{\hat{A},p}]$ which is expressed as:

$$MSE[s_{\hat{A},p}{}^*] = Var[s_{\hat{A},p}{}^*] = (1 + \frac{r^*}{w})[1 - (1 - \frac{1}{r^*})\varpi_{AB}{}^2]\frac{\varsigma_A{}^2}{p} \tag{2.10}$$

where, $\epsilon^* = \varpi_{AB}\frac{\varsigma_A}{\varsigma_B}; r^* = \sqrt{\frac{w\varpi_{AB}^2}{1-\varpi_{AB}^2}}; \varsigma_A^2 = Var[A(\omega)]; \varsigma_B^2 = Var[B(\omega)]; \varpi_{AB} = Corr(A(\omega), B(\omega))$ being the variance correlation coefficient of $A(\omega)$ and $B(\omega)$.

[114] provides an account of application of co-kriging in multi-fidelity optimization. [115] and [116] discussed kriging from the fundamentals. To make a prediction at some point x in the domain, considering uncertainty, a random variable $Y(x)$ is considered having a mean of μ and variance ς^2. Considering two distinct points x_i and x_j and assuming that the associated functional values are $y(x_i)$ and $y(x_j)$; these functional values are more likely to be close if the distance $|x_i - x_j|$ is small. The correlation between the random variables is given as:

$$Corr[Y(x_i), Y(x_j)] = exp(-\sum_{l=1}^{d} \theta_l \, |x_{il} - x_{jl}|^{pl}) \tag{2.11}$$

If the distance $|x_i - x_j|$ is infinite, the correlation tends to be zero and if the distance is zero, the correlation tends to be 1. The θ_l parameter controls the sensitivity of the correlation in the lth coordinate direction. The p_l parameter controls the smoothness of the correlation in the lth coordinate function. The uncertainty about the function's value at the n points can be expressed as:

$$y = \begin{pmatrix} Y(x_1) \\ \\ \\ Y(x_n) \end{pmatrix} \tag{2.12}$$

By equating the derivative of log-likelihood function with ς^2 and μ to zero,

$$\hat{\mu} = \frac{1^{'} R^{-1} y}{1^{'} R^{-1} 1} \tag{2.13}$$

$$\hat{\varsigma^2} = \frac{(y - 1\hat{\mu})^{'} R^{-1} (y - 1\hat{\mu})}{n} \tag{2.14}$$

Replacing the above expression in the log-likelihood function becomes:

$$-\frac{n}{2} log(\hat{\varsigma^2}) - \frac{1}{2} log\,|R| \tag{2.15}$$

The function may be maximized to estimate $\hat{\theta}_l$ and $\hat{p}_l$ $(l = 1, 2, 3, ...d)$, as the expression depends on R. These estimated values may be used to derive $\hat{\mu}$ and $\hat{\varsigma^2}$. To predict values at an unknown point x^*, a function y^*, is assumed. To assess its accuracy, the point (x^*, y^*) is added to the observed data as the $(n+1)^{th}$ observation and the likelihood function is computed using parameter values determined in maximum likelihood estimation. Using the determined fixed parameters, the log-likelihood is a function of y^* and the corresponding y^* that maximizes the likelihood function is the kriging predictor. The standard formula of kriging predictor is:

$$y(\hat{x^*}) = \hat{\mu} + r^{'} R^{-1} (y - 1\hat{\mu}) \tag{2.16}$$

[114] provides the fundamentals from co-kriging. Assuming there are two data sets, one with HF data y_e at points X_e and LF data y_c at points X_c $(X_e \subset X_c)$. The combined set can be expressed as:

$$X = \begin{pmatrix} X_c \\ X_e \end{pmatrix} = (x_c^1, ...x_c^{n_c}, x_e^1, ...x_e^{n_e})^T \tag{2.17}$$

The value at point X is a sample from a Gaussian random variable.

$$Y = \begin{pmatrix} Y_c(X_c) \\ Y_e(X_e) \end{pmatrix} = (Y_c(x_c^1), ...Y_c(x_c^{n_c}), Y_e(x_e^1), ...Y_e(x_e^{n_e}))^T \tag{2.18}$$

It is considered that, if the value of the HF model output is known at x^i, no further information can be obtained from the LF model at that point. Gaussian processes $Z_c(\bullet)$ and $Z_e(\bullet)$ represent the local features of the LF and HF models. The HF model function can be expressed as:

$$Z_e(x) = \rho Z_c(x) + Z_d(x) \tag{2.19}$$

Where, ρ is a scaling function and represents a Gaussian process defining the difference between $Z_e(x)$ and $\rho Z_c(x)$. The co-variance is defined as:

$$cov\left\{Y_c(X_c), Y_c(X_c)\right\} = cov\left\{Z_c(X_c), Z_c(X_c)\right\} = \varsigma_c^2 \psi_c(X_c, X_c) \tag{2.20}$$

$$cov\left\{Y_e(X_e), Y_c(X_c)\right\} = cov\left\{\rho Z_c(X_c) + Z_d(X_c), Z_c(X_e)\right\} = \rho\varsigma_c^2 \psi_c(X_c, X_e) \tag{2.21}$$

$$cov\left\{Y_e(X_e), Y_e(X_e)\right\} = cov\left\{\rho Z_c(X_e) + Z_d(X_e), \rho Z_c(X_e) + Z_d(X_e)\right\} \tag{2.22}$$

$$= \rho^2 cov\left\{Z_c(X_e), Z_c(X_e)\right\} + cov\left\{Z_d(X_e), Z_d(X_e)\right\} \tag{2.23}$$

$$= \rho^2 \varsigma_c^2 \psi_c\left(X_e, X_e\right) + \varsigma_d^2 \psi_d\left(X_e, X_e\right) \tag{2.24}$$

$$C = \begin{pmatrix} \varsigma_c^2 \psi_c(X_c, X_c) & \rho\varsigma_c^2 \psi_c(X_c, X_e) \\ \rho\varsigma_c^2 \psi_c(X_e, X_c) & \rho^2\varsigma_c^2 \psi_c(X_e, X_e) + \varsigma_d^2 \psi_d(X_e, X_e) \end{pmatrix} \tag{2.25}$$

where, $\psi_c\left(X_e, X_c\right)$ for instance is a matrix of the form ψ_c for correlations between X_e and X_c and is similar to Equation 2.20. Similar to kriging, the LF model data are evaluated independently and maximum likelihood estimate of μ_c, ς_c^2, θ_c and p_c are calculated by maximizing the log-likelihood. To estimate μ_d, ς_d^2, θ_d, p_d and ρ from the difference Gaussian Process, the following relation is considered:

$$d = y_e - \rho y_c(X_e) \tag{2.26}$$

where, $y_c(X_e)$ are the values of y_c at locations common to X_e. By maximizing the log-likelihood of d, the hyperparameters of μ_d, ς_d^2, θ_d, p_d and ρ can

be obtained. The co-kriging predictor based on the knows hyper-parameters is given as:

$$\hat{y_e}(x^{(n_e+1)}) = \hat{\mu} + u^T C^{-1}(y - 1\hat{\mu}) \tag{2.27}$$

$$u = \begin{pmatrix} \hat{\rho}\hat{\varsigma_c^2}\psi_c(X_c, x^{n+1}) \\ \hat{\rho}\hat{\varsigma_c^2}\psi_c(X_e, x^{n+1}) + \hat{\varsigma_d^2}\psi_d(X_e, x^{n+1}) \end{pmatrix} \tag{2.28}$$

Given the limitations with the simulation based and surrogate based approaches discussed above, we propose to use a special type of surrogate model, referred to as the multi-fidelity (MF) surrogate for uncertainty quantification of buried pipeline undergoing strike slip fault rupture in sand. In MF surrogate models, the training data is generated from two solvers - a computationally expensive HF solver that yields highly accurate results and a computationally efficient LF solver that yields results of reasonable accuracy. The idea is to have a small number of training samples from the HF solver (in the order of tens) and significant number of training samples from the LF solver (in the order of hundreds). Since the LF solver is relatively efficient, the data generating process in this case is relatively efficient. As the LF solver, the beam model previously discussed have been used. The 3D model developed in the authors' previous study is used as the HF solver. Among different MF surrogates available in the literature, we have used the MF Gaussian process (MF-GP) [82], also known as the co-Kriging [83] for the current study. HF models yield highly accurate results but are computationally expensive and time consuming in nature. HF models are generally more detailed, complex leading to accurate results. On the other hand, LF models yield approximate results due to the simplified nature of the models but are highly time efficient and require much less computational effort. LF models are generally more simplified in nature. Multi-fidelity approaches aim to combine the accuracy of hi-fidelity models with the efficiency of LF models to predict nearly accurate results in a reasonably efficient manner. Multi-fidelity models generally involve the construction of surrogate models, which are approximations that fit to available data of a process and define a relationship between input variables and output quantities of interest. Construction of surrogate models lead to reduction in the computational efforts required for optimization or uncertainty quantification problems. Multi-fidelity models may however consider both surrogates as well as non-surrogates.

2.5 Probabilistic ground deformation due to fault rupture and the Leech River Fault Zone

Characterizing seismic risk to buried pipeline infrastructure and other structures due to surface rupture require due consideration to the uncertainties regarding surface displacement values as a result of fault rupture. Initial studies to probabilistically characterize fault displacement hazards can be found in [117, 118]. Broadly, the work adopts the 'Probabilistic seismic hazard analysis' level 4 (PSHA) practice as provided in [119]. The approach to estimate the hazard involves several expert evaluations of seismic sources along with their potential for fault displacement. To consider for uncertainties in their evaluations, the experts propose several weighted alternative evaluations. Fault displacements are classified as principal and distributed to differentiate between the main plane of fault rupture and the secondary ruptures occurring in the region adjacent to the main plane. The basic formulation by [117] estimates the fault displacement hazard as a product of the frequency of fault displacement occurrences at a point and the conditional probability representing the fault displacement above a certain magnitude. In this regard, primarily two approaches namely the 'displacement approach' and 'earthquake approach' are used; the former uses point specific historical surface displacement data to define the frequency of fault displacement occurrences and the later uses seismic source evaluation to relate the frequency of earthquake occurrences at the source to the frequency of fault displacements. The work in [118] provides probabilistic distributions from global data sets for normal faulting.

Further improvement to [118] is [120] in which, data regarding strike-slip faulting ground deformations at faults, maps of fault trace prior to an earthquake and maps of surface rupture from various earthquakes are compiled. These data are suitably processed to generate regression equations for principal fault displacement vs. distances along the fault, distributed fault displacement magnitudes vs. perpendicular distances from the principal fault and off-fault probability of surface rupture. Data compiled includes fault displacement value and location data in addition to the corresponding magnitude of earthquakes along the principal faults and distributed fault displacement data as a function of perpendicular distance from principal fault along with corresponding earthquake magnitudes. This approach [120] uses four probability distribution functions: firstly, to characterize the earthquake magnitude and fault rupture location along the fault; secondly, to define the perpendicular distance from the considered site to the fault trace;

thirdly, to characterize the fault displacement along the principal fault and lastly to characterize distributed fault displacements at locations perpendicular to the rupture. In addition, probabilities to define the ratios of cells that have ruptured in the principal fault region, distributed fault region and to define the probability of surface rupture for a given earthquake magnitude are also used. The procedure considers uncertainty of both "epistemic" and "aleatory" origins.

An alternative approach to probabilistically characterize ground deformation due to fault rupture is proposed by [121] which uses stochastic source modelling and analytical Okada solutions instead of regression models. This method relies on analytical solution by [122]. In this method, firstly the source parameters of the rupturing fault are generated by empirical methods or other means. Uncertainties in fault rupture are considered in the analyses, both in terms of uncertainties in fault geometric parameters and fault slip distributions. In order to do so, statistical scaling relationships from [123] are used, for modelling the source of the earthquakes probabilistically, which define important features of a fault rupture. Other scaling relationships are also available based on empirical equations, such as by [124–129]. Source parameters considered include geometry parameters of the fault, statistics of the slip parameters for fault rupture and spatial distribution parameters for fault rupture slip. These scaling relationships for the source parameters based on a given rupture nature and earthquake magnitude are obtained with the use of publicly available extensive earthquake data and regression analyses. Thereafter, uncertainty is considered for the slip process [123] to stochastically generate earthquake slip. Ground displacements are finally computed probabilistically using analytical solutions based on Okada equations [122, 130]. Okada equations generate the surface displacements for both inclined shear as well as tensile faults. In Okada equations, the surface displacements are deterministically calculated in a three-dimensional field allowing to calculate differential displacement between any two points for a certain earthquake. Surface displacements calculated at different locations hold physical consistency with one another.

The Leech River Valley Fault Zone (LRVFZ) is about 60 km in length and is a potential threat for producing earthquakes having moment magnitude (MW) more than 6 [131]. This fault zone is in the proximity of the City of Victoria. [131] further highlights the destructive potential from surface ruptures arising due to earthquakes at shallow sources in the LRVFZ. [132] indicates that the LRVFZ can be divided into two parts towards the east, one on the north probably connecting with the Devil's Mountain Fault (DMF) and the other towards south probably connecting with the Southern

Whidbey Island Fault (SWIF). They further confirm the existence of crustal fault in the Victoria region and suggest the potential of micro seismicity due to slow movement of the active crustal faults. [133] mapped the DMF and indicated that the DMF and LRVFZ may be parts of the same fault network. They estimate that this fault network has the potential of generating earthquakes of MW 7.5 at very close vicinity of the City of Victoria.

[134] conducted a seismic hazard study for the Victoria region by considering the combined effects of the LRVFZ and DMF considering varying fault lengths and slip lengths as well as inter fault interplay. This hazard is thereafter included in the 2020 – 6th Generation Seismic Hazard model of Canada. Additional study, such as [135] also included LRVFZ as a potential source of seismicity to evaluate probabilistic seismic hazard at Victoria. They predicted an increase of 1 to 23 percent from National Building Code of Canada (NBCC) 2015 uniform hazard spectra ground motions due to the inclusion of LRFZ as an earthquake source. Uncertainties with respect to LRVFZ source is suitably considered in this study. [136] conducted a probabilistic seismic hazard analysis of the Victoria region due to seismicity from the LRFZ-DMF system using a probabilistic method based on the fault source of this region. Their study concluded a 10 to 30 percent increase in seismic hazard in the Victoria region due to the inclusion of LRVFZ-DMF as a potential cause of earthquake.

2.6 Probabilistic pipeline strain risk analysis

Methods to convert seismic hazard to pipeline strain risk using pipeline structural analysis can be found in works by [18] and [17]. In this approach, the seismic hazard is represented by a fault displacement vs mean annual rate of exceedance. The pipeline structural analysis provides a relation between fault displacement and generated strain. Pipeline strain risk is determined by combining pipeline structural analysis and seismic hazard as a relation between mean annual rate of exceeding strain values vs the corresponding strains. In this work, a comprehensive study on the pipeline response for a wide range of independent fault displacement components are conducted. However, it is highlighted that, an efficient way would be perform only a set of structural analysis for fault displacement components specific to the pipe fault crossing system at hand.

[19] performed a study to evaluate probabilistic pipeline risk based on probabilistic permanent ground deformation hazard. The method computed failure probability of buried continuous pipelines under different permanent

fault displacement levels as well as pipe cross-section properties. The study combined probabilistic fault displacement hazard, pipeline mechanical response due to fault displacement loads and empirical fragility functions to derive annual exceedance rate of pipeline failure. [137] deals with simulation based seismic risk assessment of gas distribution networks. [138] provides an assessment framework for seismic risk assessment of a gas pipeline infrastructure at a regional scale. The method employs fragility functions from literature to estimate losses resulting from liquefaction and landslide hazard due to earthquake. The basic framework consisted of hazard assessment and risk assessment components. [97] conducted a comprehensive seismic risk analysis using spatial coordinates of Azerbaijan natural gas pipeline in Iran; the objective being to estimate corresponding losses.

Chapter 3

Finite Element Modelling and Evaluation of Buried Pipeline Response undergoing Fault Rupture Deformations

3.1 Introduction

Literature review suggested that no study until now has been attempted to use non-linear soil strength constitutive relations to investigate pipeline response under fault movements. Employment of non-linear soil strength include considerations to suitably evaluate soil non-linear mobilized shear strength behavior in FE model with respect to triaxial test results for 3D applications. Further, the objective of this study is to develop an improved 3D FE model for buried pipeline undergoing fault rupture in sand using suitable properties for the non-linear sand relevant for a large scale pipe-soil test. The novelty of this work is two folds. First, we have incorporated an experimentally evaluated non-linear soil constitutive model with pre-peak hardening and post-peak softening behavior. Secondly, the soil model is calibrated suitably based on direct-shear soil test data corresponding to a large-scale experimental test.

To that end, the Mohr-Coulomb soil model has been modified based on experimentally derived constitutive relations available in the literature. The updated Mohr-Coulomb model with pre-peak hardening and post-peak softening behavior has been imported into the FE package ABAQUS by developing a user-defined subroutine, USDFLD. This developed model is then suitably calibrated for a large-scale test based on direct shear soil test data for that experiment. Thereafter, this calibrated soil model is used to simulate large scale experiment of a pipe undergoing fault rupture. The accuracy

of the developed FE model is evaluated in two-stages. First, we evaluate the material model with triaxial test results available in the literature. The model used in this study is found to yield good results as quantified later on. Second, the detailed three-dimensional FE analysis results are compared against other numerical results and experimental results of a full-scale test carried out at Cornell University [1, 2, 39]. The developed FE model is found to yield the best results.

The rest of the paper is organized as follows. In section 3.2, details about the physical system considered in this study has been provided. The details about the developed FE model is discussed in section 3.3. Evaluation of the material model and the developed FE model are presented in section 3.4. Finally, section 3.5 provides the concluding remarks.

3.2 Physical model of buried pipeline

We consider the large-scale experimental test carried out at Cornell University. Two separate case studies are considered. The experiments considered no internal pressure and no operating temperature on the pipeline and are carried out using split-boxes. The tests involved fixing one end of the pipe, its associated soil mass and applying a displacement on the other end of the pipe and its associated soil mass. Displacement applied is a combination of displacement along the lateral direction of the pipe and a displacement along the axial direction of the pipe. One of the tests involved a lateral displacement along with an axial compressive displacement and the other test involved a lateral displacement along with an axial tensile displacement. The difference between the two experiments considered resides in the fact that one exerted compressive force in the pipe in addition to bending and the other exerted tensile force in the pipe in addition to bending due to the experimental displacement arrangement.

Soil used for the large-scale tests are well graded glacio-fluvial sand. The experimental sand is tested using direct shear tests with normal stresses of 15 kPa which is similar to the vertical stresses developed at a depth of 1.25 m in sand situated above water table. This is the expected vertical stress at a depth to the centerline of the HDPE pipes used for these experiments. The length of the pipeline used in the experiments are 10.6 m in length. The experimental setup consisted of two soil boxes containing the pipe. Each half of the soil box is 6.6 m in length by 3.2 m in width by 2.3 m in depth. Total length of the setup is however, 10.6 m. The boxes are aligned at 65° with respect to the pipe. The pipe ran perfectly horizontally through the

boxes. The pipeline is reported to be fixed at each end of the box [139]. Figure 3.2 shows the experimental configuration of the 'tensile' strike-slip test as a FE mesh. The FE mesh is generated to closely represent the actual experimental setup. Hence, the soil blocks are arranged to be staggered initially and gradually displaced along the fault plane. The pipe is modelled to be placed close to the right edge of the stationary soil mass similar to the experimental arrangement. Soil strength are determined using direct shear tests. Consistent peak shear strength is maintained for the tests. The sand used for the large-scale test is termed "RMS graded sand". The mean grain size D_{50} of the soil is 0.67 mm [40]. It is reported that a consistent direct shear peak friction angle of $39° - 40°$ and dry density of 15.5-15.8 kN/m^3 is maintained for these tests. A schematic representation of the described model is shown in Figure 3.1. 'α' and 'β' in the schematic diagram are the fault angle in the vertical plane and fault angle in the horizontal plane. As stated previously, the objective of this study is to develop a detailed three-dimensional FE model for simulating the physical model described below.

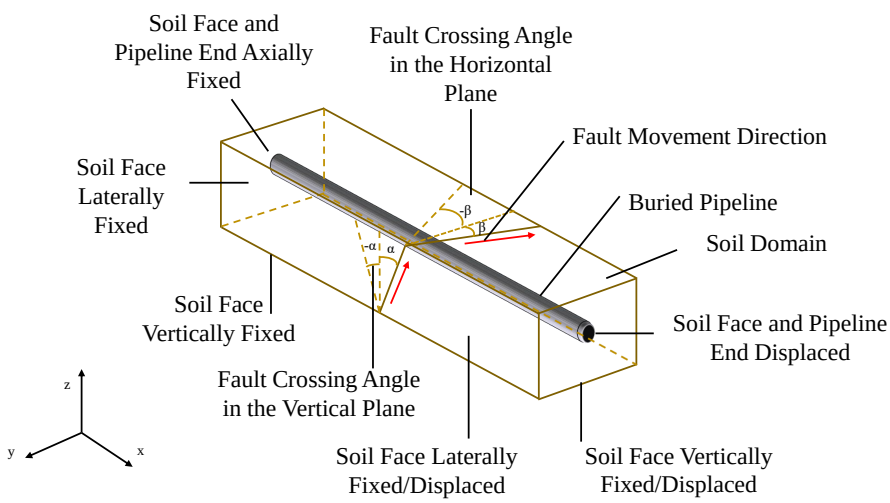

Figure 3.1: Pipeline-fault schematic diagram

3.3 Numerical modelling

The overall ABAQUS model is developed to closely represent the large-scale experimental pipe-soil specimen at Cornell University to simulate buried pipeline response under fault movement loads. Pipeline segment is considered to cross continuum soil partitioned into two blocks. One block being stationary and the other being the moving block. The two blocks are separated by a planar shear band. Since a finitely thick shear band is not modelled here, the propagation of fault rupture through the soil is not simulated here. Only the interaction of the moving and stationary soil blocks with that of the pipe and with each other is simulated. Interaction between the soil blocks in the normal direction has been modelled using "hard" contact and interaction between the soil blocks in the "tangential" direction is modelled using frictionless contact. The nature of loading on the pipe with a planar shear band is expected to be quite similar as compared to a finite thickness shear band. It is so expected as the normal stresses will get readily transferred from one block to the other due to "hard" contact and the blocks can freely slide past one another due to "frictionless" contact. The fault rupture propagation nature will however, differ with a planar shear band when compared to a finite thickness shear band; however, it is not expected to affect the pipeline performance significantly differently.

Pipe end in the stationary block is axially restrained whereas the pipe end in the moving block is modelled to move in the intended direction and magnitude along with the moving block. This arrangement of boundary conditions correspond to a buried pipeline under restrained conditions at two ends of the pipe which is expected to induce higher strains due to the imposed fault displacements. Boundary surfaces of the stationary soil block are restricted to displace in their normal directions but can move in their tangential direction. Fault movement displacement is applied in the appropriate boundary surfaces in the moving block. Modelling ensured that the soil mass rupture is initiated from the bottom. Pipeline modelled is devoid of any imperfection and soil surfaces and boundaries are modelled to be perfectly horizontal and vertical surfaces.

3.3.1 FE Modelling details

The finite element method (FEM) is used to study the performance of buried pipeline undergoing fault rupture using ABAQUS [140]. The pipe is modelled using 4-noded doubly curved general-purpose shell elements with reduced integration (ABAQUS element S4R). This element allow for trans-

verse shear deformation and based on the shell thickness, either use thick shell theory or discrete Kirchhoff thin shell theory. These properties make it suitable to model pipes of various thicknesses. These elements possess six degree of freedom at each node; three translations and three rotations defined in their global co-ordinate system. It consists of a single integration point at the mid-surface to form the element internal force vector. The number of integration points through the thickness of the element is chosen to be 5. Soil continuum are modelled using general purpose 3D stress elements (ABAQUS element C3D8R). These elements are 8-node linear brick elements with reduced integration. Reduced integration elements use a lower order integration to form the element stiffness reducing running times, especially in three dimensions [140]. The integration point is located at the center of the element. Details on pipe-soil interaction are discussed below.

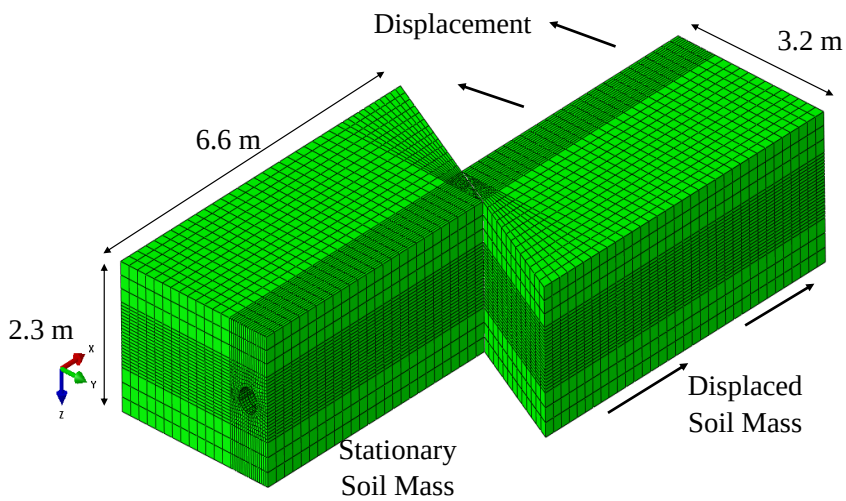

Figure 3.2: Pipeline-fault isometric mesh

The optimal mesh configuration is determined based on a convergence study. Pipe mesh size of 25 mm and soil mesh size surrounding the pipe of 10 mm are used. A schematic representation of the model is shown in Figure 3.1. The FE model developed using ABAQUS is shown in Figure 3.2

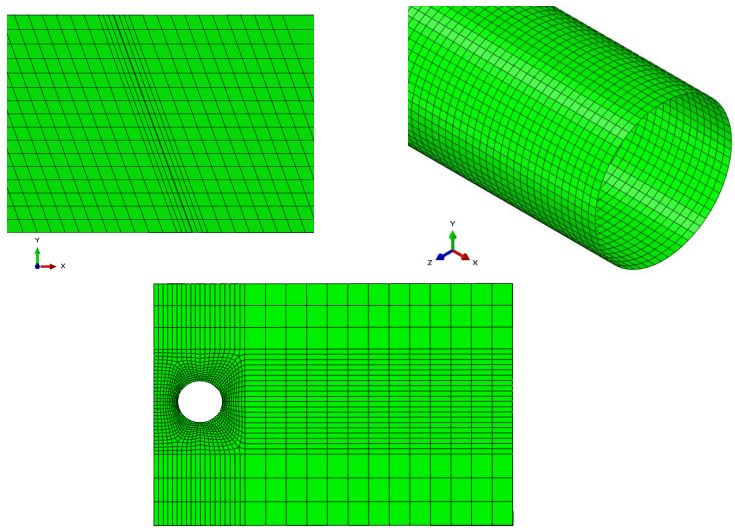

Figure 3.3: Finite element model mesh

and Figure 3.3. The shear band width for sand can range in between 3 and 25 D_{50} [65, 66]. [67] recommended a value of 16 D_{50} for sand shear band width. In the current study, for a given D_{50} of 0.67 mm and a multiplicative factor of 15, the shear band is calculated to be 10mm. [68] illustrates a method to update the strain softening factor with a scaling factor to consider for scaling effects and reduce FE mesh related inaccuracies. For fault rupture propagation, an exponential scaling factor of 1 [67, 68] is used. Additionally, an element size of 10 mm is used, which is same as the shear band width. Hence, no further modification to the strain softening factor is found necessary.

3.3.2 Soil material model

For sand, the Mohr-Column yield criterion is considered:

$$\tau = c - \sigma tan\phi \tag{3.1}$$

where c is cohesion, ϕ is internal angle of friction, σ and τ are the normal and shear stresses acting on the plane where failure occurs. The above criterion assumes σ is negative in compression and implies, larger the normal force, higher the shear the material can sustain. Primary features of stress-strain behavior of sand are its peak strength, initial elastic stiffness, pre-

peak hardening and post-peak softening [56, 58]. Shear strength of sands are influenced by its relative density, its confining pressure and are governed by its internal angle of friction [61, 68, 141–143]. Past test data show that dense sands generate plastic strains before failure and undergo softening post peak strength. Relatively softer sands exhibit lesser degrees of softening. A number of constitutive models are available in literature to define this behavior. The stress-strain behavior of dense sand can be grossly defined as elastic zone, pre-peak hardening zone [56], ranging from the initial yield surface up to the failure surface and the post peak softening zone, ranging from failure to higher deformations leading to the critical state conditions. The elastic modulus E, defining the behavior of sand in the elastic zone is computed according to [144] as:

$$E = Kp_a^{'}(p^{'}/p_a^{'})^n \tag{3.2}$$

where, the confining pressure is denoted as $p^{'}$, the atmospheric pressure is denoted as $p_a^{'}$ and following [59, 60] $K = 150$ and $n = 0.5$.

In the plastic zone, sand behaves as a nonlinear material where the friction angle and the dilation angle vary with the plastic shear strain p. Note that the variation of friction and dilation angle with the plastic shear strains are different in the pre-peak plastic zone and in the post peak softening zone. In the pre-peak plastic zone, the variation of the friction and dilation angles are represented based on [57] as:

$$\phi^{'} = \phi_{in}^{'} + sin^{-1}[(\frac{2\sqrt{\gamma^p\gamma_p^p}}{\gamma^p + \gamma_p^p})sin(\phi_p^{'} - \phi_{in}^{'})] \tag{3.3}$$

$$\psi = sin^{-1}[(\frac{2\sqrt{\gamma^p\gamma_p^p}}{\gamma^p + \gamma_p^p})sin(\psi_p)] \tag{3.4}$$

where, $\phi^{'}$ is the mobilized friction angle, ψ is the mobilized dilation angle and γ_p^p is the plastic shear strain corresponding to the instant of peak internal angle of friction and is calculated as [68]:

$$\gamma_p^p = \gamma_c^p(\frac{p^{'}}{p_a^{'}})^m \tag{3.5}$$

where, γ_c^p is a strain softening variable given as:

$$\gamma_c^p = C_1 - C_2 I_D \tag{3.6}$$

The constants $C_1 = 0.22$, $C_2 = 0.11$ and $m = 0.25$ have been used as realistic values [68], which generally need to be calibrated from experimental

data. $\phi_{in}^{'}$ is the internal friction angle at yielding. A $\phi_{in}^{'}$ of 29° has been used. $\phi_{p}^{'}$ is the peak friction angle and obtained as [61]:

$$\phi_{p}^{'} = \phi_{c}^{'} + A_{\psi} I_{R} \tag{3.7}$$

where, $\phi_{c}^{'} = 31°$ is the internal angle of friction at critical state conditions. A_{ψ} for tri-axial test conditions assumes a value of 3. The relative density index is denoted as I_R and defined as [61]:

$$I_R = I_D(Q - lnp^{'}) - R \tag{3.8}$$

where, $Q = 10$ and $R = 1$. ψ_p is the peak dilation angle and can be calculated according to [61] as:

$$\psi_p = \frac{\phi_{p}^{'} - \phi_{c}^{'}}{k_{\psi}} \tag{3.9}$$

$k = 0.5$ for triaxial conditions [61]. The post-peak nonlinear strain softening zone is defined according to [58] as:

$$\phi^{'} = \phi_{c}^{'} + (\phi_{p}^{'} - \phi_{c}^{'}) exp[-(\frac{\gamma^{p} - \gamma_{p}^{p}}{\gamma_{c}^{p}})^{2}] \tag{3.10}$$

$$\psi = \psi_{p} exp[-(\frac{\gamma^{p} - \gamma_{p}^{p}}{\gamma_{c}^{p}})^{2}] \tag{3.11}$$

Unfortunately, in ABAQUS, it is not possible to provide a varying dilation and/or friction angle. Therefore, the above equations are introduced into ABAQUS by using user-defined field (USDFLD).

An elasto-plastic representation of the soil in combination with a Mohr-Coulomb yield surface is frequently applied for soil-structure interaction analyses. The basic assumption in the Mohr criteria is that, the maximum shear stress controls failure. At yield, the critical value of shear stress is a function of the normal stress and corresponds to the point of tangency between the Mohr circle of stress and the yield surface. The Mohr-Coulomb soil model is an elastic perfectly plastic model which is widely used for the design applications in geotechnical engineering to simulate material response due to monotonic loading and is available in ABAQUS. The Mohr-Coulomb criterion assumes that yield occurs when the shear stress on any point in a material reaches a value that depends linearly on the normal stress in the same plane. The Mohr-Coulomb material model however is not equipped to produce the strain softening behavior observed in dense sand, as it employs a constant internal friction angle and dilation angle for the model.

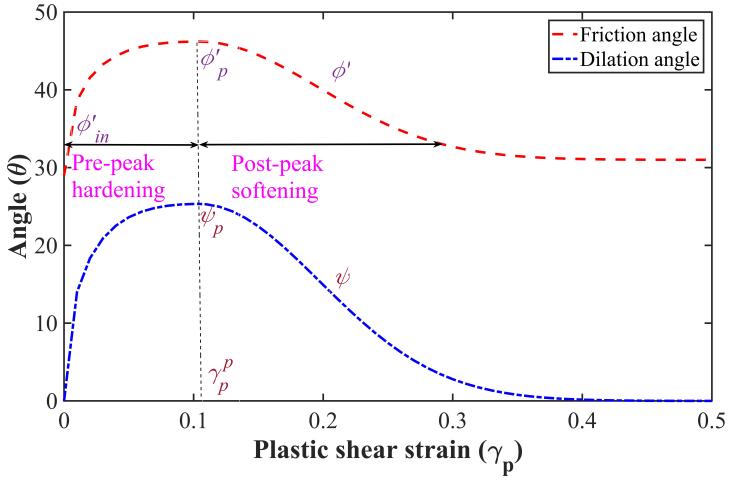

Figure 3.4: Mobilized friction angle and dilation angle

Hence, the Mohr-Coulomb model is upgraded to include a non-linear behavior using user subroutine. The modified Mohr-Coulomb model which includes pre-peak strain hardening and post-peak strain softening behavior is implemented into ABAQUS/Standard via. the user subroutine USDFLD. The subroutine allows for defining the variation of mobilized friction angle and mobilized dilation angle with the increase in deviatoric shear strain. The subroutine employs three solution dependent state variables and one field variable. In order to implement the strain softening behavior, the maximum and minimum principal plastic strain increment values are obtained for each increment using the current maximum and minimum principal plastic strains and the previous maximum and minimum principal plastic strains called from the last increment using subroutine GETVRM. These values are in-turn used to obtain the current plastic shear strain increment. The maximum deviatoric shear strain is obtained as a field variable at the end of each increment integrating the deviatoric shear strain increments over the period of analysis, which is in turn used to define the corresponding mobilized friction angle and mobilized dilation angle in the ABAQUS input file. To ensure the strain softening models validity, single element tests are carried out exhibiting softening behavior.

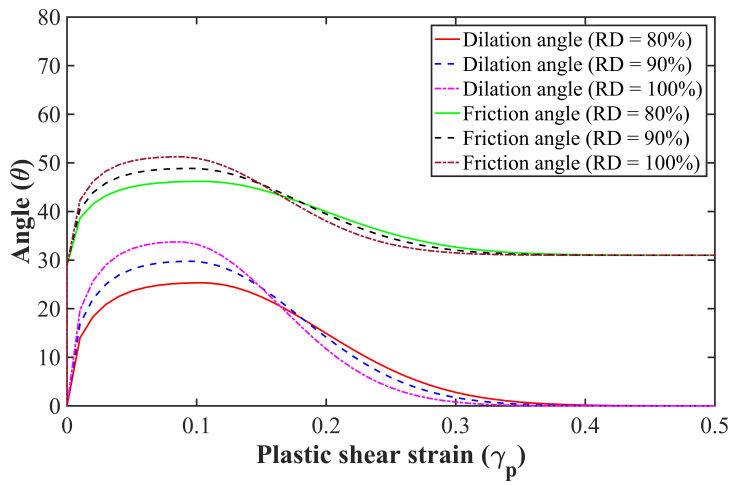

Figure 3.5: Mobilized friction angle and dilation angle for varying relative density

3.3.3 Pipe material model

Selection of proper material models are an important aspect of the FE model. The current study involves two materials – high density polyethelene (HDPE) pipe and sand. The HDPE is modelled as an elasto-plastic material. von-Mises yield criterion is adopted. The adopted stress-strain curve based on [145], considering a typical laboratory strain rate and ambient temperature of $21°C$ is shown in Figure 3.6.

3.3.4 Soil-pipe interaction modelling

Contact modelling is crucial to simulate the interaction between the soil and the pipeline in an appropriate manner. Contact between pipeline and soil introduce severe non-linearity in 3D soil-pipeline interaction problems. Pipeline outer surface and soil surface surrounding the pipe are defined as separate surfaces namely the "master" and "slave" surface for "surface to surface" contact definition. ABAQUS/Standard takes into consideration the shape of both the surfaces while defining contact using "surface to surface" contact discretization by forming equations in an average sense over regions adjacent to "slave" surface nodes. A realistic tangential friction coefficient of 0.3 is adopted for contact in the tangential direction between the surfaces. Although in reality, friction can be varying, to keep the analy-

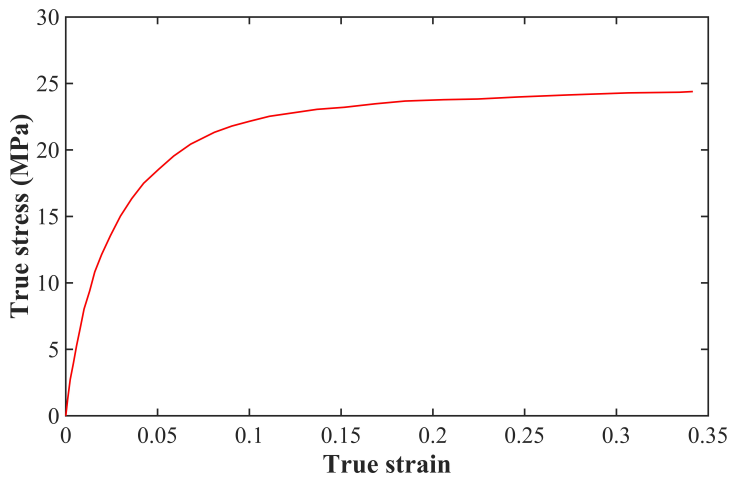

Figure 3.6: Poly ethylene stress strain curve

sis simple, a constant friction has been assumed. A "hard" contact using ABAQUS/Standard non-linear "penalty" method is adopted for contact in the normal direction between the surfaces. The non-linear "penalty" method approximates a "hard" normal contact with a nonlinear pressure-overclosure relationship between the two surfaces.

3.3.5 Solution procedure

ABAQUS/Standard with implicit formulation is used for all analyses. In ABAQUS/Standard, the solution for a non-linear problem is found by applying the specified loads gradually and incrementally towards a final solution. The process involves discretizing the analysis into numerous small load increments and obtaining equilibrium at the end of each load increment. Generally, it takes numerous iterations to determine acceptable solution to a given load increment. Hence, ABAQUS/Standard consumes significant amount of time, memory, storage and in some cases, has convergence problems in reaching the ultimate solution [140]. The Newton-Raphson method is used to solve the non-linear equilibrium equations. Displacement controlled solution strategy has been used. The desired displacement is applied as a smooth step at the boundary surfaces of the moving soil block excepting the top surface as well as the pipe end of the moving side. Axial strains along the pipe are noted for varying fault displacements at specific locations similar to what has been reported from experiments and are in turn

compared.

3.4 Results and discussion

In this section, the performance of the adopted material model and the developed FE model are presented to evaluate the accuracy of the proposed approach. For both the cases, results obtained have been compared with experimental results available in the literature. Moreover, comparison with other FE based work available in the literature have also been presented so as to evaluate the superiority of the proposed models.

3.4.1 Evaluation of material model

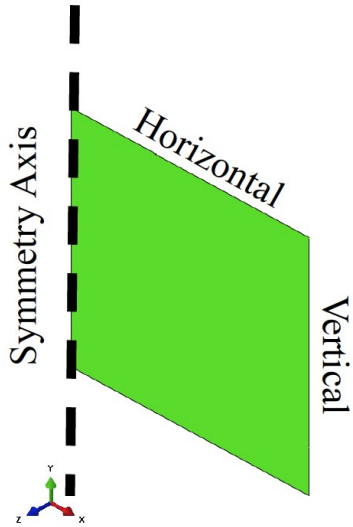

Figure 3.7: Triaxial test single axis-symmetric element

To simulate triaxial test, axisymmetric element (ABAQUS element CAX8R) is employed as shown in Figure 3.7. Based on sensitivity analysis, it is observed that the aspect ratio of the discretized element has almost no effect on the response. The optimal mesh size is found to be 100 mm. Figure 3.8 and Figure 3.9 show the variation of deviatoric stress to mean effective stress ratio with axial strains. Results obtained using triaxial test and other FE

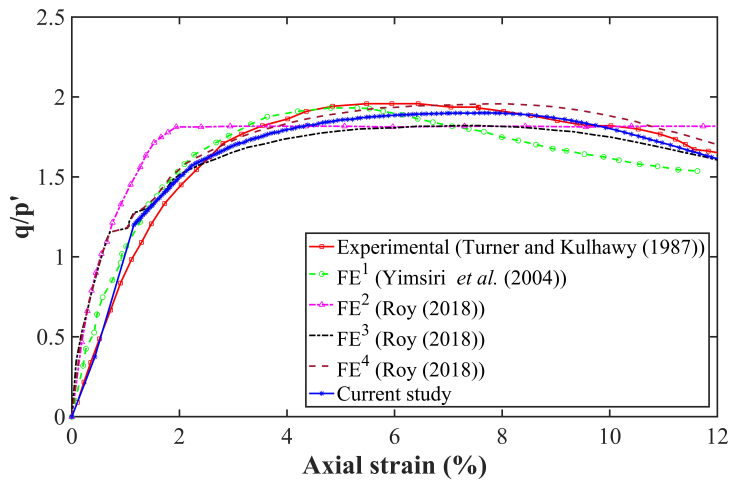

Figure 3.8: Evaluation of material model considered in this study

based models are also reported. The test performed is for a confining pressure of 39 kPa with a relative density of 80 percent. It is observed that the material model used in this study closely matches with the triaxial test results reported in [146]. To evaluate the accuracy of the current FE model, a comparison of root mean-square errors (RMSE) between FE results and experimental results are performed. Root mean-square error is calculated as

$$RMSE = \sqrt{\frac{1}{n}\sum(a_i - b_i)^2} \tag{3.12}$$

where, a_i is the FE analysis result data point and b_i is the corresponding experimental result data point. n indicates the number of data-points. RMSE of FE4 model from [68] is found to be 0.0392. RMSE from the current FE model is found to be 0.0036. Finally, the effect of relative density (RD) on the stress-strain behavior is shown in Figure 3.9. RD of 80 percent, 90 percent and 100 percent have been considered. An increase in RD results in a reduced peak strength.

3.4.2 Evaluation of full-scale FE model

Having evaluated the material model, we now focus on the evaluation of the full-scale FE model. A FE model to closely represent the Cornell University large scale test specimen is created. The geometry of the pipeline

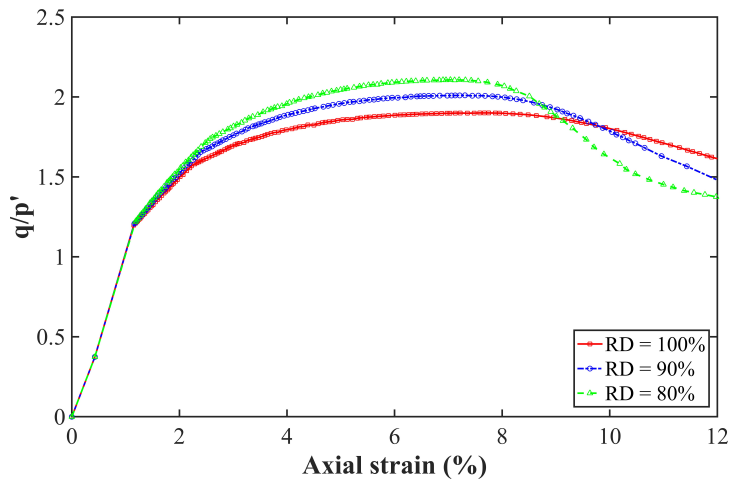

Figure 3.9: Effect of relative density on the stress strain behavior of sand

cross-section considered for this test had an outside diameter of 400.5 mm with a wall thickness of 24 mm. The displacement offset considered is 1.22 m for this test. The objective is to ensure the capability of the developed FE model to accurately simulate soil-pipe interaction mechanism and the generated pipeline strains from the large-scale experimental test. For the purpose of evaluation of the developed FE model two large scale tests from Cornell University are considered – HDPE pipe undergoing strike-slip fault rupture at a crossing angle of 65° with the fault plane under compression and tension. For sand, a ϕ'_{in} of 29° is used for this analysis similar to the triaxial test based on recommendations by [56] for typical contributions from different factors towards mobilized friction angle. A plane strain friction angle at peak direct shear strength of 43° and a plane strain cohesion of 1.2 kPa is reported by [40] for the experimental tests. [139] reported a plane strain critical state friction angle for RMS graded sand of $41° \pm 2°$. [139] presents a detailed account of direct shear strength and dilation characteristics of RMS graded sand.

In this analysis, the plane strain peak friction angle $\phi_p'^{PS}$ and plane strain critical friction angle $\phi_c'^{PS}$ are converted to triaxial peak friction angle $\phi_p'^{TX}$ and triaxial critical friction angle $\phi_c'^{TX}$ using suitable correlations. Using the set of experimentally determined constitutive equations by [61], a relative density index IR of 0.4 is obtained using A_ψ of 5.0 [61] for plane strain conditions. Based on experimental study by [147], triaxial critical state fric-

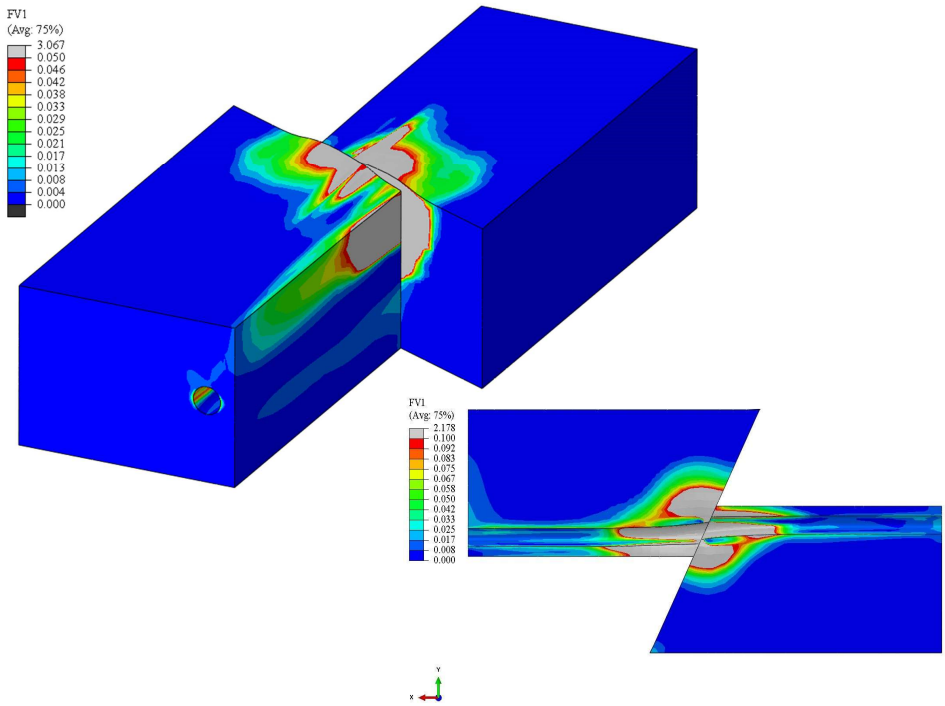

Figure 3.10: Failure plane computed using the proposed FE model

tion angle $\phi_c^{'TX}$ is considered to be about 4° smaller than the plane strain critical state friction angle $\phi_c^{'PS}$ equaling 37°. This observation is supported by other studies, such as that by [148–150]. Using equation by [61], IR of 0.4 is used to obtain the peak triaxial friction angle $\phi_P^{'TX}$ of 38.2°. A peak dilation angle of 2.4° is estimated using expression in [61]. This value is found to be consistent with peak dilation angle reported in [139] corresponding to a dry density of 15.5-15.8 kN/m3. Figure 3.10 to Figure 3.15 show the results obtained from the proposed FE model. It is observed that the FE model is able to closely predict the failure plane in the soil as shown in Figure 3.10, when compared with experimental observations in [40]. Figure 3.11 shows soil failure plane extending from pipe to the surface under a combination of axial and lateral displacement applied during the tensile faulting test. Lateral interaction between the pipe and soil being primarily concentrated at the fault, failure planes are more prominent close to the fault. Peak plastic shear strain can be located in Figure 3.11 (c) due to

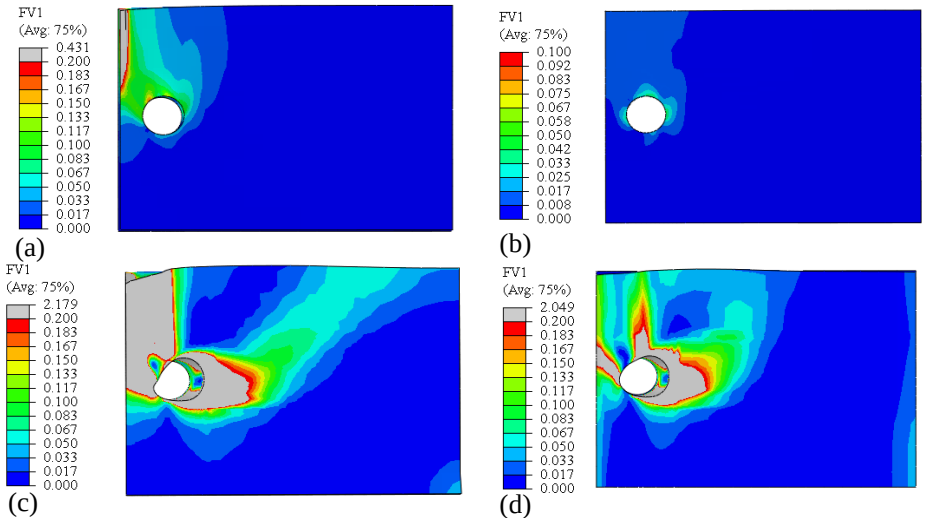

Figure 3.11: Plastic shear strain (FV1) at different locations under 300 mm displacement – (a) 2 m from fault plane on the moving soil mass (b) 2 m from fault plane on the stationary soil mass (c) vicinity of the fault plane on moving soil mass, and (d) vicinity of the fault plane on static soil mass.

the interaction between the deforming side of the pipe and the lateral soil boundary. Pipe cross-sectional east springline strain comparisons from the experimental tensile test with that of the FE analysis are presented in Figure 3.12. A close match is observed between experimental and FE analysis results. To illustrate the superior performance of the proposed approach, the RMSE between the results obtained using the FE models and the experimental results is computed. Under 300 mm displacement, RMSE for the proposed FE model is 0.0017. RMSE for the 'coupled' model and 'interface' model are found to be 0.0031 and 0.0035 respectively. Under 600 mm and 900 mm displacements as well, the proposed approach is found to predict a close match. Summary of the current FE analysis result error calculations and error calculations from other FE analysis results from literature for the experimental tensile test are shown in Table 3.1. Summary of mesh sensitivity on the peak tensile strains generated for the experimental tensile test FE analysis are presented in Table 3.2. A pipe mesh of 25 mm is selected for analyses.

Pipe axial strain comparisons from the compressive test case with that

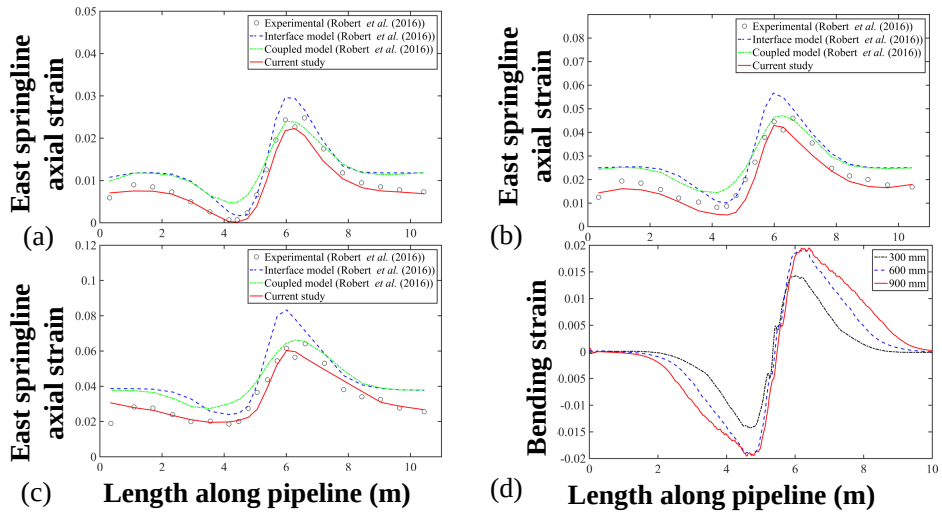

Figure 3.12: Strain profile (tensile) under a displacement of (a) 300 mm, (b) 600 mm and (c) 900 mm obtained using current study, interface model, coupled model and full-scale experimental test [1] (d) Bending strain profile from current FE analysis.

of the FE analysis are presented in Figure 3.13. Axial strains are obtained as the average of springline strains in accordance with [2]. A good match is observed between experimental results and FEA. Comparison of strain plots between current study, experimental data and beam element model by [2] are presented. Similar to the tensile case, RMSE has also been computed. Under 300 mm displacement, RMSE for current study and the beam element method are found to be 0.3766 and 0.5528, respectively. Under 600 mm displacement, RMS error for the current study is 0.5018 and RMS error for beam element model by [2] is 0.6537.

It is observed that this analysis results are not significantly better than

Table 3.1: Performance of the proposed approach in predicting the east spring line axial strain (under tension) under displacements 300 mm, 600 mm and 900 mm

Methods	Interface Model			Coupled Model			Current Study		
	0.3 m	0.6 m	0.9 m	0.3 m	0.6 m	0.9 m	0.3 m	0.6 m	0.9 m
RMSE (10E-3)	3.5	7.6	12	3.1	5.9	9.4	1.7	4.1	4.4

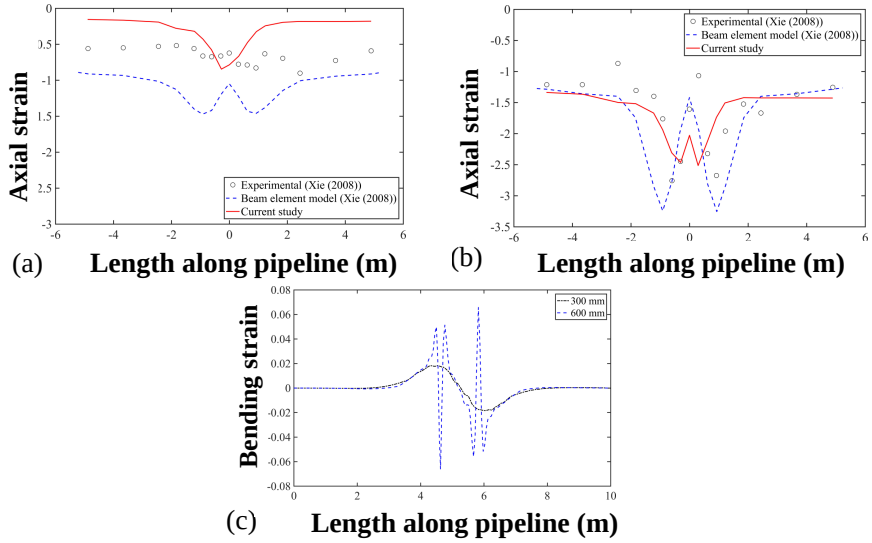

Figure 3.13: Strain profile (under compression) with a displacement of (a) 300 mm and (b) 600 mm obtained using the proposed approach, beam-element model and full-scale experimental test [2] (c) Bending strain profile from current FE analysis.

the beam on springs analyses by [2]. Detailed description of the compressive test along with its actual experimental configurations are not available in literature. It is suspected that the difference in the experimental test configuration with that of the numerical model may have contributed to not so good match between the results, or a better prediction compared to beam on spring analyses by [2].

Figure 3.14 compares the deformed shape of the pipe at varying displacements for both the compressive and tensile large-scale tests. Figure 3.15 compares the axial strain of the pipe at varying displacements for both the compressive and tensile large-scale tests. Pipe under compression failed due to initiation of local buckle as evident from axial strain plots in Figure 3.13 whereas pipe under tension failed due to tensile rupture. Initiation of local buckle resulted in an undulated axial strain profile at the center of the pipeline as can be seen in Figure 3.13.

Table 3.2: Peak tensile strains for varying mesh sizes of the pipeline for displacements 300 mm, 600 mm and 900 mm

Mesh size	15 mm			25 mm		
Fault displacement	0.3 m	0.6 m	0.9 m	0.3 m	0.6 m	0.9 m
Strain (%)	3.8	6.2	7.8	3.8	6.2	7.8
Mesh size	45 mm			75 mm		
Fault displacement	0.3 m	0.6 m	0.9 m	0.3 m	0.6 m	0.9 m
Strain (%)	3.7	6.0	7.8	3.5	5.9	-

3.5 Summary

In this study, we have developed a nonlinear three-dimensional FE model for studying structural performance of buried pipeline undergoing fault rupture displacements in sand. For modelling the constitutive relation of sand, a modified Mohr-Coulomb criterion is adopted which results in a nonlinear variation of the sand shear strength with variation in plastic shear strain. The non-linear variation in shear strength is characterized by initial linear zone, pre-peak strain-hardening and post-peak strain-softening. A USDFLD based user-subroutine is developed to include the same within ABAQUS. The adopted material model is evaluated with available experimental triaxial test results. This material model is thereafter suitably calibrated for a large-scale test based on direct shear soil test data for that experiment. Thereafter, a detailed FE model with material and geometric nonlinearity for a pipeline undergoing fault rupture displacements incorporating this new sand constitutive relation has been developed. The developed FE model is then used to simulate the full-scale test carried out at Cornell University. Results obtained using the developed FE model has been evaluated against experimental results available in the literature. In order to evaluate the performance of the developed FE model to predict pipeline strains in comparison to those already available in the literature, comparative studies have been carried out. Proposed approach is found to yield superior result than the FE models which do not consider non-linear sand constitutive relation. This indicates that the analysis methodology presented here is relevant to perform detailed FE analyses of critical fault crossings involving major energy transmission pipelines. The key findings of the study are as follows:

(1) The nonlinear material model adopted for sand successfully provided a good match with triaxial test results for sand specimen. RMSE from the current FE model is found to be 0.0036 in comparison to 0.0392 from [68].

(2) The non-linear material model adopted for sand is found to have minimal dependence on mesh size and aspect ratio of the elements. Non-linear material model FE predictions show relatively better match with respect to available numerical results in the literature.

(3) The non-linear FE model developed is found to provide good correlation with experimental results for large-scale tests. RMSE calculated for evaluation of Cornell University pipeline-fault rupture large scale "tensile" and "compressive" experiments with that of the developed FE model predictions showed errors are consistently lower than available numerical results in the literature for varying fault displacement magnitudes. At 300 mm displacement for the large-scale tensile test, an RMSE of 0.0017 is achieved in comparison to previous 0.0031 and 0.0035 for the 'coupled' and 'interface' model by [RSO16]. At 600 mm displacement for the large-scale tensile test, an RMSE of 0.0041 is achieved in comparison to previous 0.0059 and 0.0076 for the 'coupled' and 'interface' model by [RSO16]. At 900 mm displacement for the large-scale tensile test, an RMSE of 0.0044 is achieved in comparison to previous 0.0094 and 0.012 for the 'coupled' and 'interface' model by [RSO16]. At 300 mm displacement for the large-scale compressive test, RMSE for current study and the beam element method [2] are found to be 0.3766 and 0.5528, respectively. At 600 mm displacement for the large-scale compressive test, RMS error for the current study is 0.5018 and RMS error for beam element model by [2] is 0.6537. Additionally, failure patterns in the FE analysis predictions are found to closely match experimental observations.

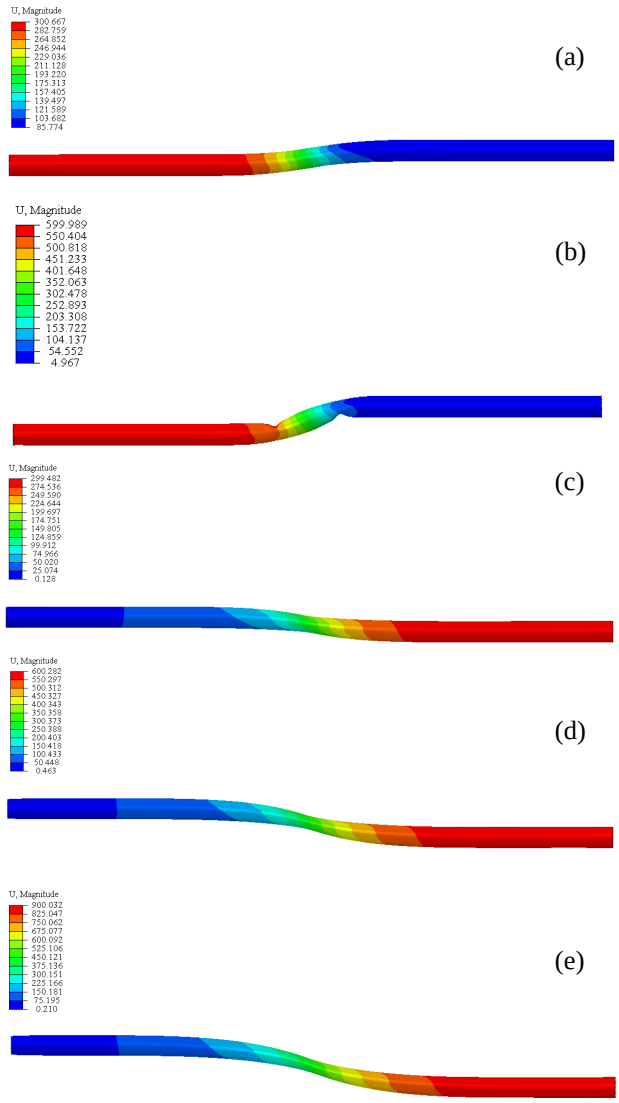

Figure 3.14: Deformation of the pipe under compression and tension at a displacement of (a) 300 mm (compression), (b) 600 mm (compression), (c) 300 mm (tension), (d) 600 mm (tension), (e) 900 mm (tension).

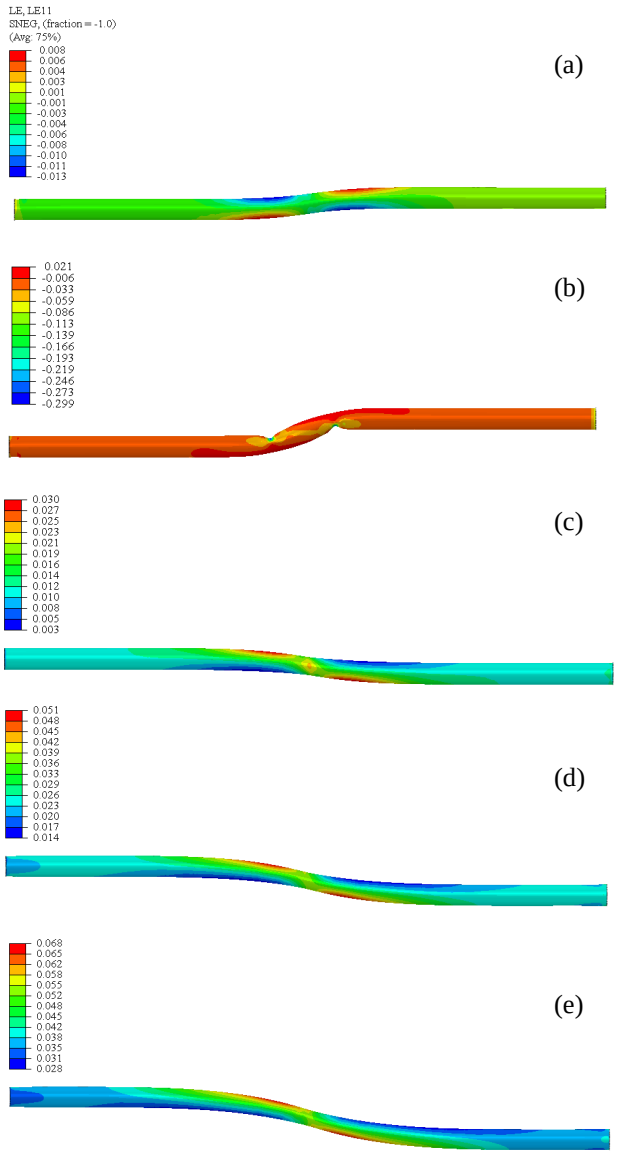

Figure 3.15: Axial strain of the pipe under compression and tension at a displacement of (a) 300 mm (compression), (b) 600 mm (compression), (c) 300 mm (tension), (d) 600 mm (tension), (e) 900 mm (tension).

Chapter 4

Multi-fidelity approach for Uncertainty Quantification of Buried Pipeline Response undergoing Fault Rupture Displacements in Sand

4.1 Introduction

A new efficient approach for uncertainty quantification of pipeline structural response undergoing reverse-slip fault rupture displacements in sand is presented using multi-fidelity Gaussian processes. Uncertainty quantification problems generally take large numbers of scenarios to be analyzed considering variations in the influencing parameters. Analysing large numbers of computationally expensive detailed geo-technical numerical models is practically not feasible. Hence, a multi-fidelity approach employing Gaussian processes is proposed to tackle this problem which combines the accuracy of a relatively few number of detailed geo-technical numerical models and the efficiency of large numbers of simplified numerical models to track the uncertainty response. The detailed model utilizes a previously evaluated pipe-soil FE model including a non-linear sand constitutive model implemented in FE software ABAQUS. The simplified model utilizes beam element pipe and bilinear soil springs. The multi-fidelity model is first trained using data from HF and LF model analyses, thereafter cross-evaluated and subsequently used to quantify uncertainty in the peak compressive strains generated and to identify the most sensitive input variables. Finally, fragility curves are derived for a site specific pipe-soil fault rupture problem.

4.2 Problem Statement

The objective of this research is to propose a solution to uncertainty quantification of detailed and complex geo-technical problems, maintaining the complexity of the numerical models capable of defining the true nature of those problems. As a demonstration, the case of a buried continuous pipeline undergoing fault rupture deformations is explored. A detailed geometrically and materially nonlinear FE model, including a nonlinear sand constitutive model implemented into it is used for this purpose.

A number of input factors are varied for the uncertainty quantification analysis. Input parameters that are varied for these analyses include outer diameter of the pipe, wall thickness of the pipe, Young's modulus of the pipe steel, yield strength of the steel, pipeline-fault crossing angle, peak friction angle calculated from the confining pressure and relative density using the adopted constitutive relations, operating temperature in the pipeline and operating pressure in the pipeline. A mean outer diameter of 609.6 mm is considered with lower and upper bounds of 600 mm and 620 mm with a coefficient of variation of 0.05. A mean pipe wall thickness of 9.52 mm is considered with lower and upper bounds of 8.57 mm and 10.47 mm, respectively with a coefficient of variation of 0.05. A truncated Gaussian distribution is adopted for both these parameters [151]. The Young's modulus mean is considered to be 207,000 MPa with lower and upper bounds to be 82,000 MPa and 331,200 MPa respectively with a coefficient of variation of 0.15. The range considered for Young's modulus is quite broad. However, since a probability distribution is considered, bulk of the data is centered in the proximity of 207,000 MPa. The yield strength mean is considered to be 414 MPa with lower and upper bounds to be 289.8 MPa and 540 MPa respectively with a coefficient of variation of 0.075. The ultimate strength mean is considered to be 517 MPa with lower and upper bounds to be 310 MPa and 725 MPa with a coefficient of variation of 0.1. A lognormal distribution is adopted for all three steel material parameters [152].

Soil confining pressure is assumed to be at a mean of 39 kPa varying from a minimum of 7.8 kPa to a maximum of 70 kPa with a coefficient of variation of 0.2 and a lognormal distribution. Relative density of the soil is assumed to be at a mean of 80 percent with a coefficient of variation of 0.025 ranging from a minimum of 55 percent to a maximum of 95 percent with a lognormal distribution. Operating temperature and pressure in the pipeline depend on the state of the pipe, if it is under operation or not. Hence, bi-modal distribution using a mixture of gaussian has been used [153]. Minimum and maximum temperature considered are $0°C$ and $56.5°C$.

Minimum and maximum pressure considered are 100 kPa and 10.35 MPa respectively. Operating mean value has been assumed as 7 MPa.

4.2.1 High-fidelity FE model

As mentioned previously, [1, 34, 41, 43, 44, 48–50, 52–55] had employed 3D soil continuum model to study the problem. [1, 53, 55] had considered linear variation of soil strength and dilatancy with varying plastic deviatoric strain in their analyses. [68] employed non-linear variation of soil strength as a relation to plastic shear strains to study 2D pipeline-soil interaction problems. The authors [154] incorporated soil constitutive model with pre-peak hardening and post-peak softening behavior in the soil model to study the structural performance of pipelines under fault movement loads using a 3D continuum soil approach. The HF model adopted here is created following the experimentally evaluated pipeline-fault model developed in [154]. The FE model created here however, considers different geometric configurations and material properties for soil as well as pipe in view of the uncertainties associated with these parameters. The model length is considered to be 100 m as shown in Figure 4.1.

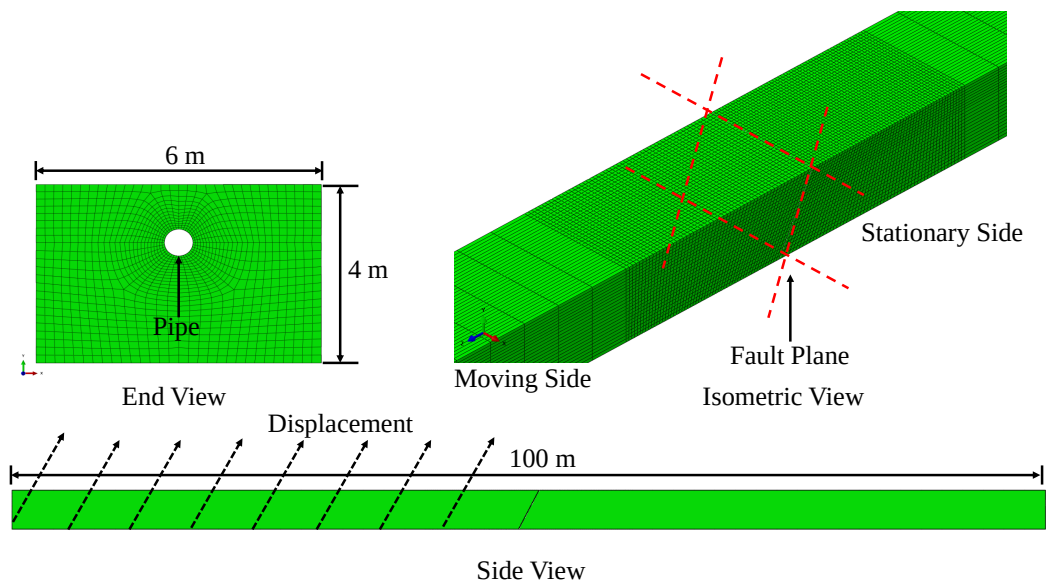

Figure 4.1: HF finite element model mesh

The FE model is created using general purpose FE analysis software

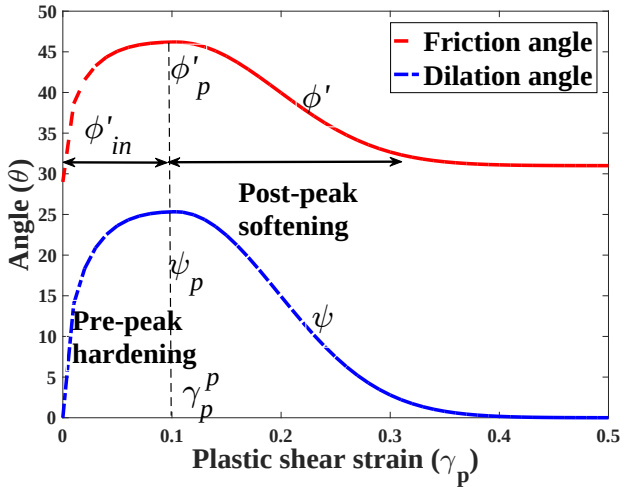

Figure 4.2: Non-linear soil constitutive relation

ABAQUS [140]. The pipeline steel is modelled using elastic-plastic behavior with yield criterion defined by von-Mises theory. The adopted stress-strain relation is defined according to Ramberg-Osgood relation [22]. For sand, the yield criterion based on Mohr-Coulomb theory is considered. Figure 4.1 shows the FE model mesh. Table 4.1 shows the effect of mesh size variation towards the generated strains for the HF models.

Salient characteristics of the mobilized soil strength for sand are its peak shear strength, stiffness in the initial elastic zone, strain hardening in the pre peak strength zone and strain softening in the post peak strength zone. This relation of sand is defined by the relative density and confining pressure of the sand. A typical non-linear sand material constitutive relation is shown in Figure 4.2. $\phi_{in}^{'}$ is the initial friction angle and $\phi_{p}^{'}$ is the peak friction angle. ψ_p is the peak dilation angle. γ_p^p is the plastic shear strain at which the peak strength is reached. Figure 4.3, Figure 4.4 and Figure 4.5 presents nonlinear mobilized friction angle curves and nonlinear mobilized dilation angle curves adopted for the 30 HF analyses. Literature review suggests the presence of a number of constitutive relations to define this behavior [57–67]. In terms of stress space, the mobilized strength behavior of sand can be grossly classified as the elastic region at low strains within the initial yield surface, pre peak strength plastic zone defining the stress space from

Table 4.1: Compressive strain percent generated for HF model analysis 1-3 for varying fault displacement and mesh size

Serial Number	Mesh Size (mm)	Analysis Number	Fault Displacement (mm)			
			25	100	200	300
1	50	1	0.0123	0.0923	0.2306	0.3855
2		2	0.0042	0.0636	0.1382	0.3640
3		3	0.0082	0.0723	0.1640	0.2443
4	75	1	0.0123	0.0923	0.2306	0.3855
5		2	0.0042	0.0636	0.1382	0.3640
6		3	0.0082	0.0723	0.1640	0.2443
7	100	1	0.0138	0.1061	0.2721	0.4240
8		2	0.0048	0.0776	0.1741	0.4331
9		3	0.0096	0.0846	0.1887	0.2858
10	200	1	0.0159	0.1144	0.2951	0.4934
11		2	0.0051	0.0788	0.1755	0.4695
12		3	0.0100	0.0919	0.2067	0.3004

initial yield surface to the surface at failure and the post peak strength strain softening plastic zone defining the space from failure surface to critical state [56, 58].

Soil material models with Mohr-Coulomb yield criterion are extensively used in geo-technical engineering problems [155–159]. The soil material model in ABAQUS based on Mohr-Coulomb theory is upgraded to enable it to simulate the true nature of the sand behaviour in compliance with the constitutive relations discussed above. An user subroutine USDFLD is used to implement this behaviour.

4.2.2 Low-Fidelity FE model

The objective of utilizing a LF model is to arrive at approximate results using limited computational resources. LF models use simplified material models, formulations and geometry of the actual problem. However, the material properties, geometrical dimensions and loads in both the HF and LF models are same for a given case. A beam element FE model [17, 34, 45, 46] is adopted as the simplified model to simulate the pipeline response under going fault displacement using ABAQUS/Standard analysis software. Two types of elements are used to prepare the model. The pipe itself is modelled using PIPE32 elements which employ Timoshenko beam formulation allowing for both shear and bending deformation. These elements are 3 node quadratic beam elements. The elements representing mutually perpendicular soil springs supporting the pipelines are modelled using PSI34

(three-dimensional pipe-soil interaction elements). These elements allow for bi-linear elastic perfectly plastic stiffness definition in the axial, lateral and vertical directions. One end of these springs are connected to the pipeline and the other end are connected to the ground. The intended fault displacements are applied in the moving side of the fault at the soil spring nodes representing ground. Fault displacements are also applied on the pipe end on the moving side. The intended resultant fault displacement is converted to axial, lateral and vertical components and applied to the axial, lateral and vertical springs respectively. Soil spring nodes representing ground on the stationary side and the pipe end on the stationary side are kept restrained. The complete model consisted of 400 elements with nominal element length of 0.5 m. Based on a mesh sensitivity study, the element length is found to yield satisfactory results where, no difference in results are noticed with further decrease in mesh size. The length of the pipeline section in the model is considered to be 100 m. The steel pipeline material is modelled with a bi-linear elastic-perfectly plastic stress-strain relation. The von-Mises yield criterion is used to define the steel material properties. Elastic perfectly plastic relations are utilized for the steel. Various yield strength values are used based on the distributions as discussed in section 4.2. Static analyses are performed to analyze this problem. Figure 4.6 shows 1D schematic diagram of the LF pipe-soil model.

Soil springs are calculated using the fundamental soil properties based on [4] guidelines. For all analyses, drained soil properties are assumed. Since, cohesionless soil, such as sand can drain water readily, drained soil properties are used for this study. To derive the drained soil properties, undrained shear strength value is not used in the prescribed equations by [4]. Peak effective friction angle is used instead to obtain the peak forces.

For axial soil springs, coefficient of pressure at rest is obtained based on the internal friction angle. Maximum force values in the axial direction are calculated based on pipe diameter, depth to pipe centerline, co-efficient of pressure at rest and interface angle of friction for pipe and soil as shown in (Equation 4.1):

$$T_U = \pi D \omega c + \pi D H \bar{\gamma} \frac{(1 + K_0)}{2} tan\delta \tag{4.1}$$

where D is pipe outside diameter, c soil cohesion representative of the soil back fill, H is the depth to pipeline center line, $\bar{\gamma}$ is effective unit weight of soil, K_0 is coefficient of pressure at rest, ω is adhesion factor, δ is interface angle of friction for pipe-soil.

For lateral springs, maximum force values are calculated based on inter-

nal friction angle of soil, pipe diameter, depth to pipe centerline and effective unit weight of soil as shown in (Equation 4.2):

$$P_u = N_{ch}cD + N_{qh}\bar{\gamma}HD \tag{4.2}$$

where N_{ch} is horizontal bearing capacity factor for clay, N_{qh} is horizontal bearing capacity factor for sand.

For vertical uplift springs, maximum force values are obtained using internal friction angle of soil, depth to pipe centerline, pipe diameter, effective unit weight of soil as shown in (Equation 4.3):

$$Q_u = N_{cv}cD + N_{qv}\bar{\gamma}HD \tag{4.3}$$

where N_{cv} is vertical uplift factor for clay, N_{qv} is vertical uplift factor for sand.

For vertical downward springs, maximum force values are obtained based on internal friction angle of soil, depth to pipe centerline, pipe diameter, total unit weight of soil as shown in (Equation 4.4):

$$Q_d = N_c cD + N_q\bar{\gamma}HD + N_\gamma\gamma\frac{D^2}{2} \tag{4.4}$$

where N_c, N_q and N_γ are bearing capacity factors and γ is total unit weight of soil.

4.3 Uncertainty quantification using multi-fidelity surrogate

One of the primary challenges in uncertainty quantification in buried pipelines is scarcity of data. Simulating the buried pipeline response undergoing fault rupture deformations using HF FE method is quite expensive from a computational resource point of view. As a result, one can only afford to run the simulator a limited number of times. An alternative is to resort to LF simulators however, this will result in a loss of accuracy. In this work, we propose to use multi-fidelity Gaussian process (MF-GP) for uncertainty quantification of buried pipeline undergoing reverse-slip fault rupture in sand. MF-GP combines data generated from a HF simulator with data generated from a LF simulator. This enables it to learn from very few (in the order of tens) HF data. In this section, we first provide a brief description of MF-GP followed by its use in uncertainty quantification.

4.3.1 Multi-fidelity Gaussian process

MF-GP is a type of Gaussian process (GP) where one uses LF and HF data by using a autoregressive scheme [160]:

$$Z_e\left(x\right) = \rho Z_c\left(x\right) + Z_d\left(x\right), \tag{4.5}$$

where Z_e is the MF-GP model also representing the HF model, Z_c is a GP representing the LF model, Z_d is a GP representing the difference model $Z_e - \rho Z_c$ and, in this setting, ρ is a scaling factor. The MF-GP model Z_e can be developed in two steps [161]. The first step involves training the GP model Z_c with respect to the LF training data (X_c, Z_c), which consists of tuning the Z_c hyper-parameters through maximization of the log-likelihood function. The second step involves training the Z_d GP model with respect to the difference training data $(X_e - \rho X_c, Z_e - \rho Z_c)$, by simultaneously optimizing the corresponding Z_d model hyper-parameters and the ρ constant, again using log-likelihood maximization (see [161] for details). Each one of the GP models Z_c and Z_d consists of a mean function and a correlation function. If it is assumed herein that the same form of mean functions $f(x)$ are considered for models Z_c and Z_d. The MF-GP best linear unbiased estimator $\widehat{Z}_e$ is then given as:

$$\widehat{Z}_e(x) = h(x)^T\widehat{b} + v(x)^T\mathbf{V}^{-1}\left(Y - \mathbf{H}\widehat{b}\right), \tag{4.6}$$

where $Y = \left[{Y_c}^T, {Y_e}^T\right]^T$, $h(x) = \left[\rho f(x)^T, f(x)^T\right]^T$, $\widehat{b} = \left(\mathbf{H}^T\mathbf{V}^{-1}\mathbf{H}\right)^{-1}\mathbf{H}^T\mathbf{V}^{-1}Y$, and $v(x)$ is computed as:

$$v(x) = \begin{bmatrix} \rho\xi_c^2 r_c(x, x_c) \\ \rho^2\xi_c^2 r_c(x, x_e) + \xi_d^2 r_d(x, x_e) \end{bmatrix}, \tag{4.7}$$

the $\mathbf{H}$ matrix is given as:

$$\mathbf{H} = \begin{bmatrix} f\left(x_1^c\right)^T & 0 \\ \vdots & \vdots \\ f\left(x_{n_c}^c\right)^T & 0 \\ \rho f\left(x_1^e\right)^T & f\left(x_1^e\right)^T \\ \vdots & \vdots \\ \rho f\left(x_{n_e}^e\right)^T & f\left(x_{n_e}^e\right)^T \end{bmatrix}, \tag{4.8}$$

and the covariance matrix $\mathbf{V}$ takes the form,

$$\mathbf{V} = \begin{bmatrix} \xi_c^2\mathbf{R}_c\left(X_c, X_c\right) & \rho\xi_c^2\mathbf{R}_c\left(X_c, X_e\right) \\ \rho\xi_c^2\mathbf{R}_c\left(X_e, X_c\right) & \rho^2\xi_c^2\mathbf{R}_c\left(X_e, X_e\right) + \xi_d^2\mathbf{R}_d\left(X_e, X_e\right) \end{bmatrix}. \tag{4.9}$$

Correlation matrices $\mathbf{R}_c$ and $\mathbf{R}_e$ in Equation 4.9 are defined in a similar way as for an ordinary GP model, with the difference that there are now two of them, corresponding to models Z_c and Z_d, respectively. The same hold for correlation vectors r_c and r_e in Equation 4.7. For further details on GP and how correlation matrices are defined in GP, interested readers may refer to [162, 163].

The kernel function to define the correlation between the random variables is given as Equation 4.10:

$$cor[Y(x^i), Y(x^l)] = exp(\sum_{j=1}^{k} \theta_j |x_j^i - x_j^l|^{p_j}) \tag{4.10}$$

In this study constant terms are selected as mean functions of the two GP models, denoted as μ_c and μ_d for models Z_c and Z_d, respectively. With this, the MF-GP estimator (Equation 4.6) is now written as:

$$\widehat{Z}_e(x) = \widehat{b} + v(x)^T \mathbf{V}^{-1} \left(Y - \mathbf{1}\widehat{b} \right), \tag{4.11}$$

where $\widehat{b} = \left(\mathbf{1}^T \mathbf{V}^{-1} 1\right)^{-1} \mathbf{1}^T \mathbf{V}^{-1} Y$ and $\mathbf{H} = 1$, a vector of ones. Additionally, the prediction variance at x is [161]:

$$\widehat{\xi}_e^2(x) = \widehat{\rho}^2 \widehat{\xi}_c^2 + \widehat{\xi}_d^2 - v(x)^T \mathbf{V}^{-1} v(x). \tag{4.12}$$

One of the important challenges with ML algorithms is its extrapolation capability. MF-GP being a Bayesian ML algorithm addresses extrapolation problems based on priors. In this work, we have used GP priors.

4.3.2 Uncertainty quantification using MF-GP

The uncertainty in the pipeline response is a function of all the variabilities in the input parameters, such as fault-pipe crossing angle, soil properties etc. A total of 30 HF and 500 LF models are analyzed. The number of HF and LF models are selected based on trial and error to achieve a high coefficient of determination with minimal computational effort. Table 4.3 presents the improvement in coefficient of determination of MF-GP model trained with increasing number of HF models. Input parameters are randomly selected from uniform probability distributions of the upper and lower bound ranges for the numerical analyses inputs. Data (peak compressive strains) generated from the numerical analyses are fed to train the multi-fidelity surrogate model. Subsequently, the surrogate model is used to predict peak compressive strains for a separate set of prediction data

where the input parameter values are randomly selected from corresponding predefined probability distributions of the input parameters as discussed in section 4.2. Figure 4.7 shows the MF-GP uncertainty quantification process through a flowchart.

The vulnerability of a structure can be expressed as a cumulative probability of it reaching a failure limit state as a function of the load intensity it is subjected to. Generally, a fragility function is used for this purpose and assumes the shape of a log-normal function. The cumulative lognormal function is adopted in accordance with [164] as shown below in (Equation 4.13):

$$P\left(di|IM = x\right) = \upsilon\left(\frac{ln(\frac{x}{\theta})}{\lambda}\right) \tag{4.13}$$

wherein, the probability that a structure will be at a failure state (di) caused by a load intensity $IM = x$, is $P\left(di|IM = x\right)$; υ denotes the standard normal cumulative distribution function; θ is the load intensity level denoting a failure probability of 50 percent; λ signifies the standard deviation for $ln(IM)$. Initially, realistic values for the parameters defining the fragility equation are assumed. The parameters are finally obtained by maximizing the logarithm of the likelihood function as shown below (Equation 4.14) :

$$\left\{\hat{\theta}, \hat{\lambda}\right\} = argmax \sum_{j=1}^{m} \left\{ln\left(\frac{n_j}{z_j}\right) + z_j ln\phi\left(\frac{ln(\frac{x_j}{\theta})}{\lambda}\right) + \left(n_j - z_j\right) ln\left(1 - \phi\left(\frac{ln(\frac{x_j}{\theta})}{\lambda}\right)\right)\right\} \tag{4.14}$$

where, m is the number of load intensity levels. At each load intensity level $IM = x_j$, it is assumed that the structural analyses produce z_j failures out of n_j analyses. To derive the fragility curves, the multi-fidelity model is trained at incremental fault displacements and strains are predicted for the prediction data set. Number of failure instances are calculated for each fault displacement using [22] compressive strain limit criterion. The load intensity (fault displacement) vs probability of failure data points are thereafter used for generation of the fragility curves. The same procedure is repeated for models trained with only HF data points and only LF data points.

4.4 Results and discussion

Results presented include comparison of HF model vs LF model peak compressive strains generated with increasing fault displacements. Compressive strains are studied since the pipeline fails under compression due

Table 4.2: Coefficient of determination for surrogate models trained with only 30 HF models, only 500 LF models and combination of 30 HF and 500 LF multi-fidelity models

Serial Number	Fault Displacement (mm)	HF Model Results	LF Model Results	Multi-fidelity Model Results
1.	25	0.699	0.620	0.897
2.	100	0.604	0.576	0.944
3.	300	0.476	0.571	0.924

Table 4.3: Coefficient of determination for multi-fidelity models trained with varying number of HF models and constant 500 LF models

Serial Number	Fault Displacement (mm)	20 HF 500 LF	25 HF 500 LF	30 HF 500 LF
1.	25	0.759	0.885	0.897
2.	100	0.800	0.907	0.944
3.	300	0.696	0.911	0.924

to buckling under reverse fault rupture displacements. Additionally, results include cross-evaluations of the developed multi-fidelity model predictions with HF model predictions, sensitivity of the input parameters towards the generated peak compressive strains, probability distribution of the peak compressive strains at various fault displacement levels and development of pipeline fragility curves for this specific problem.

4.4.1 Cross-evaluation test

The peak compressive strain outputs obtained from the HF and LF FE analysis models at different fault displacements are used to train the multi-fidelity model. Figure 4.8 shows a representative stress plot of the HF FE model. Figure 4.9 to Figure 4.11 shows the comparison between HF and LF model peak generated compressive strains vs fault displacement values. Comparisons from a total of 30 analyses which are performed both for the HF and LF models are presented. The multi-fidelity models are cross-evaluated using the k-fold cross-evaluation technique. Using this technique, the HF data set are split into 'k' number of sections.

In the first step, the first section is used to test the model and the remaining sections are used to train the multi-fidelity model. In the second step, the second section is used to test the model and the remaining sections are used to train the multi-fidelity model. Likewise, this process is repeated for all the 'k'-sections. The multi-fidelity model test prediction data from the k-fold are then compared with the original HF model observations. The accuracy of the multi-fidelity model is then checked using the coefficient of determination (R-square). Figure 4.12, Figure 4.14 and

Figure 4.16 show excellent coefficient of determination of 0.897, 0.944 and 0.924 for cross-evaluation tests at fault displacements of 25 mm, 100 mm and 300 mm, respectively. Figure 4.13, Figure 4.15 and Figure 4.17 also show the cross evaluation attempts on only HF data trained surrogate model and only LF data trained surrogate model. Table 4.2 shows the comparison of coefficient of determination obtained from the multi-fidelity model, only HF data trained surrogate model and only LF data trained surrogate model. Table 4.3 shows the coefficient of determination for the MF-GP model with a fixed number of 500 LF model data and varying number of HF model data. It is observed that the coefficient of determination increases with the increase in number of HF model data. At 25 mm fault displacement, the MF-GP model bias error and variance are found to be 5.85E-6 and 2.15E-6 respectively. At 100 mm fault displacement, the MF-GP model bias error and variance are found to be 0.00036 and 2.42E-5 respectively. At 300 mm fault displacement, the MF-GP model bias error and variance are found to be 0.312 and 4.095 respectively.

As mentioned previously, the MF-GP model allowed the use LF models with its significantly less run time of 15 minutes in contrast to 48 hours of the HF models for 500 runs and still achieve high accuracy in comparison to the HF models as demonstrated in Table 4.2 coefficient of determination results.

4.4.2 Sensitivity analysis and generation of fragility curves

After the multi-fidelity model for pipeline crossing fault rupture to estimate peak compressive strains at certain fault displacement levels is evaluated, the model is used to predict peak compressive strains at those fault displacement levels. Suitable distributions of input parameters (10 parameters) as described previously are fed to the the multi-fidelity model to predict distribution of peak compressive strains.

The current study uses the Pearson's correlation coefficient for sensitivity analyses. Two of the most sensitive input parameters are identified as the pipe-fault angle and the sand confining pressure as shown in Figure 4.18 for 25 mm and 100 mm fault displacements. For 300 mm displacement as shown in Figure 4.18, the most sensitive parameter is however pipe outer diameter as larger diameter pipes are more prone to local buckle. Other input parameters which had their sensitivity within 10 percent include internal pressure, pipeline temperature, soil relative density, pipe steel ultimate strength, pipeline yield strength, steel yield strength, steel young's modulus and pipe wall thickness. Pipe outer diameter had a sensitivity of around 30 percent.

Since, the primary mode of failure in this problem is compressive buckling, the pipe-fault angle which governs the amount of compressive displacement is one of the most sensitive parameters. Similarly, the pipe outer diameter which greatly influences buckling is significantly sensitive here since, the primary mode of failure for this problem is buckling. Confining pressure has significant sensitivity due to its influence towards soil strength with which the soil loads the pipe. Positive sensitivity indicates that the quantity of interest, peak compressive strain increases with the increase in the parameter value. Negative sensitivity indicates that the quantity of interest, peak compressive strain decreases with the increase in the parameter value. In this regard, yield strength and young's modulus can be seen having negative sensitivity at lower displacements. However, their sensitivity changes to positive at higher displacements. At smaller displacements, higher young's modulus and yield strength leads to lower peak compressive strains due to higher resistance. However, at higher displacements as buckles starts to form, higher yield strength and young's modulus will result in higher forces feeding into the buckle, resulting in higher peak compressive strains.

Figure 4.19 - Figure 4.20 shows the variations of the predicted peak compressive strains with pipe-fault angle and sand confining pressure for different fault displacement values. At 25 mm fault displacement, fault rupture angle on the higher side showed no variation in compressive strains with the variation in sand confining pressure. However, for lower fault rupture angles, where the pipe is subjected to a higher degree of compressive loading, higher sand confining pressure resulted in higher compressive strains due to larger soil resistance. At 100 mm fault displacement, irrespective of the fault rupture angle, increase in sand confining pressure resulted in increased peak compressive strains, quite reasonably due to higher soil resistance. Compressive strains are noted to be increasing with lesser fault rupture angle which will impart more compression loading to the pipe in comparison to a larger fault rupture angle. At 300 mm fault displacement however, no specific trend is observed with respect to the above two parameters and is most likely due to the fact that at such high displacements, the pipe has undergone local buckling failure irrespective of the loading pattern and soil resistance. It is observed that with the increase in fault displacement the mean peak compressive strains increased and also the range of uncertainty increased. Figure 4.21 shows the probability distributions of the peak compressive strain predictions at 25 mm, 100 mm and 300 mm fault displacements.

Figure 4.22 shows the fragility curves derived for this specific problem which plots probability of pipeline failure as a function of fault displacement.

Results show that the fragility curve obtained using the MF-GP has a significantly different characteristic than the surrogate models which used only the HF model data and LF model data. The HF surrogate model showed higher failure probabilities at lower fault displacements (less than 350mm) in comparison to both the MF-GP and LF surrogate model. The LF surrogate model on the other hand showed significantly lower failure probabilities at lower fault displacements in comparison to the MF-GP and HF surrogate models. This is due to the fact that, the LF models in general predicted significantly lesser peak compressive strains than the corresponding HF ones. At higher fault displacements (350 mm and more) however the HF model predicted failure strains for lesser number of cases as a proportion of the total number of cases analyzed in comparison to the LF model, resulting in a smaller slope of the fragility curve post 350 mm fault displacement. Overall, it is observed that the multi-fidelity model reduces conservatism in the pipeline design in comparison to the HF surrogate model and at the same time captures the structural vulnerability of the pipeline which is not captured by the LF surrogate model.

4.5 Summary and future work

In this paper, a multi-fidelity approach employing Gaussian processes to study uncertainty in pipeline response subjected to fault displacement loads is developed. The multi-fidelity approach developed uses a previously developed and evaluated detailed pipe soil continuum model with a nonlinear soil constitutive model implemented into it, as the HF model. The multi-fidelity model uses a beam element pipe supported by bi-linear soil springs as the LF model. Important inputs in the analysis that may contribute to peak compressive strain uncertainty are identified. Numerical analyses of both the HF and LF models are performed to generate the training data for the multi-fidelity model. There after the evaluated multi-fidelity model is used to quantify uncertainty in the pipeline strains generated and develop fragility curves. Results obtained have been summarized accordingly.

The key findings of the study are as follows:

(1) Uncertainty quantification in a complex geo-technical engineering problem, such as pipeline undergoing fault rupture deformations can be studied efficiently employing multi-fidelity Gaussian processes.

(2) Excellent coefficient of determinations are achieved between HF observed values and multi-fidelity model predicted values during cross-evaluation of results, there by establishing the validity of the multi-fidelity model. Co-

efficient of determinations obtained for the multi-fidelity surrogate models for fault displacements of 25 mm, 100 mm and 300 mm are 0.897, 0.944 and 0.924 respectively.

(3) Among the input parameters considered, the pipeline-fault crossing angle and the confining pressure of the soil are found to be the most sensitive parameters in influencing the peak compressive strains generated. Other input parameters which had their sensitivity within 10 percent include internal pressure, pipeline temperature, soil relative density, pipe steel ultimate strength, pipeline yield strength, steel yield strength, steel young's modulus and pipe wall thickness. Pipe outer diameter had a sensitivity of around 30 percent. Since, the primary mode of failure in this problem is compressive buckling, the pipe-fault angle which governs the amount of compressive displacement is one of the most sensitive parameters. Similarly, the pipe outer diameter which greatly influences buckling is significantly sensitive here since, the primary mode of failure for this problem is buckling. Confining pressure has significant sensitivity due to its influence towards soil strength with which the soil loads the pipe.

The current case study entails uncertainty quantification of the structural performance of a buried continuous pipeline undergoing fault rupture loading in an efficient and accurate manner using MF-GP. The case study undertaken here considers a site specific pipeline-fault movement case with due regards to variations in the input parameters with respect to a specific site. Further extension to this work would be to characterise the regional seismic risk to pipelines due to fault rupture which involves integration of pipeline uncertainty quantification at a specific site to probabilistic regional ground deformation hazard due to fault rupture.

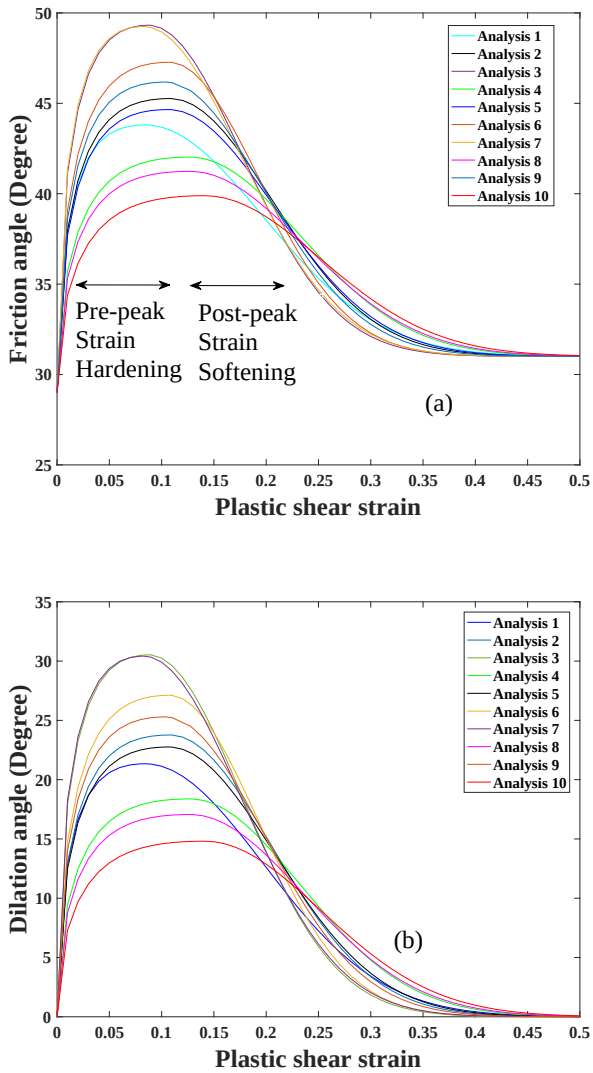

Figure 4.3: Non-linear variation of (a) mobilized friction angle and (b) mobilized dilation angle with plastic shear strain used in HF soil material models for analyses 1 to 10 among a total of 30 analyses

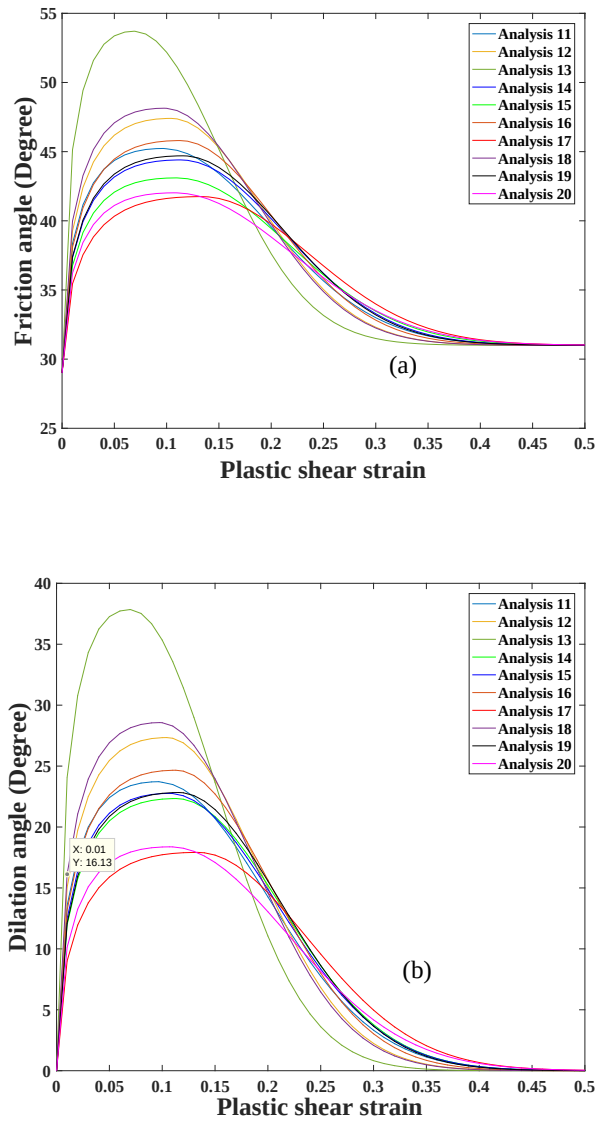

Figure 4.4: Non-linear variation of (a) mobilized friction angle and (b) mobilized dilation angle with plastic shear strain used in HF soil material models for analyses 11 to 20 among a total of 30 analyses

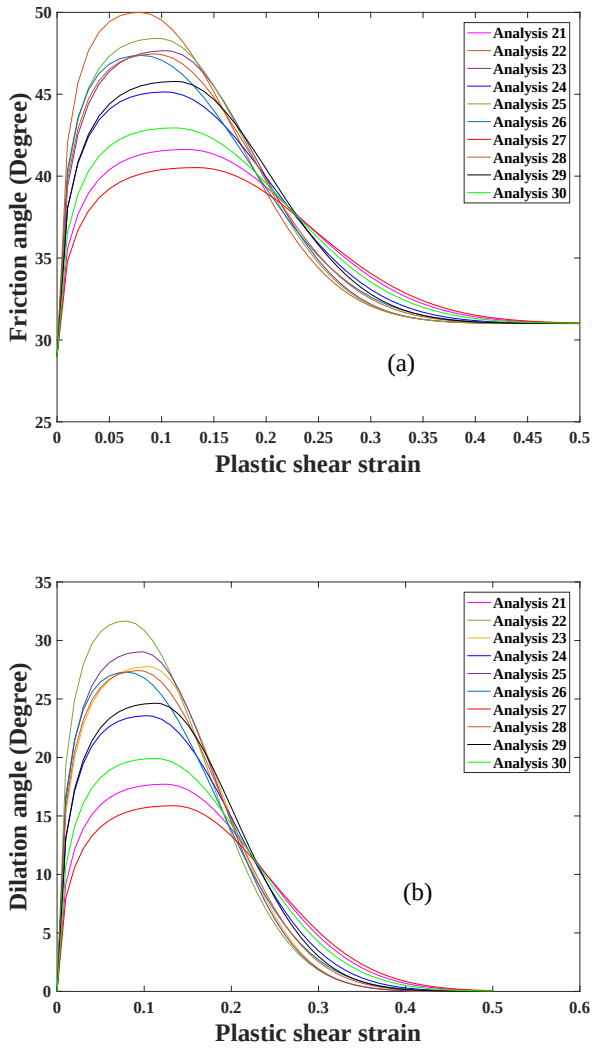

Figure 4.5: Non-linear variation of (a) mobilized friction angle and (b) mobilized dilation angle with plastic shear strain used in HF soil material models for analyses 21 to 30 among a total of 30 analyses

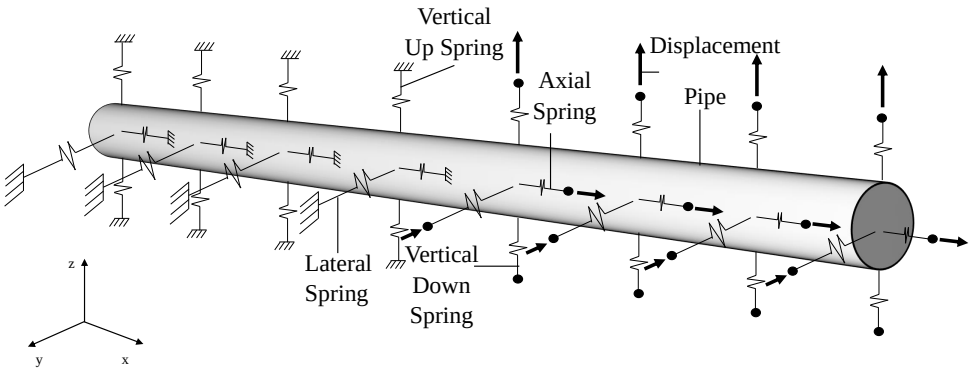

Figure 4.6: Schematic diagram of LF pipe-soil model

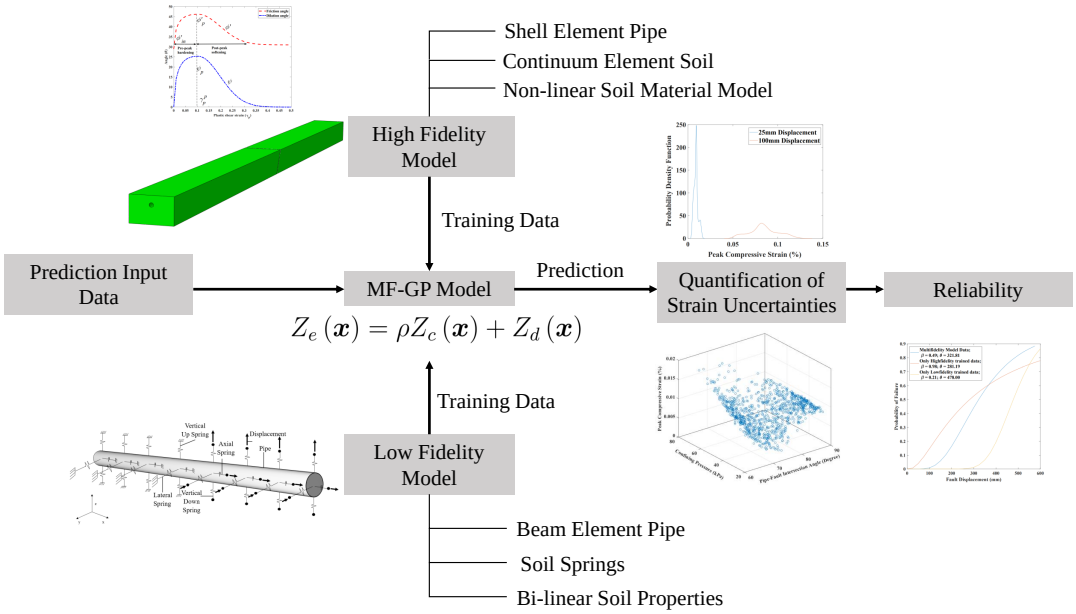

Figure 4.7: MF-GP uncertainty quantification flowchart

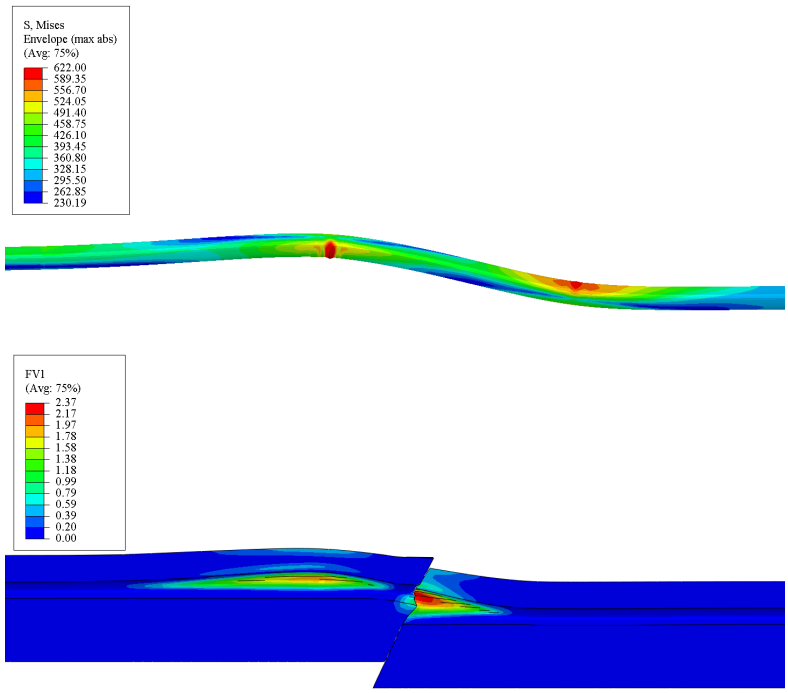

Figure 4.8: HF pipe-soil model: pipe von Mises stress plot and soil plastic shear strain plot

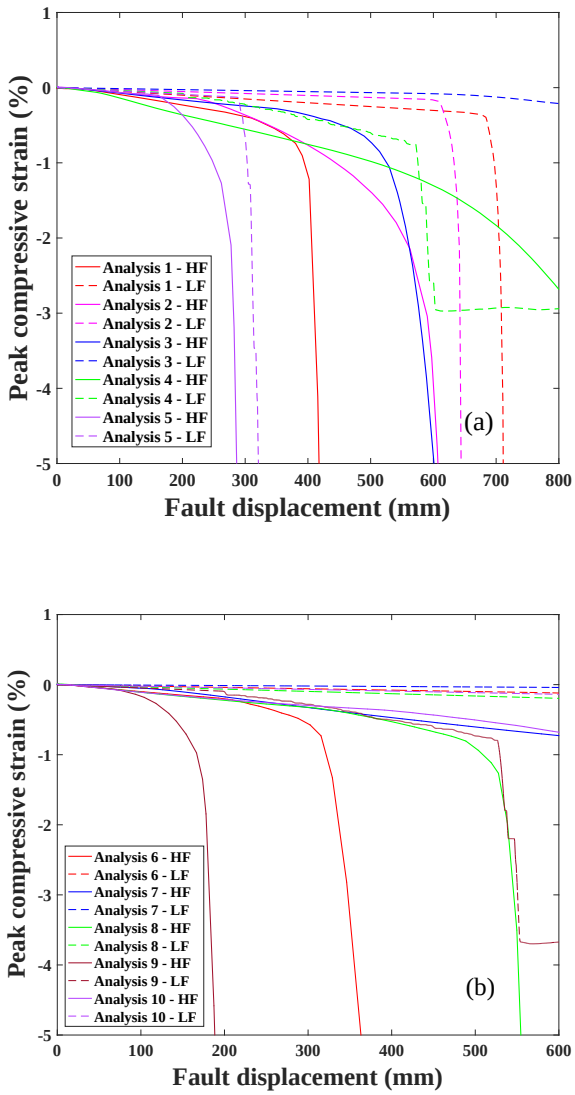

Figure 4.9: Peak compressive strain percent generated in the pipe at various instants with increasing fault displacements: (a) analysis 1 - 5 (b) analysis 6 - 10

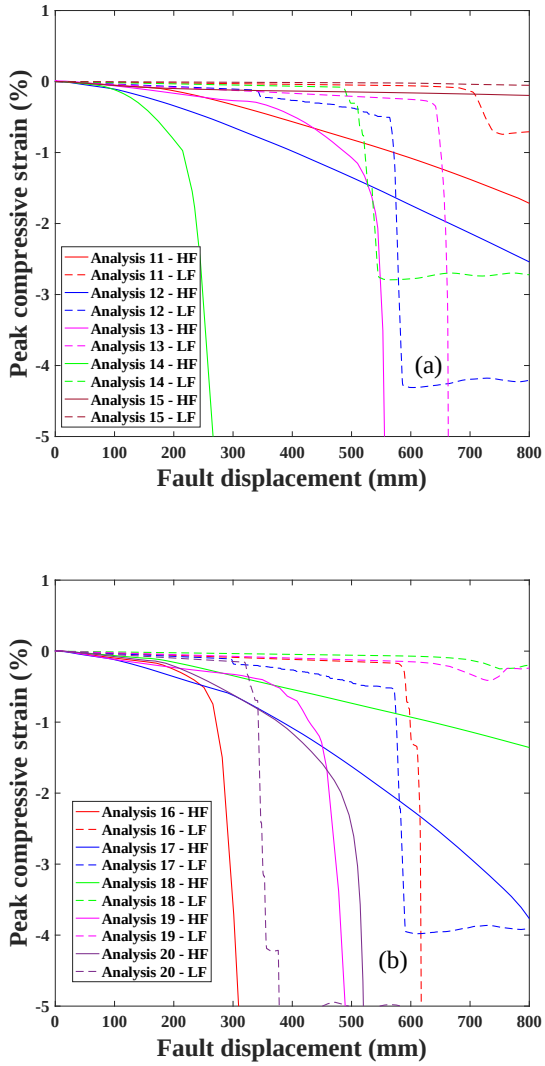

Figure 4.10: Peak compressive strain percent generated in the pipe at various instants with increasing fault displacements: (a) analysis 11 - 15 (b) analysis 16 - 20

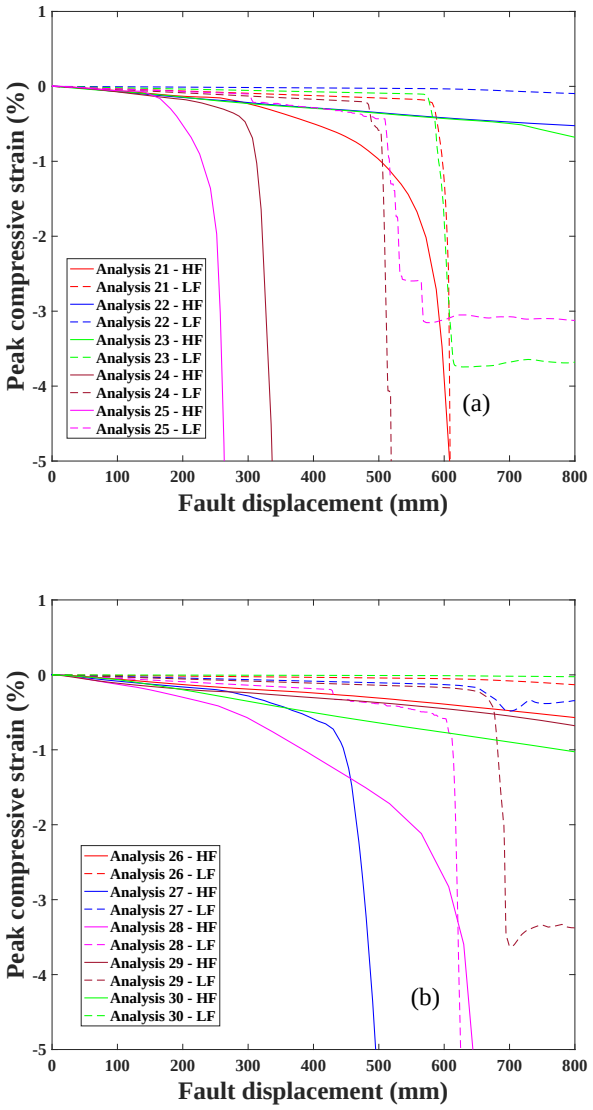

Figure 4.11: Peak compressive strain percent generated in the pipe at various instants with increasing fault displacements: (a) analysis 21 - 25 (b) analysis 26 - 30

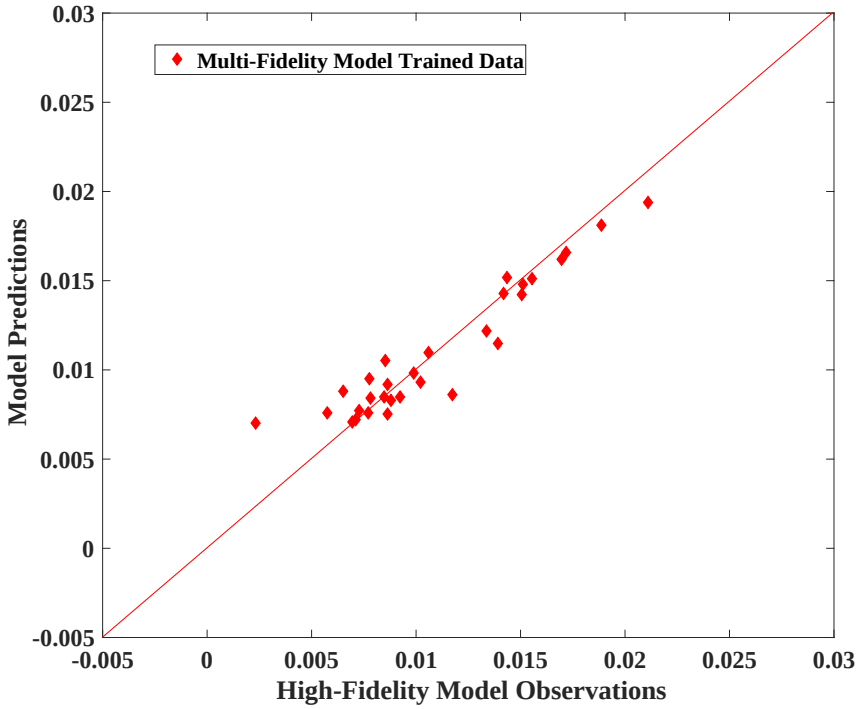

Figure 4.12: Cross-evaluation data (peak compressive strain percent) at 25 mm fault displacement for multi-fidelity model trained with both HF and LF data

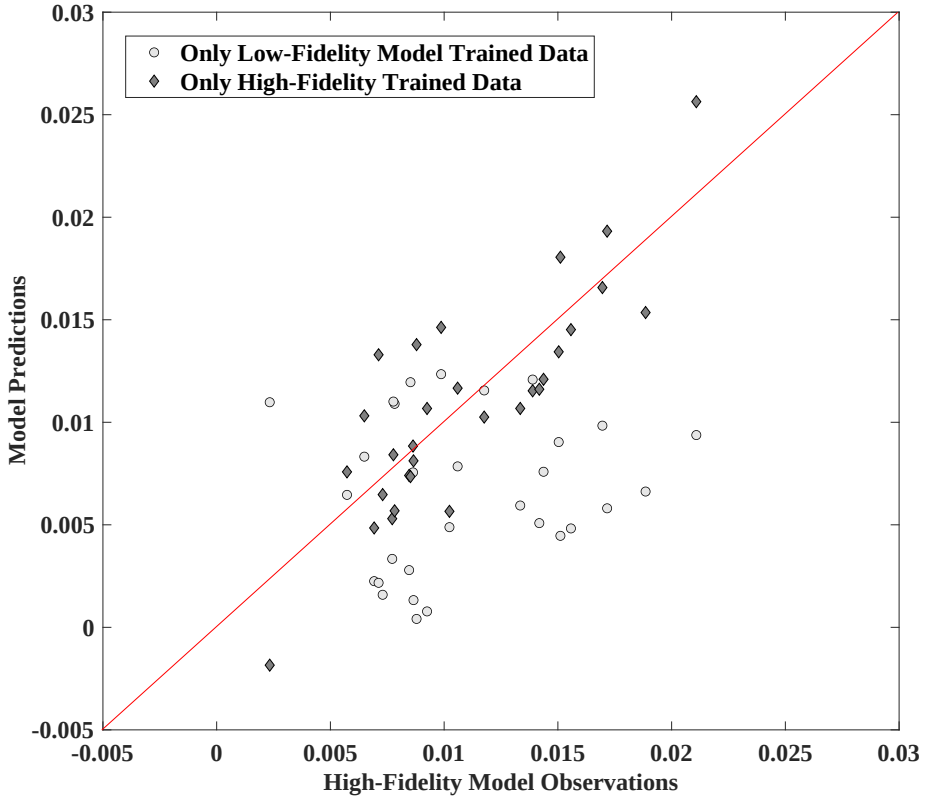

Figure 4.13: Cross-evaluation data (peak compressive strain percent) at 25 mm fault displacement for multi-fidelity model trained with only HF or LF data

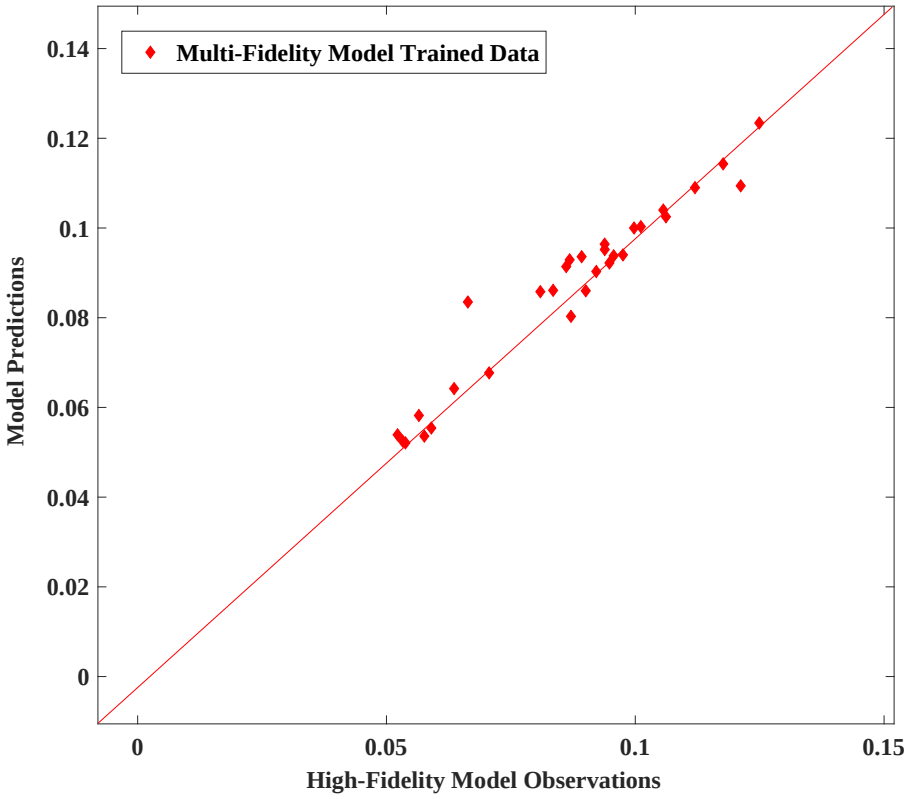

Figure 4.14: Cross-evaluation data (peak compressive strain percent) at 100 mm fault displacement for multi-fidelity model trained with both HF and LF data

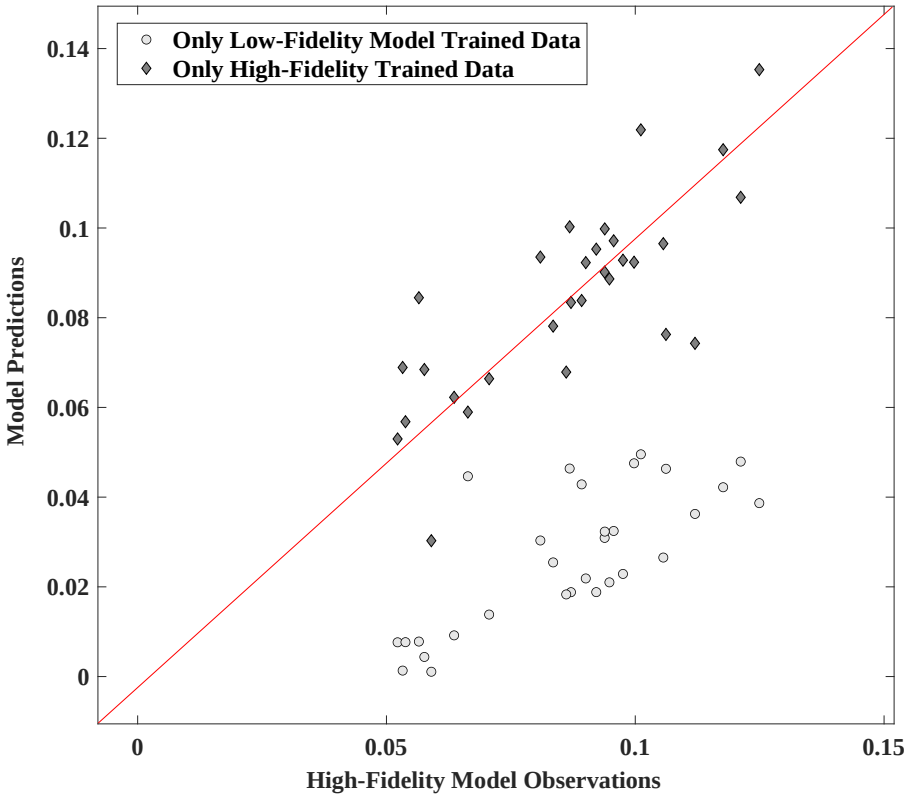

Figure 4.15: Cross-evaluation data (peak compressive strain percent) at 100 mm fault displacement for multi-fidelity model trained with only HF or LF data

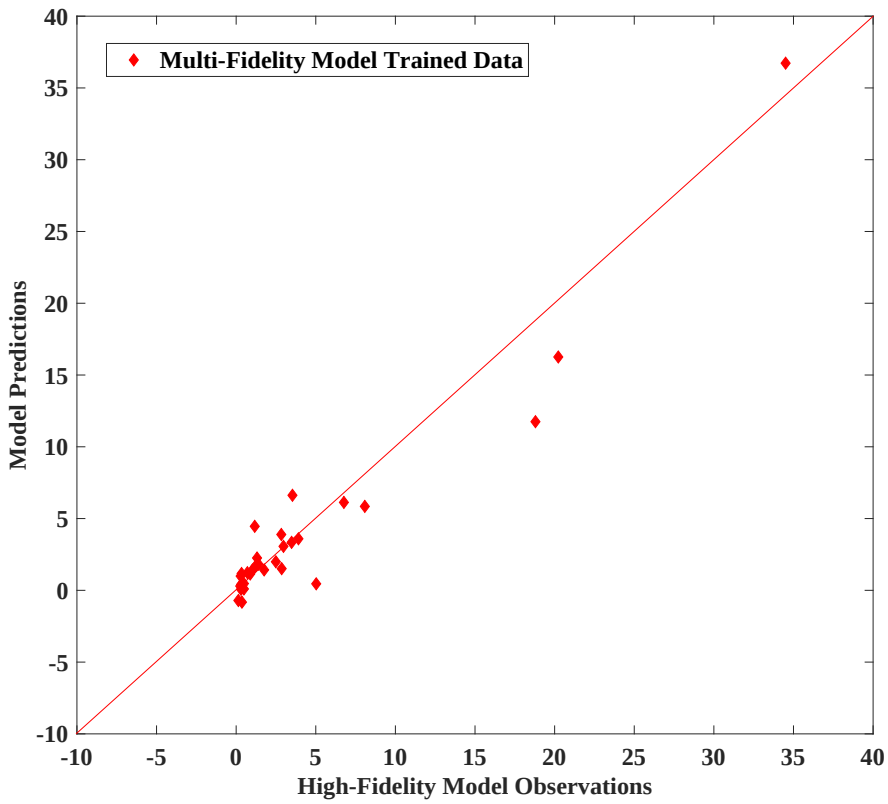

Figure 4.16: Cross-evaluation data (peak compressive strain percent) at 300 mm fault displacement for multi-fidelity model trained with both HF and LF data

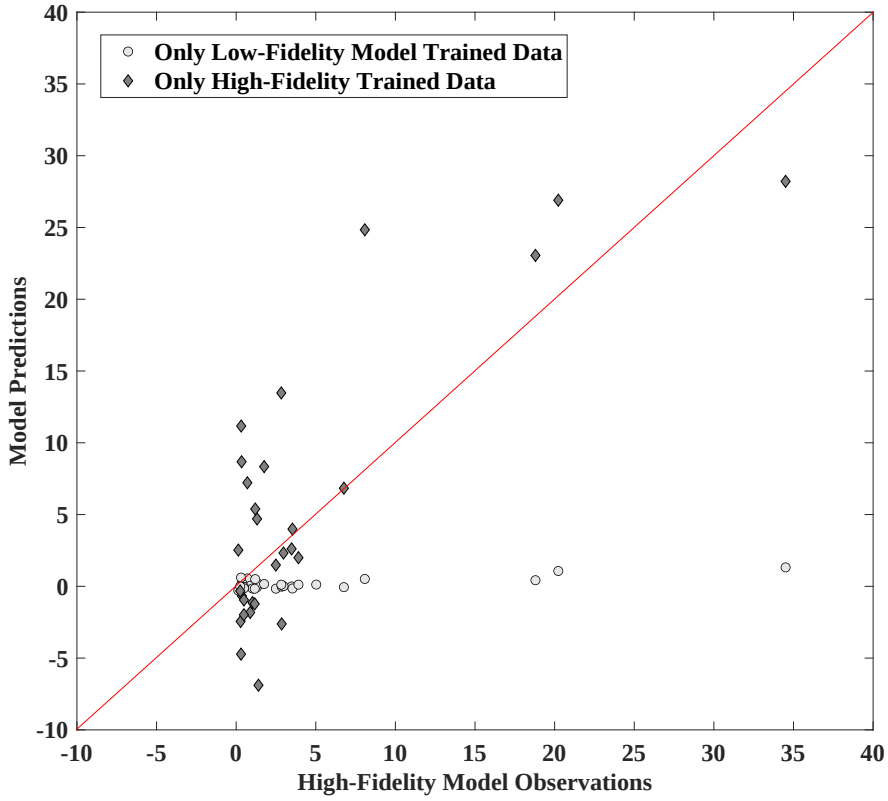

Figure 4.17: Cross-evaluation data (peak compressive strain percent) at 300 mm fault displacement for multi-fidelity model trained with only HF or LF data

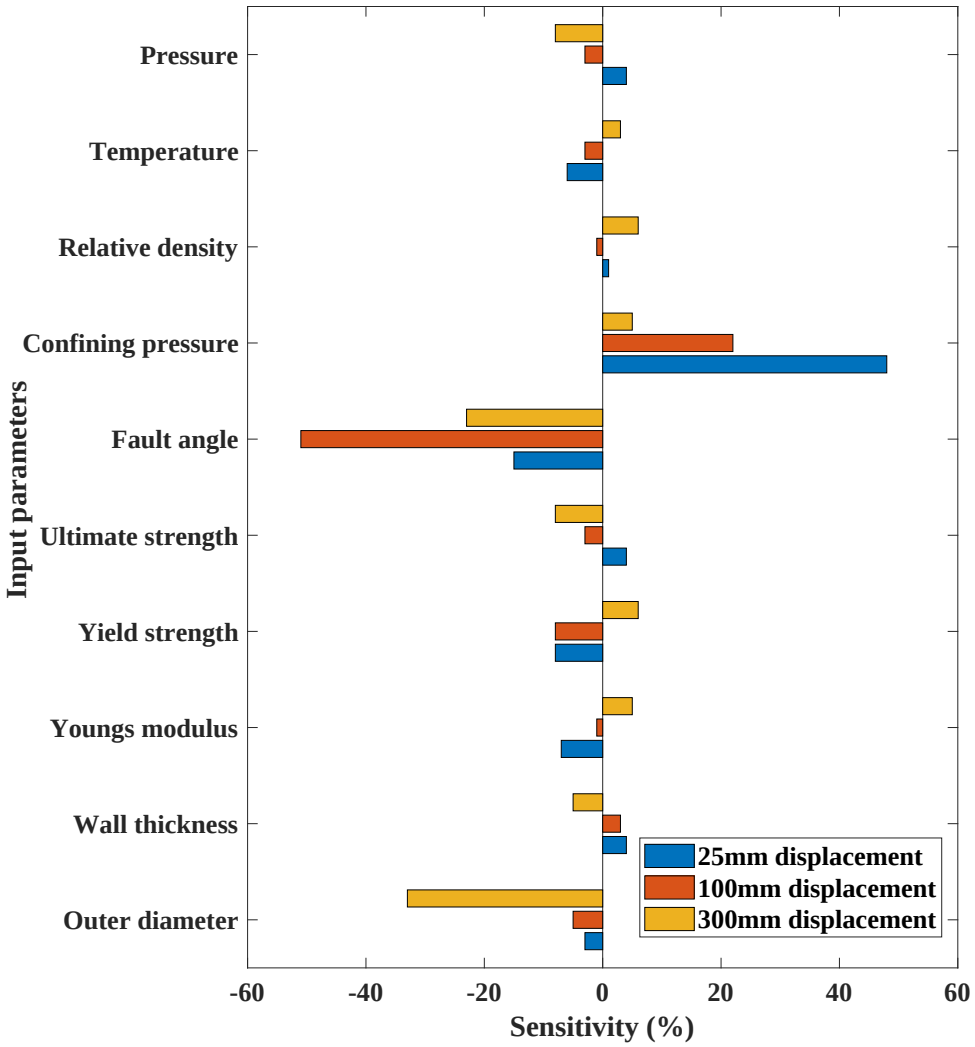

Figure 4.18: Sensitivity of input variables at 25 mm, 100 mm and 300 mm fault displacements

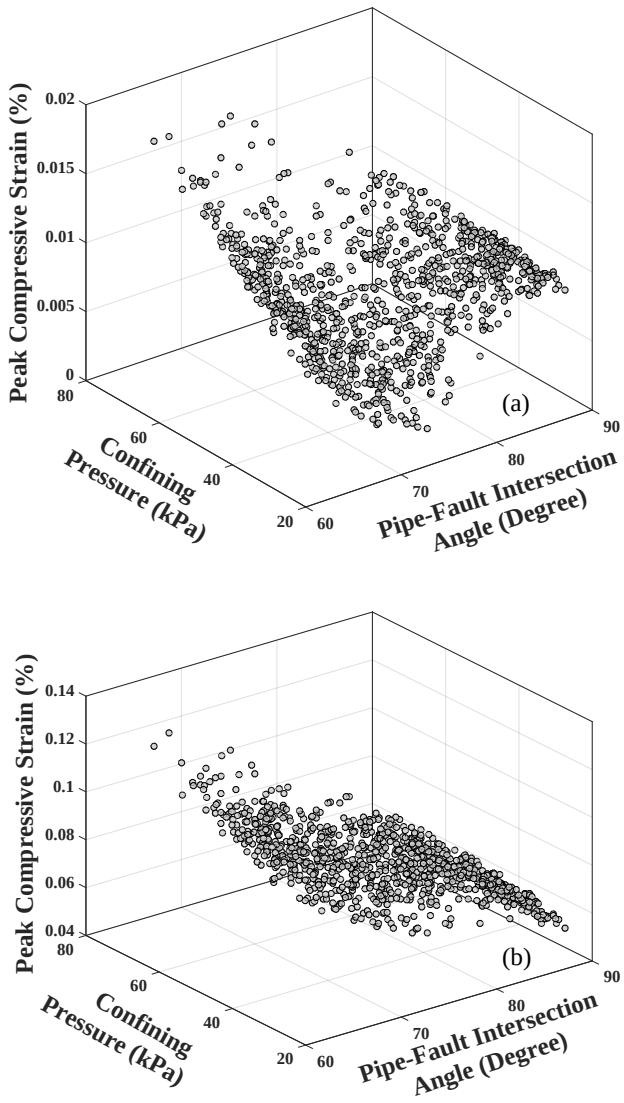

Figure 4.19: Peak compressive strain predictions at (a) 25 mm fault displacement and (b) 100 mm fault displacement

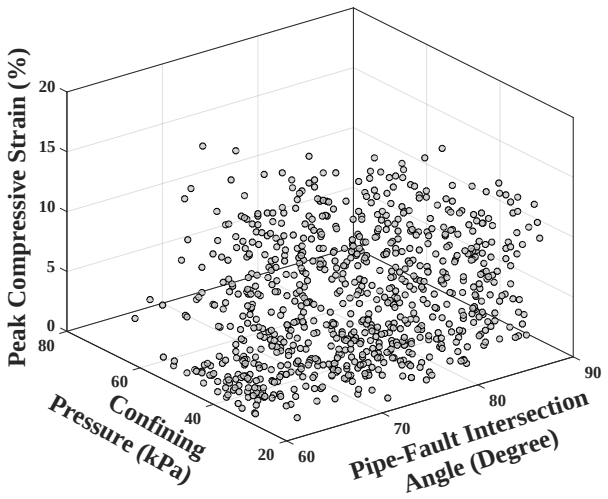

Figure 4.20: Peak compressive strain predictions at 300 mm fault displacement

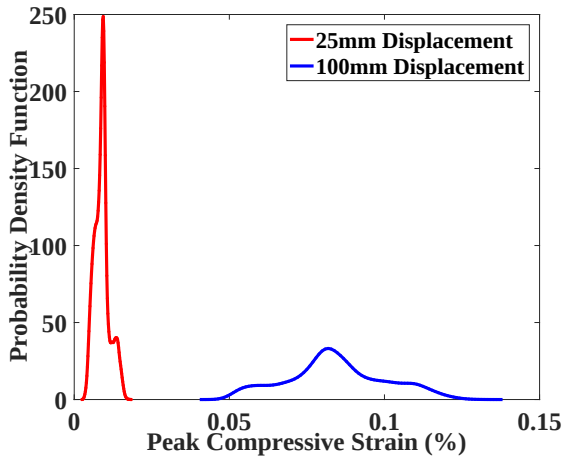

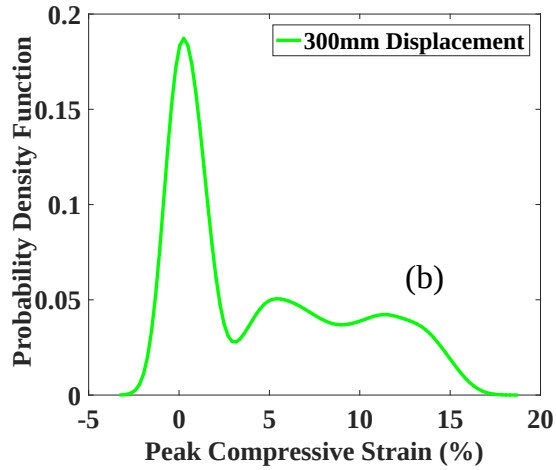

Figure 4.21: Peak compressive strain predictions at (a) 25 mm fault displacement and (b) 100 mm fault displacement

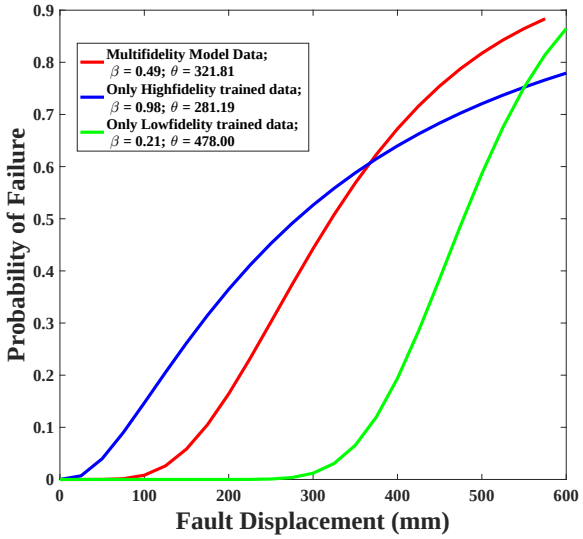

Figure 4.22: Fragility curve for pipeline failure under compression

Chapter 5

Regional Probabilistic Seismic Risk Analysis of Buried Pipelines due to Permanent Ground Deformation Hazard for Victoria, British Columbia, Canada

5.1 Introduction

A novel method to estimate regional seismic risk to buried continuous pipelines probabilistically, due to earthquake rupture induced permanent ground deformations has been proposed. The seismic risk assessment method has been illustrated for buried gas pipeline in the City of Victoria considering seismic risk from the Leech River Fault Zone (LRVFZ). The method considers uncertainty in a comprehensive manner on various aspects and levels of the assessment, as well as utilizes experimentally evaluated complex geotechnical numerical models in an efficient manner. Major improvements of this method over existing studies include: (1) Stochastic source modelling and analytical Okada solutions to regionally generate ground deformations instead of regression equations to characterize ground deformation along a fault (2) Complex experimentally evaluated geotechnical FE models employing non-linear soil constitutive relations instead of simple soil spring – beam element pipe models to evaluate pipeline response (3) Use of multi-fidelity Gaussian processes to ensure efficiency and limit required computational resource, given the high number of runs necessary for uncer-

tainty quantification exercises and the computationally expensive nature of complex geotechnical FE models used. Probabilistic regional ground deformations generated has been suitably applied to the FE models, to transfer the uncertainty in ground deformation towards the pipeline response.

The current study aims to quantify uncertainty in buried gas pipeline response in the City of Victoria due to permanent ground deformations resulting from LRVFZ fault rupture. The study probabilistically generates the ground deformations over a region to capture uncertainty and considers variations in pipe geometry, soil conditions, operating conditions together using a multi-fidelity Gaussian processes (MF-GP) analysis framework in association with FE analysis [154, 165]. The significance of this study in comparison to existing comparable studies [18, 19] is integration of probabilistic regional ground deformation with MF-GP surrogate model. Stochastic source modelling and analytical okada equations are used to characterize probabilistic ground deformation regionally. On the other hand, MF-GP surrogate model enabled experimentally evaluated complex pipe-soil numerical models are used to quantify uncertainty of pipeline response. The case study performed for the City of Victoria due to permanent ground deformations resulting from LRVFZ fault rupture indicated potential for significant differential ground deformations at many instances and locations. A fragility curve is generated for pipe failure at a specific site based on [4] strain limit.

5.2 Integrated risk assessment method for buried pipelines

The proposed methodology for integrated risk assessment of buried pipelines first characterizes the permanent ground deformation over a region, probabilistically using the approach by [121]. Thereafter, the pipeline response is evaluated using FE analysis coupled with multi-fidelity Gaussian processes (MF-GP) surrogate model [165]. To consider uncertainties in the pipe response, variations in pipe geometry, soil conditions and operating conditions are considered in this method. The integrated assessment of uncertain permanent ground deformation and uncertain pipeline response result in the seismic risk assessment of pipelines due to permanent ground deformation. Figure 5.1 presents the method in a flow chart form.

The probabilistic ground deformation approach computes ground deformations over a region using statistical models for earthquake source parameters, simulated earthquake slip models and analytical Okada equations. To do so, fault geometry is defined based on regional geological and seismo-

logical studies and is discretized into sub-faults to allow heterogeneous slip distribution over a fault plane. An earthquake scenario is defined based on regional seismicity and are typically represented by truncated exponential and characteristic earthquake recurrence models. A logic tree approach is used to consider uncertainties in various parameters involved in the earthquake occurrence modelling. Thereafter, based on an earthquake scenario, earthquake source parameters are sampled from statistical scaling relationships derived from the earthquake rupture model database. Subsequently, realistic fault slip fields are generated and ground deformations computed using Okada equations, all constrained to the fault geometry set initially. The resultant probabilistic ground deformations are strictly of tectonic origin and can be obtained at any locations within a region. More importantly, differential probabilistic ground deformation between any two points can also be estimated.

To consider uncertainty in the pipeline response, large numbers of scenarios considering variations in input parameters are required to be analyzed. In addition to variation in pipe operating conditions, soil material properties, pipe geometry, variation of differential ground deformation between two ends of the pipe section are also to be considered. This variability in differential ground deformation between the two ends of the pipe is obtained from the generated probabilistic ground deformation. From pipeline infrastructure maps and fault alignments, potential sites for pipeline risk assessment can be identified. The probabilistic differential ground deformations between two surface points can be converted to local co-ordinates corresponding to the pipe section under consideration and included in the FE analysis. In case of the HF type of FE models, these variations in differential ground deformations will translate to varying interface fault angles between the two soil blocks both in the horizontal plane and vertical plane. Additionally, these will translate to variations in the axial, lateral and vertical differential displacements between the two sides of the pipeline, true for both the HF and LF models. To derive training data for the MF-GP surrogate model, the HF and LF models are to be fed with uniformly randomly sampled axial, lateral and vertical differential displacements. These differential displacements are to be obtained from the range of probabilistic differential ground deformations between two surface points of interest in local co-ordinates corresponding to the pipe section.

Finally, to assess pipeline risk, the two primary variables of interest namely peak axial tensile strain and peak axial compressive strain are extracted from the pipeline at the end of both the HF and LF analyses. These data are used to train the MF-GP model. Data from a small number of

HF models (tens) and a large number of LF models (hundreds) can be combined to predict the uncertainty in the pipeline response by leveraging the accuracy and complexity of the HF models and the efficiency of the LF models in a MF-GP surrogate model framework. MF-GP surrogate models use Gaussian processes to approximate relationship between the input and output variables by fitting available data. To ensure reliability of the MF-GP model, it is first to be cross-evaluated and then used to study the uncertainty response of the buried pipelines.

5.3 Probabilistic ground deformation hazard assessment for Victoria, British Columbia

The LRVFZ is located in the vicinity of the City of Victoria and is of important consideration for seismic risk assessment in the region [131, 131, 133]. To generate ground deformations probabilistically due to fault rupture, the method proposed in [121] is adopted. Broadly, it involves the definition of an earthquake scenario comprising of earthquake magnitude and faulting type. Additionally, it requires the selection of a fault rupture source region, which reflect the seismological information of fault rupture in the region. The source region is subsequently divided into a number of sub-faults to enable random generation of candidate rupture models to consider uncertainty. To model the fault rupture source stochastically, first earthquake source parameters comprising of geometry and slip distribution parameters are randomly sampled from [123]. Then, the geometry of the fault plane is selected and slip distribution is defined. Finally, Okada equations [122] are employed to generate surface deformations. The final ground deformations calculated are solely of tectonic origin and can be used to characterize probability distributions of ground deformations in the North-South, East-West, and Up-Down directions.

5.3.1 Leech River Valley Fault Zone (LRVFZ) Source Characterization and Rupture Occurrence

The LRVFZ consists of a North-North East dipping zone [132]. The North-East ward reverse faulting dipping region of the LRVFZ is close to 70° steep and extends for about 60 km [131, 134, 135]. The fault geometry of the LRVFZ in the current study has been adopted from [134], with a fault length of 67.8 km. A dipping angle of 70° is used [134], resulting in a width of 25 km. The fault geometry is, thereafter, divided into a

total of 525 sub-faults: 35 along strike and 15 along dip. Fault ruptures in the LRVFZ fault plane are simulated by rectangular finite-fault sources. The earthquake magnitudes are modelled based on [166, 167]. A truncated exponential model and characteristic model are used to define the magnitude vs. annual frequency relationship. Details of the earthquake modelling approach for the LRVFZ can be found in [165]. To this end, first the slip rate is obtained by considering the representative slip rate of 0.25 mm/year [3, 134, 168]. The fault zone area is calculated based on the adopted fault length and width. A shear modulus of 35 GPa is adopted in the calculations [136]. A value of 0.796 is used for the slope parameter of the truncated exponential model [169].

A minimum magnitude of 6 is used [134]. The magnitude intervals to define probability density value for the characteristic part and the magnitude intervals for the characteristic part is set to 1.0 and 0.5 [134, 166]. For each of the two earthquake magnitude models, variations of discrete values of these parameters are considered. These parameters are randomly selected using a logic-tree approach in association with a combination of characteristic and truncated exponential magnitude-annual frequency relationships to characterize a fault rupture and their occurrence. Once, a fault rupture occurs within a specified magnitude range of 0.1 bin in between 6.0 and 7.7, earthquake magnitude is generated from a discrete distribution and subsequently, stochastic source models are generated [121] for that given earthquake magnitude using earthquake source scaling relationships [123], which consider uncertainties in fault rupture by means of variations in both geometrical parameters and slip distributions. 1000 stochastic sources are generated for the selected magnitude range of 0.1 and one of them are randomly selected for extraction of fault plane and fault slip information.

5.3.2 Probabilistic Ground Deformation Hazard Assessment

In the ground deformation computation phase, the randomly selected source parameters based on magnitudes are utilized to define the fault plane. Additionally, an earthquake slip field is generated randomly based on the spatial slip distribution parameters which are also generated from the scaling relationships [123]. An iterative approach is adopted to ensure consistency between the generated fault length, fault width and mean slip by matching the target and simulated seismic moment. Subsequently, Okada equations are used to compute surface displacements of an elastic half space due to a rupture in a rectangular fault. The inputs for the Okada computations are

rake angle and slip value in addition to the rupture geometry, such as the strike angle, dip angle, fault length, fault width and depth. Depth indicates the depth of the fault centroid, strike is the azimuth angle of fault trace with respect to North, dip angle is the angle between the fault plane and horizontal plane, fault length is the dimension of the fault along the strike, fault width is the dimension of the fault along the dip, rake angle is the angle between the hanging wall movement direction with that of the strike and slip defines the value of hanging wall movement. To limit computational time, Okada equations are pre-computed at locations of interest in the East-West, North-South and Up-Down directions for every sub-fault by considering an unit displacement (reverse faulting). A thorough review of the gas pipeline network for the City of Victoria is performed and a pipe location susceptible to differential permanent ground deformation (48°25'59.49"N, 123°31'42.80"W) and (48°26'27.67"N, 123°29'6.64"W) is identified. Post stochastic synthesis of slip for all sub-faults, pre-computed deformation values for unit slip can be scaled to derive the final ground deformations using Okada equations [122]. Since the ground deformation computed using Okada equations are physically consistent for a given rupture, differential deformations in the East-West, North-South and Up-Down directions can also be evaluated at the two sites of interest and used for FE analyses.

5.4 Finite Element Models of Buried Pipelines

The FE models used in the analyses involve both HF models and LF models. The FE models are created in ABAQUS [140]. [1, 34, 41, 43, 44, 48–50, 52–55] previously employed shell pipes with surrounding continuum soil to analyze pipeline response undergoing fault rupture deformations. The HF model in the current study employs shell pipeline and continuum soil with geometric and material nonlinearity. The HF and LF models are created in accordance with [165] which successfully performed a multi-fidelity uncertainty quantification analysis for buried pipeline undergoing fault rupture displacements. The HF model is based on [154]. The model employs tri-axial test evaluated nonlinear soil constitutive models. It is based on a full-scale pipeline fault rupture experimental test evaluated FE model. [18, 34, 45, 46] employed beam elements to study this problem in a simplified FE approach.

5.4.1 Variation in Model Parameters

To conduct an uncertainty quantification exercise, variation in pipeline geometrical parameters, such as pipe diameter and wall thickness is con-

sidered. The pipeline diameter at the location of study is 114 mm (email communication with Fortis BC). Variations of pipe wall thickness from 104 mm to 124 mm is considered. Pipe wall thickness varies from 6.02 mm to 17.1 mm, which is the available range of wall thickness for the given pipe diameter. Additionally, among operating conditions, internal pressure varies from no pressure up to a maximum of 550 kPa (email communication with Fortis BC). The soil conditions at the concerned site is sandy in nature (BC Soil Information Finder Tool). Uncertainty in the sandy soil conditions is considered by varying confining pressure and relative density. Mean confining pressure of 39 kPa is assumed with values ranging from 7.8 kPa to 70 kPa and mean relative density of 80 percent is assumed with values ranging from 55 percent to 95 percent. The effect of uncertainty in permanent ground deformation due to fault rupture is considered by varying the axial, lateral, and vertical displacement boundary conditions in the FE analyses. The uncertainty in permanent ground deformation is estimated from the probabilistic regional ground deformations, as discussed in section 3. The differential North-South, Up-Down and East-West probabilistic ground deformations between the two ends of the pipeline section under consideration are converted into the pipe axial, lateral and vertical directions and applied in the FE model. In this analysis, differential East-West, North-South and Up-Down displacements are varied as -0.185 m to 0.216 m, -0.458 m to 0.079 m, and -1.238 m to 0.219 m respectively which is consistent with the values obtained from the probabilistic ground deformation at the site of interest.

5.4.2 High-Fidelity FE Model

A total of 30 HF models are created. The pipeline segment is modelled by employing 4-noded general reduced integration shell elements (S4R element). The soil continuum is modelled using three-dimensional reduced integration stress elements (C3D8R element). A mesh convergence study is performed and an optimal mesh size is chosen accordingly. Pipe mesh size of 25 mm and soil mesh size surrounding the pipe of 10 mm are used. Figure 5.2 shows how the displacement boundary conditions for the FE analyses are obtained from the regional ground deformations (section 3). The pipe material is polyethelene PE80 and accordingly, a Young's modulus of 800 MPa, poison's ratio of 0.4, yield strength of 21 MPa and ultimate strength of 30 MPa are considered. A yield criterion based on von-Mises criteria is adopted. The soil material model is adopted based on the Mohr-Coulomb yield criterion with non-linear constitutive relations. Sand shear strength response is a function of the confining pressure and relative density and is directly dependent on

the internal angle of friction [61, 68, 141–143]. The salient features of a sand constitutive relation are its elastic stiffness, pre-peak hardening behavior, peak strength, and post-peak softening behavior [56, 58]. The default Mohr-Coulomb model in ABAQUS is not capable of modelling varying mobilized friction angle and dilation angle. The Mohr-Coulomb model in ABAQUS is hence modified using the user-defined field subroutine (USDFLD).

5.4.3 Low-Fidelity FE Model

The pipe is modelled using 3-noded quadratic PIPE32 elements, constituting Timoshenko beam formulation allowing for both shear and bending deformation. The soil springs supporting the pipe in the mutually perpendicular axial, lateral, and vertical directions are modelled using 3D pipe-soil interaction elements PSI34. These elements allow for bi-linear elastic perfectly plastic force displacement response in simulating the soil resistance to the pipeline. One end of these springs are connected to the pipe nodes and the other end are connected to the ground. The ground ends are assigned to be fixed on the stationary side of the fault. The ground ends are assigned a certain movement displacement boundary condition on the moving side of the fault. The LF FE model represents a 100m-long pipe segment and is made up of a total of 400 elements. Based on a mesh-sensitivity study the element length is chosen to be 0.5 m. Out of the 400 elements, 200 elements are PIPE32 elements and 200 elements are PSI34 elements. The soil resistances are calculated based on [4].

5.5 Uncertainty Quantification using Multi-Fidelity Surrogate Modelling

Uncertainty in pipeline response can be due to variations in the pipe geometry, soil conditions, operating conditions as well as variations in the ground deformations resulting out of fault rupture. It is evident from [69–71, 73–76, 78–80] that variations in soil conditions can impact pipeline response significantly. Additionally, pipe geometry, such as diameter and wall thickness, can also influence pipeline response [73, 78, 80]. Uncertainty quantification studies typically require large numbers of scenarios to be analyzed to gather information on structural response under varied conditions. Some of the more commonly used uncertainty quantification techniques include simulation-based techniques, such as Monte-Carlo simulation [82, 83] or surrogate model-based techniques, such as polynomial chaos expansion

[89, 90], neural networks [73, 91], radial basis function [92] and kriging [93, 96]. Monte-Carlo simulations require large numbers of scenarios to run in order to achieve desirable accuracy. Similarly, surrogate model-based methods involve training a surrogate model using data from several analyses and using it to predict data for a large number of cases using Monte-Carlo simulation. Both approaches practically require a large number of analyses to be performed. Traditionally, uncertainty quantification exercises for buried pipelines are performed using simplified numerical models or analytical models [18, 19, 69–71, 73–76, 78–80] requiring minimal computational efforts.

An uncertainty quantification exercise allowing for maintaining the intricacy and reliability associated with detailed pipe-soil numerical models will provide deeper and realistic insight of the behavior of the pipeline. Solving detailed pipe-soil numerical analysis problems, such as the current one at hand involving continuum elements with non-linear soil constitutive relations as well as geometric nonlinearity and contact nonlinearity requires significant amount of computational efforts. Hence, a multi-fidelity surrogate; multi-fidelity Gaussian processes (MF-GP) [170, 171] is used to quantify uncertainty in buried pipeline response in Victoria, British Columbia due to fault rupture induced ground deformations. [165] successfully applied the technique to study this problem for a hypothetical reverse faulting case. MF-GP learns from a small number of HF data (in the order of 10s) and a large number of LF data (in the order of 100s) and predicts data as good as HF. This approach helps in reducing enormous amounts of computational efforts as it allows for learning from a large number of computationally inexpensive LF data instead of an equal number of computationally expensive HF data.

5.6 Results and Discussion

This section presents results regarding probabilistic ground deformation in the City of Victoria and its further application to quantify uncertainty in structural response of buried pipelines. The results also include cross-evaluation of the MF-GP surrogate model for both the pipeline response parameters of interest namely, peak axial compressive strains and peak axial tensile strains. Uncertainty in pipeline response has been studied by generating probability density functions of pipeline peak axial compressive and tensile strains as well as their relationship with the most sensitive input variables. A sensitivity analysis has also been included to identify the most

influential parameters towards the pipeline response.

5.6.1 Probabilistic Ground Deformation Hazard Estimation for LRFZ

Figure 5.4 and Figure 5.5 presents some of the critical rupture scenarios including the slip distribution along the fault as well as computed ground deformations in the North-South, East-West and Up-Down directions. It is to be noted that the location of interest in this study as identified by a square and circle in Figure 5.4 and Figure 5.5 is seen to be having significant differential ground deformations. Since, ground deformations computed using Okada equations regionally are physical consistent, the ground deformations computed for each scenario at point 1 and point 2 hold physical dependency. Thus, once the probabilistic ground deformations are computed at point 1 (48°25'59.49"N, 123°31'42.80"W) and point 2 (48°26'27.67"N, 123°29'6.64"W), the differential probabilistic ground deformations are obtained by computing the difference in ground deformation between point 1 and point 2 in the corresponding North-South, East-West and Up-Down directions. Figure 5.8 and Figure 5.9 shows the differential probabilistic ground deformation between point 1 and point 2.

5.6.2 Cross-evaluation and uncertainty quantification of pipeline response

The peak axial compressive strains and peak axial tensile strains from the HF and LF FE models are utilized to train the MF-GP surrogate model. Thereafter, to ensure the validity of the models a k-fold cross-evaluation method is used. To do so, HF data are divided equally into 6 parts . Thereafter, the first part is used to test the surrogate model and the rest of the data are used to train the surrogate model. Similarly, the second part is then used to test the surrogate model and the rest of the data are used to train the surrogate model. This process is repeated for all the parts. The validity of the MF-GP surrogate model is measured with the coefficient of determination (R-square). Figure 5.7 presents the cross-evaluation results for both the axial tensile strains and axial compressive strains. High values of the coefficient of determination of 0.92 and 0.96 are obtained for the axial compressive strains and axial tensile strains, respectively. For peak axial tensile strains, the most sensitive parameters are identified to be pipe outer diameter, sand confining pressure and differential ground deformation in the up-down direction. For peak axial compressive strains, the most sensitive

parameters are identified to be sand relative density, differential ground deformation in the North-south direction and differential ground deformation in the Up-down direction.

Figure 5.10 presents variations of the peak axial tensile strains and compressive strains with their corresponding most sensitive input variables. The variation of peak axial tensile strain with outer diameter is non-linear in nature. The variation of peak axial compressive strain with relative density is linear in nature and the strains increase with the increase in relative density. Figure 5.11 presents the generated histograms for the pipeline peak axial tensile and compressive strains for the given location and considered set of input parameters and their respective variations. The peak tensile strain histogram gradually increases from 0 to about 0.025 and thereafter, drops drastically. The compressive strain histogram gradually increases from to 0 to about 0.014 and thereafter, drops drastically. A cumulative lognormal function based on [164] is used to generate fragility curve for the pipeline at the site. To evaluate damage, strain limit based on [4] has been used. Figure 5.12 shows the probability of pipeline damage at the site of interest as a function of differential ground deformation. It is to be noted here that, based on ultimate strain capacity of PE 80 pipes, no significant failure is observed.

5.7 Summary

In this paper, an integrated risk assessment technique for buried pipelines under fault rupture induced permanent ground deformation hazard is developed. It can be applied both regionally and at specific sites. To do so, a previously available probabilistic ground deformation approach has been employed. Additionally, a previously developed method to quantify uncertainty in pipeline response using a MF-GP surrogate model has been used. The primary contribution of this work has been to bridge these two approaches suitably to present an integrated risk assessment approach for buried pipelines. The method considers regional fault source characteristics, site specific soil conditions, pipeline geometry and operating conditions to quantify uncertainty in pipeline response. The method considers uncertainty in a comprehensive manner on various aspects and levels of the assessment as well as utilizes experimentally evaluated complex geotechnical numerical models in an efficient manner. The method uses MF-GP surrogate model to ensure efficiency.

The developed method is used to illustrate a case study for the city of

Victoria buried gas pipeline. Pipeline risk assessment is conducted due to rupture in the LRVFZ. The MF-GP surrogate model is successfully cross-evaluated with excellent coefficient of determinations of 0.92 and 0.96 between HF observed values and MF predicted values for peak axial compressive strains and peak axial tensile strains, respectively. Finally, the uncertainty in peak axial tensile and compressive strains are presented as histograms. Additionally, a fragility curve based on [4] strain limit is developed. Its is also found that based on ultimate strain capacity of PE 80 pipe no appreciable failure is identified at this site. Although the case study performed here is for a specific pipe location, the same approach can be used for multiple locations of concern over a region. In that case, either separate MF-GP surrogate models can be created for each site or, a global MF-GP surrogate model can be created with wide variations in the input variables considering every situation for all the sites and then separate prediction data can be used to evaluate each site individually.

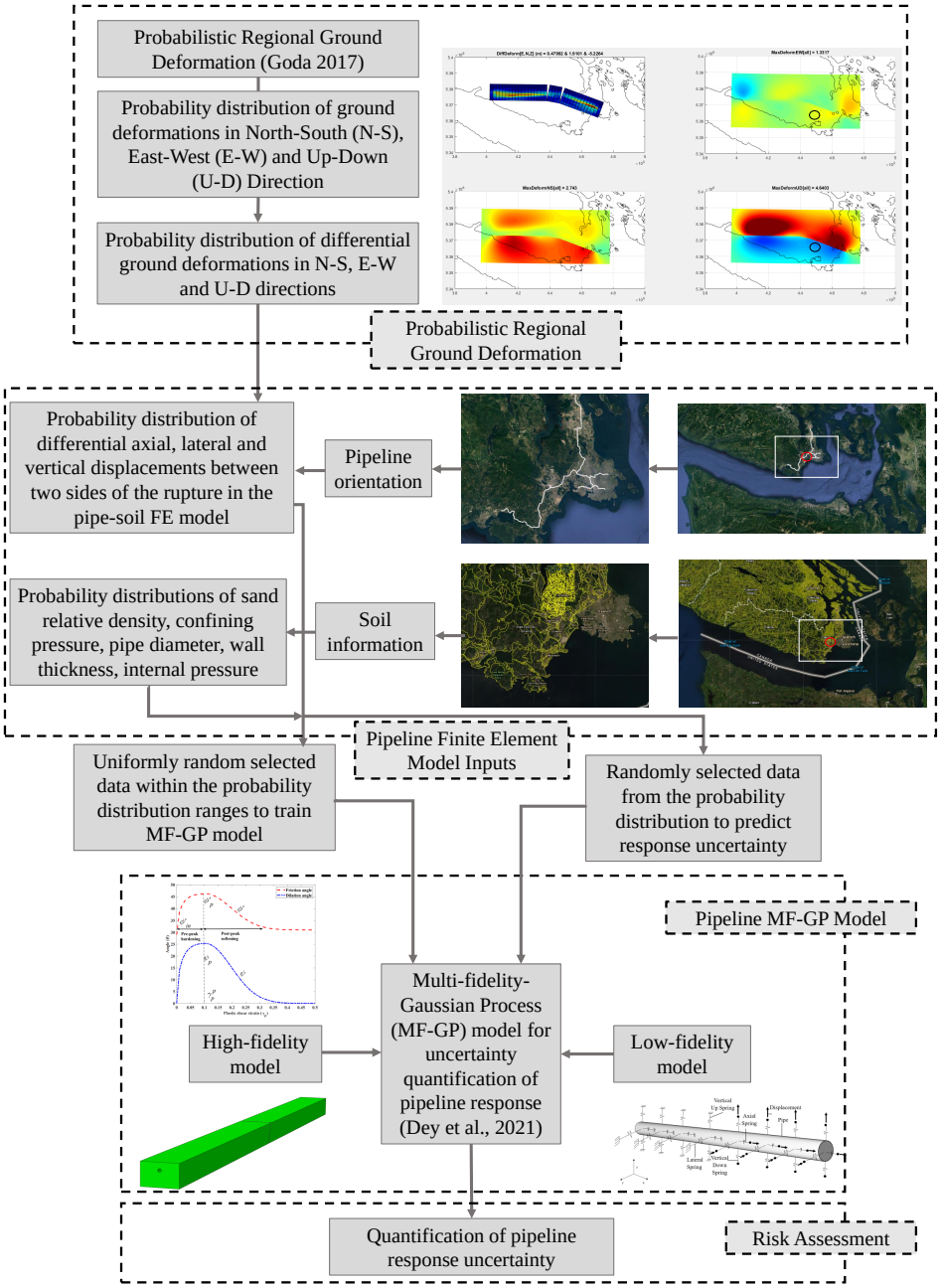

Figure 5.1: Integration of regional probabilistic ground deformation with pipeline response uncertainty quantification

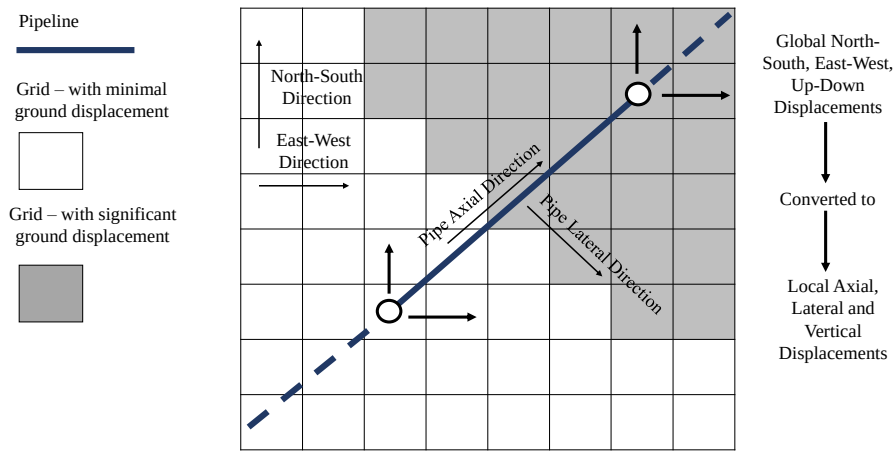

Figure 5.2: Schematic diagram of FE model displacement boundary conditions derivations from probabilistic ground deformation analyses

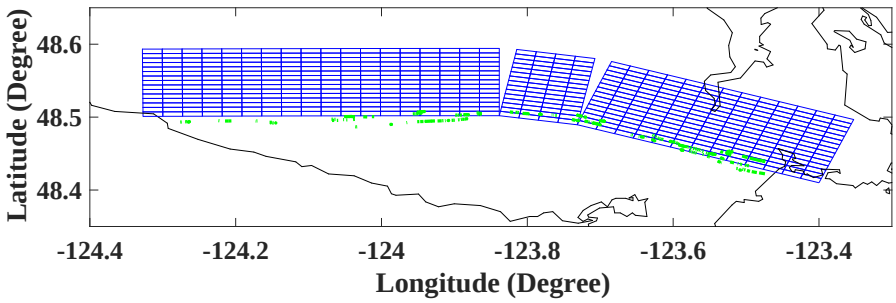

Figure 5.3: LRFZ finite fault model and sub-fault discretization along with [3] fault scarp information

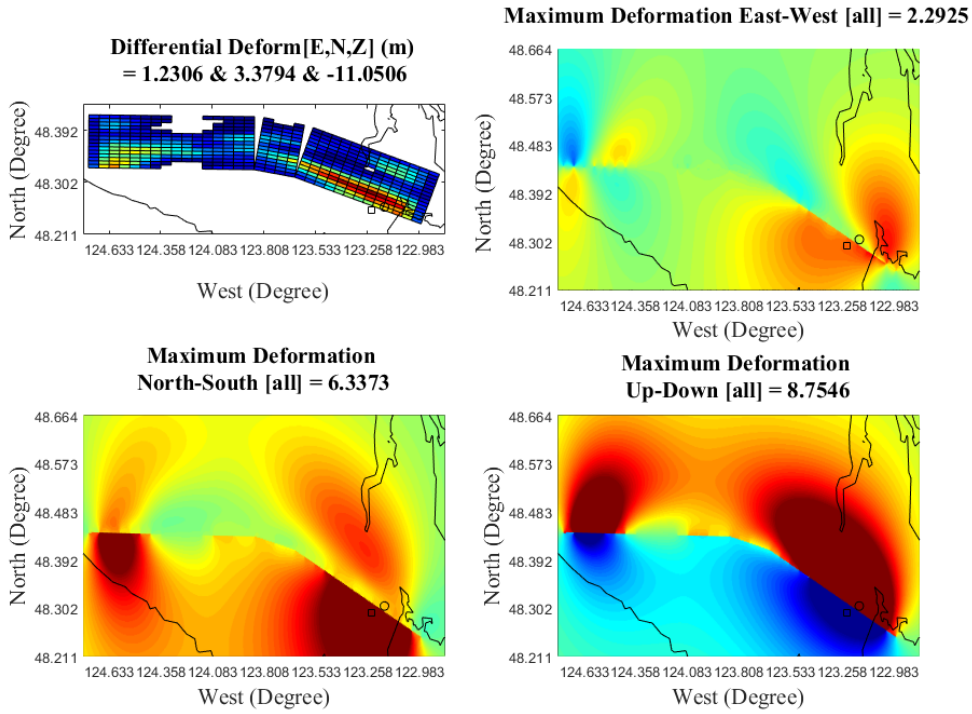

Figure 5.4: Sample critical rupture scenario slip distribution and regional ground deformation profiles in the East-west, North-south and Up-down direction in the City of Victoria

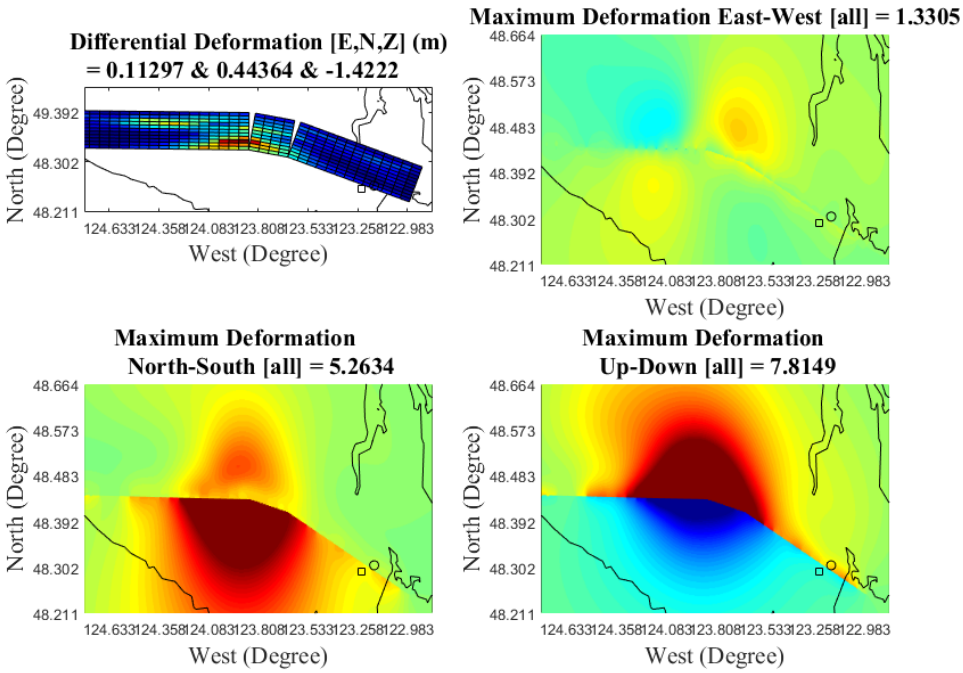

Figure 5.5: Sample critical rupture scenario slip distribution and regional ground deformation profiles in the East-west, North-south and Up-down direction in the City of Victoria

Figure 5.6: City of Victoria buried gas pipeline network under consideration

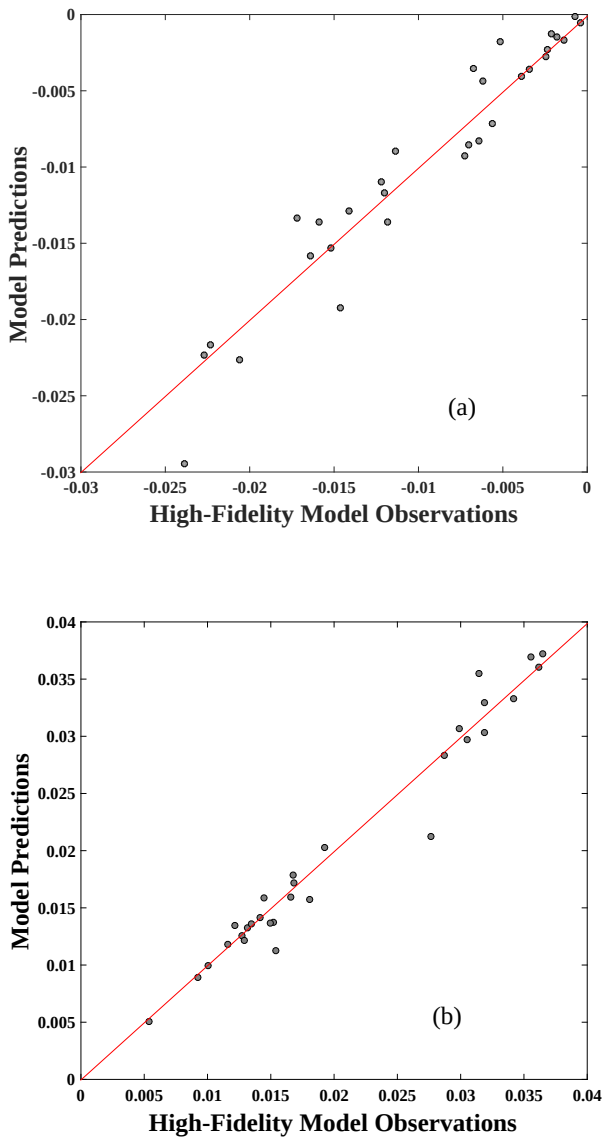

Figure 5.7: Cross-evaluation of MF-GP surrogate model for (a) peak axial compressive strains and (b) peak axial tensile strains

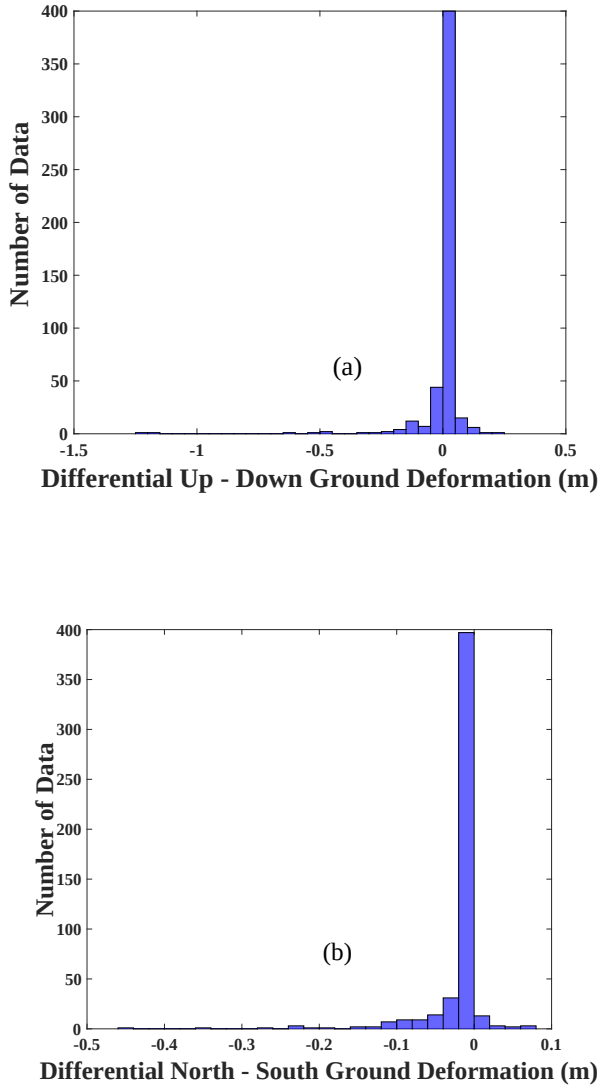

Figure 5.8: Histograms of the simulated differential ground deformations in the (a) Up-Down and (b) North-South direction at the location of interest

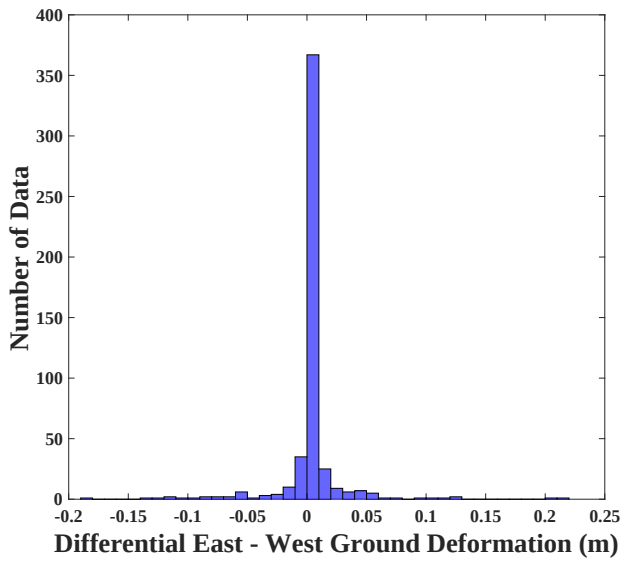

Figure 5.9: Histograms of the simulated differential ground deformations in the East-West direction at the location of interest

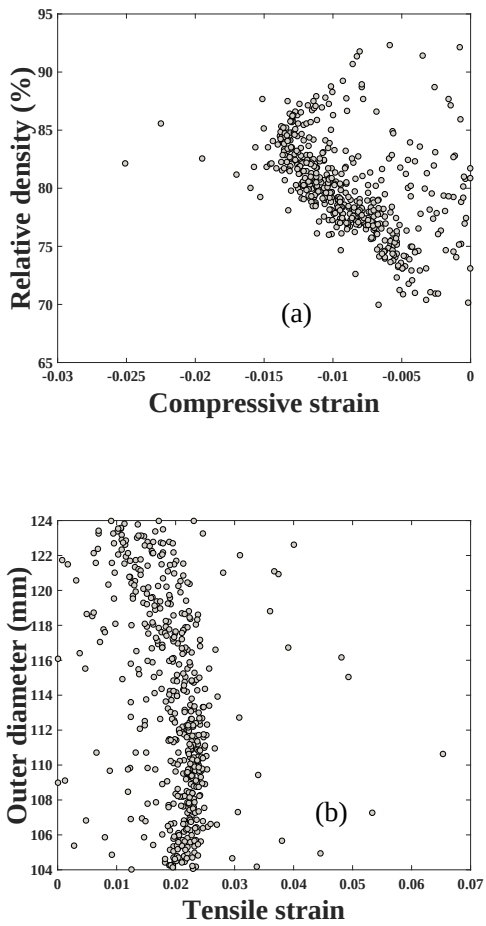

Figure 5.10: Variation of predicted peak axial strains with the most sensitive parameters at the location of interest (a) compressive strain vs relative density (b) tensile strain vs outer diameter

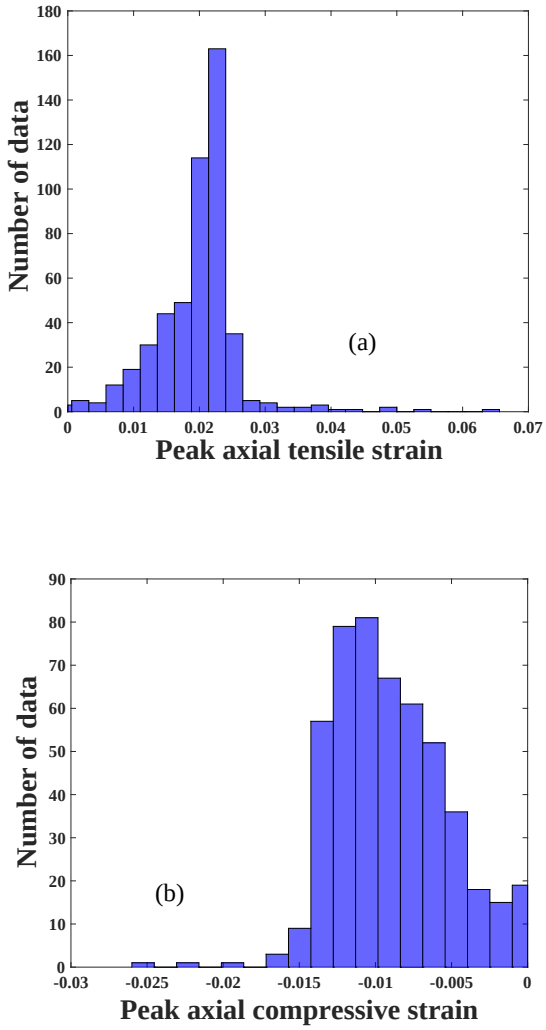

Figure 5.11: Histograms of the pipeline peak axial (a) tensile strains and (b) compressive strains generated at the location of interest

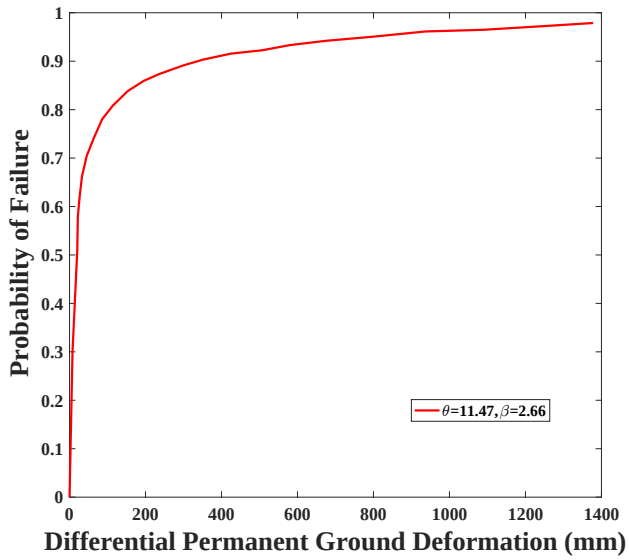

Figure 5.12: Fragility curve for pipeline damage using [4] strain limits

Chapter 6

Design of Buried Pipeline undergoing Fault Rupture Deformations in Sand using Taguchi Design of Experiments

6.1 Introduction

Nonlinear structural response of buried continuous steel pipeline undergoing fault rupture deformation is studied in a systematic manner. A detailed and efficient analysis framework for design is proposed and explained with a case study. A three-dimensional nonlinear FE model previously developed and evaluated by the authors is used for this study. Taguchi method for design of experiments is employed to evaluate the structural performance of buried pipeline. It is also used to identify the influence of different parameters, such as the fault crossing angle, faulting type (Reverse/Normal, Strike-slip), the operating conditions of the pipeline, geometry of the pipe cross-section and material properties of the pipe and soil on the structural behavior of buried pipelines. The proposed method can be successfully employed to derive peak strain demands as a function of fault displacements for a given set of input conditions in an efficient manner leading to an efficient and safe design solution to this problem. A case study involving NPS 24 steel pipeline with a maximum operating internal pressure of 9.1 MPa is also carried out. The method presented here is suitable for pipeline strain hazard analysis, applicable for major oil and gas transmission lines crossing seismically active faults.

6.2 Problem statement

The objective of the research includes establishing an appropriate framework to quantitatively evaluate the structural performance of buried continuous steel pipelines undergoing fault rupture deformations in a comprehensive manner. The aim is establishing a detailed structural analysis method for this problem suitable for design purposes which is highly efficient and reliable. To quantitatively evaluate the structural performance, engineering demand parameters, such as tensile and compressive strain demand are required to be obtained from systematic FE analyses. The structural performance of the pipeline is affected by several parameters, such as fault type, fault-pipe crossing angle, pipe material grade, pipe diameter, pipe internal pressure, pipe temperature and soil conditions. Considering the nonlinearity of the system, the influence of the concerned parameters towards the peak pipeline strains generated is characterized by significant variability.

To address this, the research employs a previously developed and experimentally evaluated FE model by the authors [154]. The pipe-soil FE model employs pipe material (steel) and soil (sand) non-linear material properties as well as geometric non-linearity. The steel is modeled using von-Mises yield criterion and elastic plastic Ramberg-Osgood non-linear stress strain relation. Non-linear soil strength relations are used to model the soil. section 6.4 provide further specifics of the steel and soil material properties used. An experimentally evaluated Mohr-Coulomb yield criterion for sand with pre-peak strain hardening and post-peak strain softening is adopted using suitable constitutive relationships. The adopted FE model [154] provides a better match with experimental results in comparison to numerical studies in literature. For the material model evaluation, root mean square error (RMSE) of the [154] model is found to be 3.6E-03 in comparison to 3.9E-02 for the model by [68]. For large scale tensile experimental test [40] evaluations, RMSE of the [154] model at 300 mm, 600 mm and 900 mm fault displacements are found to be 1.7E-03, 4.1E-03 and 4.4E-03 respectively in comparison to 3.1E-03, 5.9E-03 and 9.4E-03 respectively for the [1] 'coupled' model and 3.5E-03, 7.6E-03 and 12E-03 for the [1] 'interface' model. For large scale compressive experimental test [40] evaluations, RMSE of the [154] model at 300 mm and 600 mm fault displacements are 0.3766 and 0.5018 respectively in comparison to 0.5528 and 0.6537 respectively for the [2] model.

A process employing Taguchi method to efficiently study several important parameters affecting the structural performance of pipeline undergoing fault-rupture deformations is presented. The Taguchi method is employed

to project the peak compressive and tensile strains generated for varying fault displacement values as well as to study the influence of the variation of the factors towards the peak projected strains. These peak strain values provide the strain demand. The research presents details of the method adopted and the analysis technique employed to obtain pipeline strain demand for a chosen pipe diameter and maximum internal pressure in concert with [22], as a case study. This analysis methodology is applicable to perform pipeline strain hazard analysis for buried energy pipelines due to fault rupture.

6.3 Taguchi's Method for Sensitivity Analysis

Buried continuous energy pipeline undergoing fault rupture displacement is a complex phenomenon and the pipeline response is expected to be highly non-linear. The effect of non-linear soil strength which includes pre-peak strain hardening followed by post-peak strain softening, on the pipeline response has not been studied till now. The influence of soil type on the pipeline response is also expected to be non-linear. [46] reported that with the increase in pipe diameter to wall thickness ratio, a reduction in peak compressive strain is noted. Contrary to that, a pipeline with higher diameter to wall thickness ratio is expected to undergo local buckling more readily, resulting in higher strains. In another study, [46] reported a reduction of compressive strain with the increase in pipe wall thickness. Hence, the effect of diameter to wall thickness ratio towards the maximum pipeline strains generated with increasing fault displacements can vary. [46] reported that, the faulting angle with respect to the pipe can have varying effects toward the pipeline failure. [172] showed that the relation between maximum compressive strain generated with the fault crossing angle is highly non-linear and characterized by significant variability. [173] reported that the critical fault displacement to initiate buckling increased with the increase in the internal pressure up to an optimum level, beyond which, the critical fault displacement decreased with the increase in internal pressure. [48] showed that, the influence of pipe internal pressure towards the maximum strains may vary depending on the value of other concerned parameters. Instead of a parametric analysis approach as conducted by [1, 17, 31–38, 40–46, 48–50, 52–55], the method proposed here consider all the important factors influencing the pipeline structural behavior in a comprehensive manner suitable for design purposes.

Figure 6.1 summarizes the proposed methodology. Firstly, the uncertain

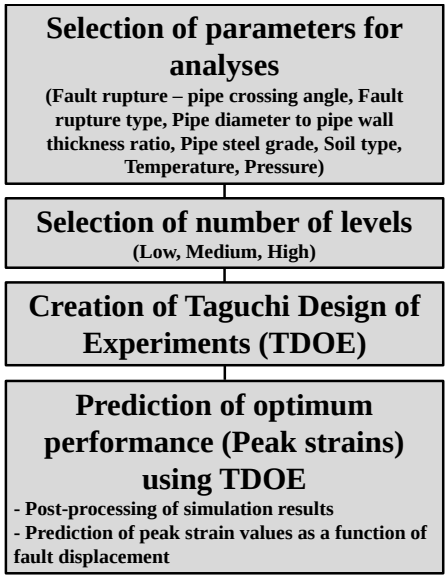

Figure 6.1: Analysis methodology using Taguchi design of experiments

factors affecting the pipeline response are to be identified, such as pipe-fault crossing angle, pipe geometric factors, soil and pipe material properties and pipe operating conditions. Range of steel grade, pipe wall thickness, operating temperature can be decided based on concerned design codes and project requirements. Likewise, range of soil types can be decided based on available data. Other important parameters, such as range of pipe-fault crossing angle and faulting types (Reverse/Normal, Strike-slip) can be decided based on regional seismological information.

Parametric analyses involving large numbers of factors and their respective levels are not feasible, considering a full factorial design given the computationally expensive nature of the complex FE models used. To overcome this, design of experiment employing Taguchi method is proposed. Basics of Taguchi method can be found in [106]. Taguchi method includes a series of orthogonal arrays to cover a wide range of experimental situations as well as methods to analyze results. Design of experiments using orthogonal arrays provide high experimental efficiency, however, are more suitable for cases where there is minimal interaction between the factors. Details of the method and analysis technique adopted to generate strain envelopes are explained here supported by a case study. After selecting concerned parameters, a set of experiment is planned based on Taguchi approach. Pipeline

undergoing fault rupture deformation being a complex mechanism and the non-linear pipeline response being characterized by significant variability as discussed, it's difficult to predict the appropriate combination of level for various factors involved, that may lead to maximum strains for increasing fault displacements. The Taguchi method allows for predicting the maximum strains possible at increasing values of fault displacement by projecting the maximum value of the compressive and tensile strains. Subsequently, these strain values at discrete fault displacement values are combined to generate maximum compressive and tensile strain envelope curves as a function of fault displacement.

The mixed level orthogonal array employed for this study consists of 6 factors of 3 levels each and one factor of 6 level. The array $A_{18}(6^1 by 3^6)$ considered for this study is a matrix of 18 rows and (1+6) = 7 columns in which the first 1 column has all the 6 elements and each of the next 6 columns have 3 elements each. Additionally, another property of this array is that, in every 2 columns all the ordered pairs of levels appear a fixed number of times. The construction of the array involves difference matrix, Kronecker sums, saturated orthogonal arrays and column replacement. Taguchi's $A_{18}(6^1 by 3^6)$ are based on [109] approach employing difference matrix D_6^3. A difference matrix D_6^3 is a 6 by 6 matrix whose columns have the property that the differences between any two columns is a column where each of the 3 elements occur equally often. Taguchi's D_6^3 matrix is given by Table 6.1 :

Table 6.1: Matrix 1

0	0	0	0	0	0
0	0	1	1	2	2
0	1	0	2	1	2
0	2	2	1	1	0
0	1	2	0	2	1
0	2	1	2	0	1

The Kronecker sum of a 6 by 6 difference matrix D6(3) and a 3 x 1 vector b of 3 elements, column vector (0,1,2) is a matrix of 6 x 3 = 18 rows and 6 columns created by adding the finite arithmetic from each element of the vector b to each element of the difference matrix D_6^3. Hence, the Kronecker sum can be determined as Table 6.2:

The matrix $A_{18}^{3^6}$ is further expressed as Table 6.3.

To generate the final target orthogonal array, a matrix is constructed, comprising of 6 times 3 = 18 rows. 6 columns of the matrix are created from the Kronecker sum of the generated D_6^3 difference matrix and column vector

Table 6.2: Matrix 2

0 + 0	0 + 0	0 + 0	0 + 0	0 + 0	0 + 0
0 + 1	0 + 1	0 + 1	0 + 1	0 + 1	0 + 1
0 + 2	0 + 2	0 + 2	0 + 2	0 + 2	0 + 2
0 + 0	0 + 0	1 + 0	1 + 0	2 + 0	2 + 0
0 + 1	0 + 1	1 + 1	1 + 1	2 + 1	2 + 1
0 + 2	0 + 2	1 + 2	1 + 2	2 + 2	2 + 2
0 + 0	1 + 0	0 + 0	2 + 0	1 + 0	2 + 0
0 + 1	1 + 1	0 + 1	2 + 1	1 + 1	2 + 1
0 + 2	1 + 2	0 + 2	2 + 2	1 + 2	2 + 2
0 + 0	2 + 0	2 + 0	1 + 0	1 + 0	0 + 0
0 + 1	2 + 1	2 + 1	1 + 1	1 + 1	0 + 1
0 + 2	2 + 2	2 + 2	1 + 2	1 + 2	0 + 2
0 + 0	1 + 0	2 + 0	0 + 0	2 + 0	1 + 0
0 + 1	1 + 1	2 + 1	0 + 1	2 + 1	1 + 1
0 + 2	1 + 2	2 + 2	0 + 2	2 + 2	1 + 2
0 + 0	2 + 0	1 + 0	2 + 0	0 + 0	1 + 0
0 + 1	2 + 1	1 + 1	2 + 1	0 + 1	1 + 1
0 + 2	2 + 2	1 + 2	2 + 2	0 + 2	1 + 2

Table 6.3: Matrix 3

0	0	0	0	0	0
1	1	1	1	1	1
2	2	2	2	2	2
0	0	1	1	2	2
1	1	2	2	0	0
2	2	0	0	1	1
0	1	0	2	1	2
1	2	1	0	2	0
2	0	2	1	0	1
0	2	2	1	1	0
1	0	0	2	2	1
2	1	1	0	0	2
0	1	2	0	2	1
1	2	0	1	0	2
2	0	1	2	1	0
0	2	1	2	0	1
1	0	2	0	1	2
2	1	0	1	2	0

Table 6.4: Matrix 4

0	0	0	0	0	0	0
0	1	1	1	1	1	1
0	2	2	2	2	2	2
1	0	0	1	1	2	2
1	1	1	2	2	0	0
1	2	2	0	0	1	1
2	0	1	0	2	1	2
2	1	2	1	0	2	0
2	2	0	2	1	0	1
3	0	2	2	1	1	0
3	1	0	0	2	2	1
3	2	1	1	0	0	2
4	0	1	2	0	2	1
4	1	2	0	1	0	2
4	2	0	1	2	1	0
5	0	2	1	2	0	1
5	1	0	2	0	1	2
5	2	1	0	1	2	0

given by (0,1,2). This matrix forms the columns 2 to 7 of the target matrix and is an $A_{18}^{3^6}$ matrix. Now, the target matrix is generated by adding column 1 to the previously constructed matrix. Column 1 is created consisting of three 1s, three 2s, three 3s, three 4s, three 5s and three 6s. The resulting saturated orthogonal array $A_{18}(6^1 by 3^6)$ is given as Table 6.4.

To project the maximum value of the desired performance output the following technique is adopted. For this problem, a total of 7 factors can be considered namely, 'A', 'B', 'C', 'D', 'E', 'F', 'G'. 'A' is fault-pipe crossing angle, 'B' is fault type, 'C' is wall thickness, 'D' is steel grade, 'E' is soil type, 'F' is temperature and 'G' is internal pressure. 'A' can be considered to comprise of 6 levels, 'B' to 'G' can be considered to consist of 3 levels each. Possible input corresponding to a specific factor along with its level can be expressed as say, 'A1'. 'A1' being the input corresponding to factor 'A' and level '1'. Average of the performance output from all the set of experiments consisting a particular set of factor and level say, factor 'A' and level '1' can be expressed as 'A1". For a given fault displacement, this parameter needs to be evaluated for all possible combinations of factors along with their respective levels. Subsequently, maximum values of the

parameter need to be stored for every factor and the corresponding levels influencing the maximum value need to be identified. The combination of the factors along with their respective levels influencing the maximum values define the optimum condition of input variables for a maximum desired performance output. Once the optimum condition of input variables is identified as say, 'A2'B3'C2'D3'E2'F1'G1", projected peak performance output can be expressed according to [106] as Equation 6.1:

$$O_{projected} = X/M + (A_2^{'} - X/M) + (B_3^{'} - X/M) + (C_2^{'} - X/M) + ... + (G_1^{'} - X/M) \tag{6.1}$$

where, 'X' is the sum of all the results and 'M' is the number of results.

6.4 Case study

The case study illustrates the proposed method using taguchi design of experiments to efficiently design buried pipelines faced with fault rupture hazard. To achieve this, the previously developed experimentally evaluated FE modelling technique by [154] is used. To consider for variations in some of the most influential input factors in an efficient manner, taguchi design of experiments is employed to obtain the strain envelope curves and to study influence of various factors towards the generated strains. NPS24 pipeline is considered for the case study. A maximum operational internal pressure of 9.1 MPa is selected and steel grades of Gr 290, Gr 386 and Gr 483 are selected. [22] is used to select a minimum wall thickness based on pressure design criteria considering the lowest grade from the selected steel grades. Subsequently, [22] is used to determine a maximum operating temperature of $47°C$.

6.4.1 Design of experiment using Taguchi method

A series of numerical experiments are first designed using taguchi method and subsequently performed to investigate the effects of various factors towards the structural performance of the pipeline. Structural performance measures considered are tensile and compressive strains. Since, the number of possible combinations for the input factors and their respective levels in a full-factorial experimental design is very large, a logical test plan involving orthogonal arrays based on Taguchi approach is adopted. The numerical simulations planned here are devoid of any repetitions for a specific test combination. To study the nonlinear effect of the factors a minimum of

three levels are considered for all the factors. Six levels are considered for the pipe-fault crossing angle factor to investigate a range of values. Hence, a mixed level array is employed. The design of experiment assumed that the factors are independent of one another. Hence, no interaction between the factors are considered.

The faulting mechanism type factor is assigned two levels namely, strike slip type and normal/reverse faulting type. The primary difference between these two categories is that, in the former, the rupture propagates from the lateral direction and the gravity load acts out of the bending plane of the pipe; where as in the later, the rupture propagates from the base and the gravity load acts in the bending plane of the pipe. The experimental design adopted here considers six three-level factors and one six-level factor. Hence, to accommodate two levels for the faulting type factor in the experiment plan, a degraded column approach is adopted, wherein the third level is replaced with reverse/normal type faulting. The taguchi design of experiment adopted can be found in the Table 6.5. To summarize, analyses parametric factors consisted of fault-pipe crossing angle (-33.33°, -20°, -6.67°, 6.67°, 20° and 33.33°); faulting type (Reverse/Normal and Strike-slip); pipe wall thickness (12.7 mm, 14.27 mm and 17.48 mm); steel grade (Gr 290, Gr 386 and Gr 483); soil type (soft sand, medium sand and dense sand); temperature ($0°C$, $23.5°C$ and $47°C$) and pressure (0 MPa, 4.6 MPa and 9.1 MPa).

6.4.2 Analysis of results using Taguchi method and development of envelope strain demand curves

Figure 6.2 to Figure 6.3 show plastic shear strain mobilized from the analyses conducted at various instances and locations. Structural response of the pipeline is evaluated in terms of the engineering demand parameters of interest namely, the maximum compressive strain and maximum tensile strain. Projection of peak values of engineering demand parameters are conducted for varying fault displacements. For simplicity, fault displacement magnitudes are discretized into a number of bins and peak strain values are projected for each of those bins. Peak strain envelopes are obtained as functions of fault displacements. Figure 6.6 shows the maximum tensile strains obtained from the 18 numerical analyses with increasing fault displacements. 9 of the 18 analyses showed no accumulation of noticeable compressive strains. Figure 6.6 also shows the maximum compressive strains obtained from 9 of the 18 numerical analyses with increasing fault displacements. Figure 6.6 presents the developed compressive strain envelope and

tensile strain envelope curves.

Under reverse faulting or compressive strike slip faulting, the pipe failed in buckling; whereas, under normal faulting and tensile strike-slip faulting the pipe failed in tensile rupture. Peak compressive strain is found to increase linearly with increase in fault displacement up to a certain level before assuming very large values. Its evident from the curve that with the onset of buckling, strains tend to reach very high values. Peak tensile strains are found to increase fairly linearly with increase in fault displacement before reaching a plateau and increasing thereafter. The nature resembles somewhat similarity to the steel stress-strain relation. Figure 6.4 and Figure 6.5 show influence of all the factors towards the generated peak compressive and tensile strains. Influence of a factor towards the generated strains are studied by keeping all other factors at a constant level. Case 1 corresponds to results where all other factors are at their lowest level and case 2 corresponds to results where all other factors are at their highest level. Results are obtained at two discrete fault displacement values of 300 mm and 750 mm.

Results on the variance analysis (ANOVA) to evaluate the relative influence of different input variables on the variance of the generated strains are provided in Table 6.6 and Table 6.7. Peak strains are extracted at discrete fault displacement values and variance analysis is performed for both compressive and tensile strains. Tables presenting the results for tensile strains and compressive strains are presented there. Pipe-fault crossing angle is identified as the most prominent factor influencing the variance of peak strains generated.

Strain response as a function of variation of the input factors are found to be non-linear in nature, as shown in Figure 6.4 and Figure 6.5. Figure 6.4 shows that, compressive strains increased significantly with the decrease in pipe-fault crossing angle and vice versa for the tensile strains. This is reasonable since, decrease in pipe-fault angle results in more contraction in the pipe and increase in pipe-fault angle results in more extension of the pipe. For compressive strains, reverse faulting resulted in higher strains in comparison to strike-slip faulting as shown in Figure 6.4. Higher strain levels resulted due to thinner pipe walls as shown in Figure 6.4 due to increase in severity of local failure with decrease in pipe wall thickness. Strain levels are found to decrease with increase in steel grade as shown in Figure 6.5 primarily due to sooner yield in the lower grades. However, the strain response is found to be varying mildly in relation to the steel grades. In general, higher peak strains are observed with the presence of internal pressure as shown in Figure 6.5 due to increase in severity of local failure zones in the

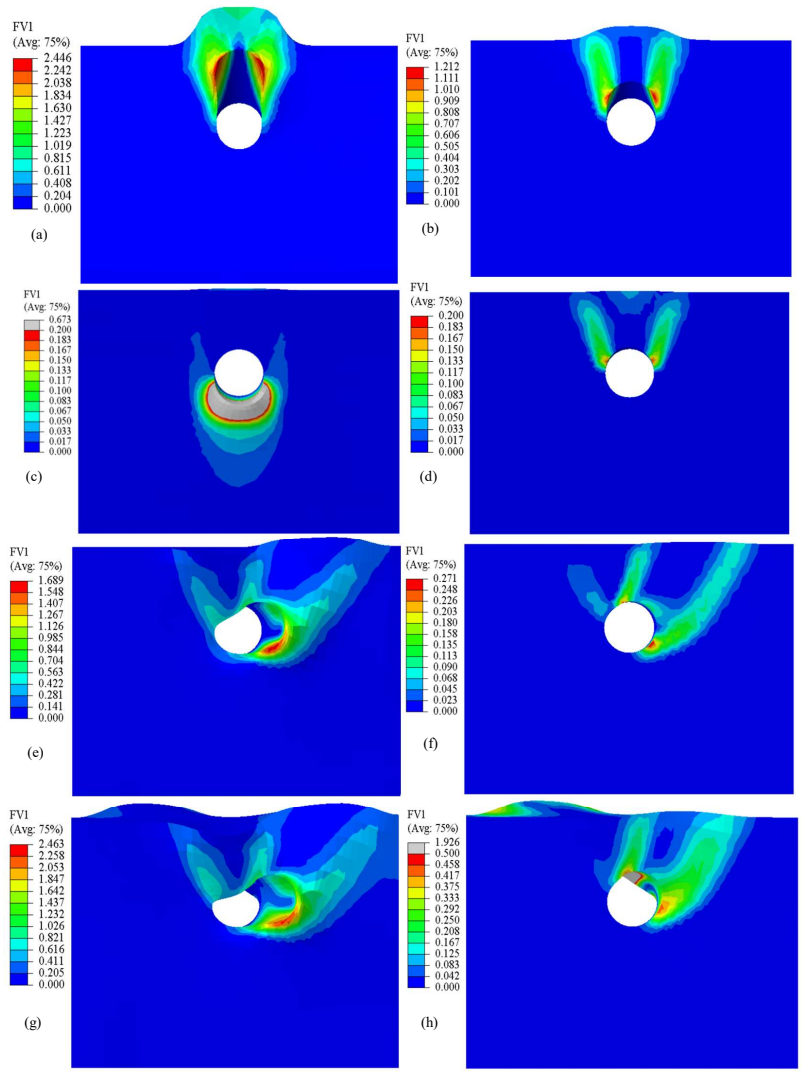

Figure 6.2: Plastic shear strain in sand corresponding to analysis 7 (a) at fault side 1 in the vicinity of the fault (b) at fault side 1, 5 m away from fault (c) at fault side 2 in the vicinity of the fault (d) at fault side 2, 5 m away from fault; analysis 8 (e) at fault side 1 in the vicinity of the fault (f) at fault side 1, 5 m away from fault (g) at fault side 2 in the vicinity of the fault (h) at fault side 2, 5 m away from fault

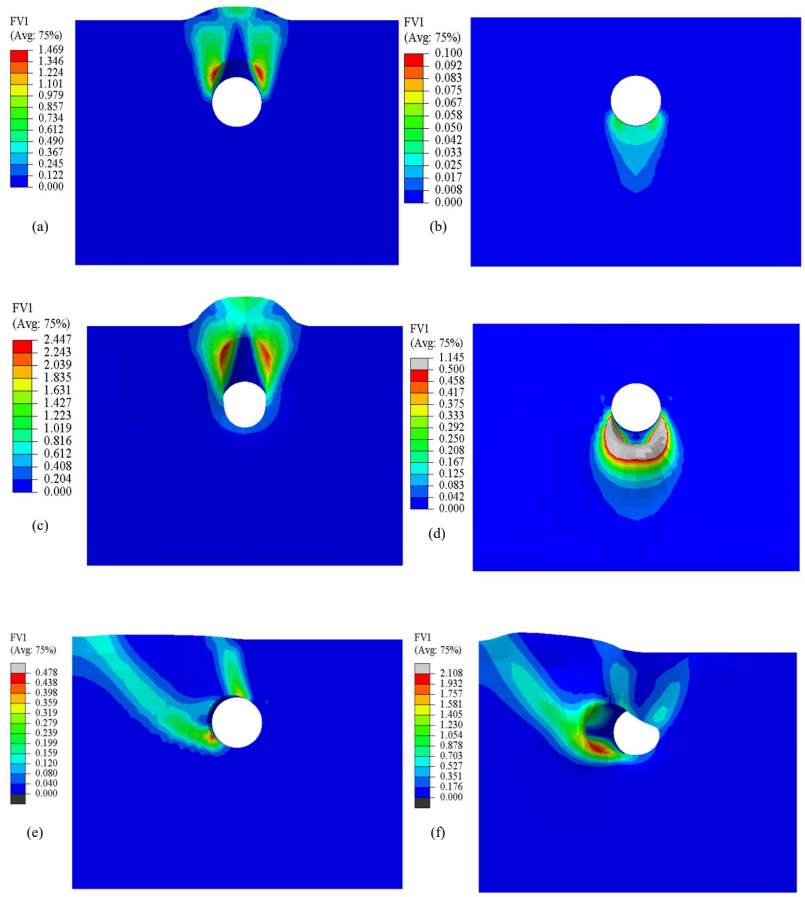

Figure 6.3: Plastic shear strain in sand corresponding to analysis 12 (a) at fault side 1 in the vicinity of the fault (b) at fault side 1, 5 m away from fault (c) at fault side 2 in the vicinity of the fault (d) at fault side 2, 5 m away from fault; analysis 11 (e) 5 m away from fault (f) at the vicinity of fault

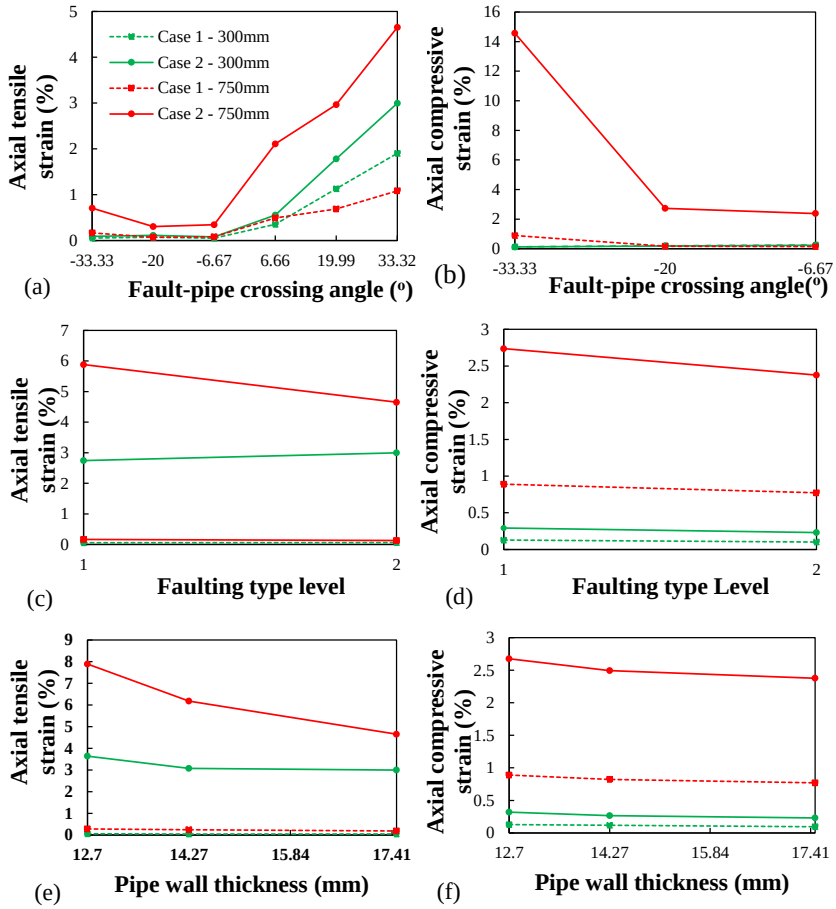

Figure 6.4: Influence of fault-pipe crossing angle on the peak axial strains generated at 300 mm and 750 mm fault displacements: (a) tensile strain (b) compressive strain; Influence of faulting type: (c) tensile strain (d) compressive strain; Influence of pipe wall thickness: (e) tensile strain (f) compressive strain

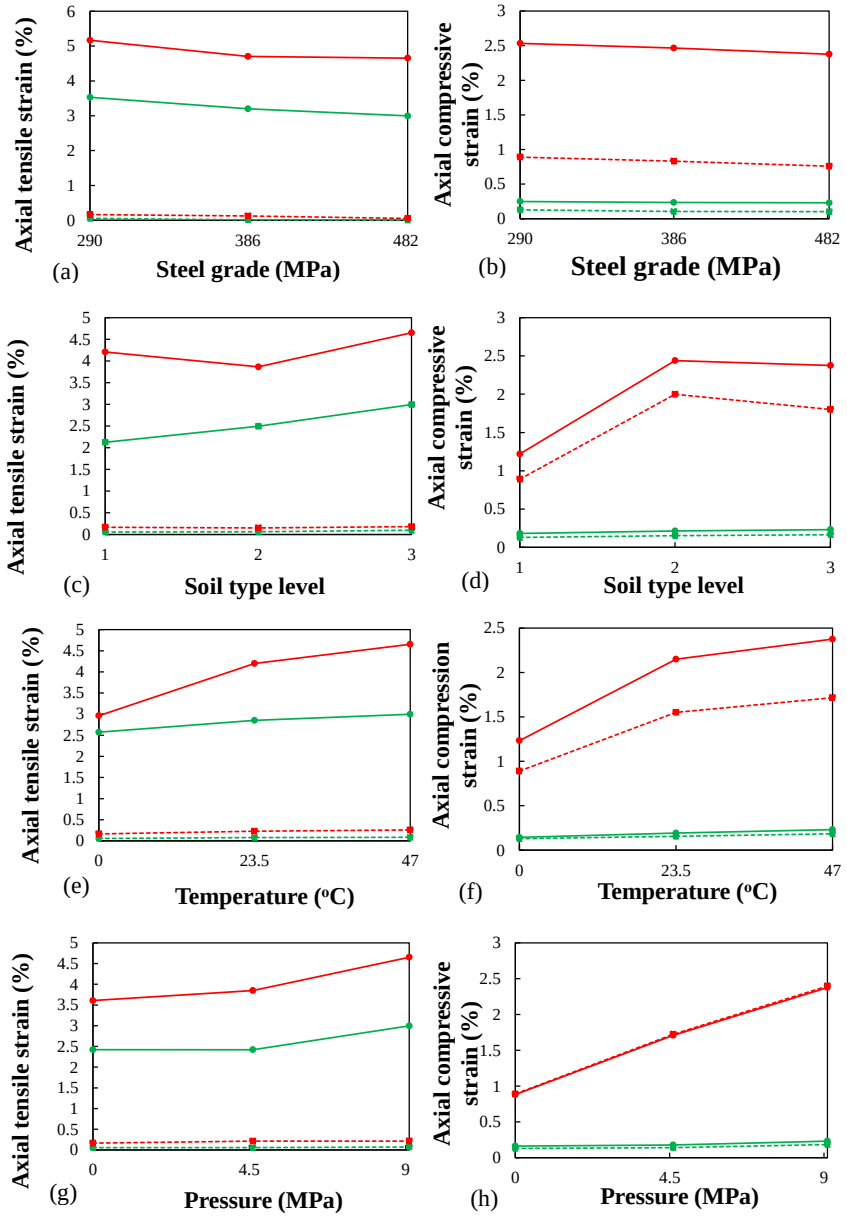

Figure 6.5: Influence of steel grade on the peak axial strains generated at 300 mm and 750 mm fault displacements: (a) tensile strain (b) compressive strain; Influence of soil type level: (a) tensile strain (b) compressive strain; Influence of temperature: (a) tensile strain (b) compressive strain; Influence of pressure: (a) tensile strain (b) compressive strain

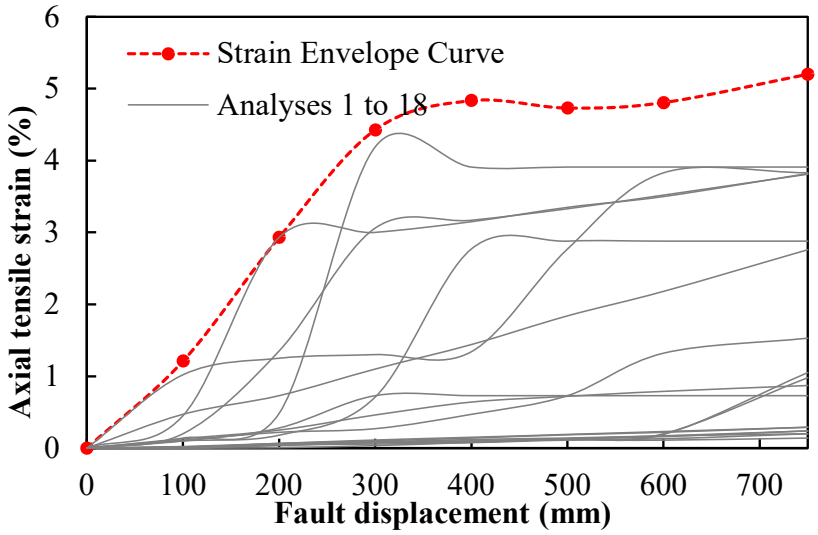

(a)

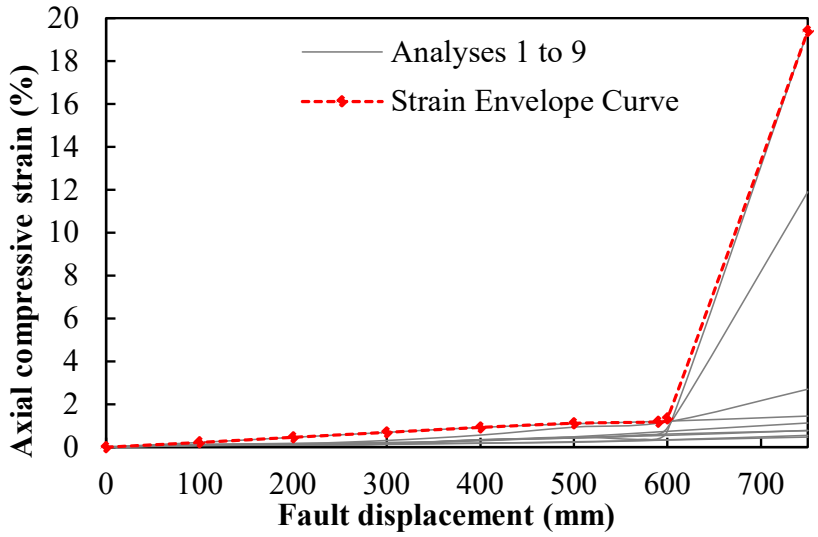

(b)

Figure 6.6: Peak strain envelope as a function of fault displacement: (a) tensile (b) compressive

Table 6.5: Taguchi design of experiment for the problem under consideration

Serial number	Fault-pipe crossing angle (degree)	Fault type	Wall thickness (mm)	Steel grade (MPa)	Soil type	Temperature (degree C)	Pressure (MPa)
1	-33.33	Reverse/Normal	12.7	290	Soft	0	0
2	-33.33	Strike Slip	14.27	386	Medium	23.5	4.6
3	-33.33	Reverse/Normal	17.48	483	Dense	47	9.1
4	-20	Reverse/Normal	12.7	386	Medium	47	9.1
5	-20	Strike Slip	14.27	483	Dense	0	0
6	-20	Reverse/Normal	17.48	290	Soft	23.5	4.6
7	-6.67	Reverse/Normal	14.27	290	Dense	23.5	9.1
8	-6.67	Strike Slip	17.48	386	Soft	47	0
9	-6.67	Reverse/Normal	12.7	483	Medium	0	4.6
10	6.67	Reverse/Normal	17.48	483	Medium	23.5	0
11	6.67	Strike Slip	12.7	290	Dense	47	4.6
12	6.67	Reverse/Normal	14.27	386	Soft	0	9.1
13	20	Reverse/Normal	14.27	483	Soft	47	4.6
14	20	Strike Slip	17.48	290	Medium	0	9.1
15	20	Reverse/Normal	12.7	386	Dense	23.5	0
16	33.33	Reverse/Normal	17.48	386	Dense	0	4.6
17	33.33	Strike Slip	12.7	483	Soft	23.5	9.1
18	33.33	Reverse/Normal	14.27	290	Medium	47	0

pipeline due to additional pressure load. Increase in temperature also led to higher strains as shown in Figure 6.5 due to similar reasons. At lower displacements of 300mm, pipe strains are found to increase with sand density as shown in Figure 6.5 since its expected that the majority of the soil is still in their pre-peak strain hardening phase. Higher sand density that is, soil strength results in higher pipe strains. Pipeline compressive strains are found to increase for medium dense sands in comparison to loose sands and then decrease for dense sands in comparison to medium dense sands for 750 mm fault displacements. This is caused by the non-linearity in the soil mobilized shear strength comprising of strain-hardening and strain-softening. Similar non-linear response is observed for 750 mm tensile strains where the strains first decrease and then increase with increase in soil strength.

6.5 Summary

An experimentally evaluated FE model for buried continuous pipeline undergoing fault rupture deformations is adopted. Thereafter, nonlinear 3D FE analyses of buried continuous energy pipelines under fault displacement loads considering variation in faulting mechanism, such as reverse faulting, normal faulting and strike slip faulting, variation in sand type, pipe wall thickness, pipe steel grade, internal pressure, temperature are performed to evaluate the structural performance of a typical oil and gas steel buried pipeline. The analyses provided information on the tensile and compressive strain demands on the buried pipeline. The findings of the study can be

Table 6.6: ANOVA analysis results for axial tensile strains

Fault displacement (mm)	Factor	Degrees of freedom	Sum of squares	Variance	Contribution (%)
100	Pipe-fault crossing angle	5	0.559	0.111	49.14
	Fault type	1	0.069	0.069	6.12
	Wall thickness	2	0.121	0.060	10.65
	Steel grade	2	0.031	0.015	2.75
	Soil type	2	0.031	0.015	2.76
	Temperature	2	0.137	0.068	12.08
	Pressure	2	0.130	0.065	11.48
	Error	1	0.056	0.056	4.99
200	Pipe-fault crossing angle	5	5.005	1.001	53.56
	Fault type	1	0.572	0.572	6.13
	Wall thickness	2	0.198	0.099	2.12
	Steel grade	2	0.992	0.496	10.62
	Soil type	2	1.017	0.508	10.89
	Temperature	2	0.159	0.079	1.70
	Pressure	2	0.995	0.497	10.65
	Error	1	0.402	0.402	4.30
300	Pipe-fault crossing angle	5	18.904	3.780	70.50
	Fault type	1	0.054	0.054	0.20
	Wall thickness	2	1.947	0.973	7.26
	Steel grade	2	1.886	0.943	7.03
	Soil type	2	2.035	1.017	7.59
	Temperature	2	1.841	0.920	6.86
	Pressure	2	0.138	0.069	0.51
	Error	1	0.005	0.005	0.02
400	Pipe-fault crossing angle	5	19.219	3.843	66.42
	Fault type	1	0.085	0.085	0.29
	Wall thickness	2	0.953	0.476	3.29
	Steel grade	2	3.375	1.687	11.66
	Soil type	2	2.717	1.358	9.39
	Temperature	2	1.498	0.749	5.17
	Pressure	2	0.611	0.305	2.11
	Error	1	0.473	0.473	1.63
500	Pipe-fault crossing angle	5	23.841	4.768	72.28
	Fault type	1	0.476	0.476	1.44
	Wall thickness	2	0.934	0.467	2.83
	Steel grade	2	3.502	1.751	10.62
	Soil type	2	3.341	1.670	10.13
	Temperature	2	0.540	0.270	1.63
	Pressure	2	0.229	0.114	0.69
	Error	1	0.114	0.114	0.34
600	Pipe-fault crossing angle	5	28.352	5.670	74.24
	Fault type	1	1.102	1.102	2.88
	Wall thickness	2	0.985	0.492	2.58
	Steel grade	2	3.964	1.982	10.38
	Soil type	2	3.308	1.654	8.66
	Temperature	2	0.360	0.180	0.94
	Pressure	2	0.116	0.058	0.30
	Error	1	0.00	0.00	0.00
750	Pipe-fault crossing angle	5	28.408	5.681	74.34
	Fault type	1	1.295	1.295	3.39
	Wall thickness	2	0.891	0.445	2.33
	Steel grade	2	4.801	2.400	12.56
	Soil type	2	1.990	0.995	5.21
	Temperature	2	0.596	0.298	1.56
	Pressure	2	0.128	0.064	0.33
	Error	1	0.099	0.099	0.25

summarized as follows:

(1) Design of buried continuous pipelines faced with permanent ground deformation hazard due to fault rupture can be conducted using a Taguchi design of experiment approach considering variations in influential factors affecting pipeline response.

(2) The projection of peak performance approach employed using Taguchi design of experiments is an efficient way of estimating peak strain demands for tensile as well as compressive strains.

(3) Only 18 analysis are carried out instead of a full factorial design of total 2916 possible combinations to arrive at the peak strain demands for increasing fault displacement magnitudes.

(4) Maximum compressive strain envelope generated from a case study for NPS 24 pipe from Taguchi design of experiment showed linearly increasing strains up to 1.33 percent for approximately 600 mm displacement and increasing sharply thereafter. Maximum tensile strain envelope generated for the same case study showed a linear increase in strains up to 4.42 percent for 300 mm fault displacement followed by a plateau and further increase from 5.2 percent at 750 mm fault displacement.

(5) Analysis of variance showed that pipe-fault crossing angle is the most influential factor affecting the variance in pipeline strains generated.

Table 6.7: ANOVA analysis results for axial compressive strains

Fault displacement (mm)	Factor	Degrees of freedom	Sum of squares	Variance	Contribution (%)
100	Pipe-fault crossing angle	5	0.059	0.011	84.27
	Fault type	1	0.000	0.000	0.19
	Wall thickness	2	0.003	0.001	4.26
	Steel grade	2	0.001	0.000	2.73
	Soil type	2	0.002	0.001	2.82
	Temperature	2	0.002	0.001	3.53
	Pressure	2	0.000	0.000	0.86
	Error	1	0.000	0.000	1.29
200	Pipe-fault crossing angle	5	0.157	0.031	69.36
	Fault type	1	0.003	0.003	1.70
	Wall thickness	2	0.013	0.006	6.06
	Steel grade	2	0.008	0.004	3.88
	Soil type	2	0.012	0.006	5.44
	Temperature	2	0.009	0.004	4.38
	Pressure	2	0.012	0.006	5.36
	Error	1	0.008	0.008	3.78
300	Pipe-fault crossing angle	5	0.314	0.062	61.96
	Fault type	1	0.017	0.017	3.49
	Wall thickness	2	0.026	0.013	5.17
	Steel grade	2	0.024	0.012	4.88
	Soil type	2	0.023	0.011	4.67
	Temperature	2	0.023	0.011	4.54
	Pressure	2	0.045	0.022	8.95
	Error	1	0.032	0.032	6.30
400	Pipe-fault crossing angle	5	0.705	0.141	64.65
	Fault type	1	0.051	0.051	4.70
	Wall thickness	2	0.032	0.016	2.98
	Steel grade	2	0.053	0.026	4.92
	Soil type	2	0.027	0.013	2.51
	Temperature	2	0.049	0.024	4.54
	Pressure	2	0.106	0.053	9.76
	Error	1	0.064	0.064	5.91
500	Pipe-fault crossing angle	5	1.296	0.259	67.18
	Fault type	1	0.112	0.112	5.82
	Wall thickness	2	0.044	0.022	2.32
	Steel grade	2	0.050	0.025	2.63
	Soil type	2	0.053	0.026	2.76
	Temperature	2	0.057	0.028	2.96
	Pressure	2	0.220	0.110	11.44
	Error	1	0.093	0.093	4.85
600	Pipe-fault crossing angle	5	2.354	0.470	74.02
	Fault type	1	0.086	0.086	2.70
	Wall thickness	2	0.108	0.054	3.40
	Steel grade	2	0.052	0.026	1.64
	Soil type	2	0.149	0.074	4.70
	Temperature	2	0.080	0.040	2.52
	Pressure	2	0.252	0.126	7.94
	Error	1	0.097	0.097	3.05
750	Pipe-fault crossing angle	5	266.191	53.238	59.78
	Fault type	1	0.004	0.004	0.00
	Wall thickness	2	21.647	10.823	4.86
	Steel grade	2	28.260	14.130	6.34
	Soil type	2	33.094	16.547	7.43
	Temperature	2	34.026	17.013	7.64
	Pressure	2	39.602	19.801	8.89
	Error	1	22.386	22.386	5.02

Chapter 7

Summary and Conclusions

7.1 Summary

The overall purpose of this research is to develop an improved and robust method for seismic risk assessment of buried continuous energy pipelines subjected to fault rupture permanent ground deformations, considering uncertainty at various levels. The specific objectives met for this research are as follows:

1. Conducted a state-of-the art literature review of existing approaches to study pipeline structural behavior undergoing fault rupture deformations, as well as a literature review of existing easy to use soil (sand) constitutive relations. This includes review of approaches to evaluate pipeline response using analytical approaches, simplified numerical approaches and complex numerical approaches. Additional literature review are conducted on available approaches to model nonlinear mobilized soil strength properties as well as dilatancy properties.

2. Developed an experimentally evaluated FE model for soil non-linear material property and developed an experimentally evaluated detailed 3D FE model of pipeline undergoing fault rupture deformations. To do so, first a nonlinear Mohr-Coulomb soil model is implemented in FE software ABAQUS. Thereafter nonlinear mobilized soil strength and dilation behavior is incorporated in ABAQUS. Axis-symmetric uni-element is used to evaluate the model against triaxial test results for sand. Finally, this developed soil model is suitably fed with soil material properties from a large scale pipeline-soil fault rupture test and used to evaluate a FE model of pipeline undergoing fault rupture against large scale experimental tests.

3. Conducted a state-of-the art literature review of existing methods for uncertainty quantification and propagation as well as multi-fidelity-based approaches for uncertainty quantification. A detailed review on Monte Carlo simulation, surrogate based approaches and multi-fidelity surrogate approaches for uncertainty quantification is carried out.

4. Developed a multi-fidelity-based uncertainty quantification approach for buried pipeline undergoing fault rupture deformations. This includes

identifying suitable machine learning techniques applicable to this problem and implementing suitable methods for pipeline response uncertainty quantification. In this study a multi-fidelity Gaussian processes based method is used. Specifically, Gaussian processes regression has been used. Gaussian processes are probability distribution over functions and generalize multivariate Gaussian distributions. To achieve this, small number of data from HF models which are computationally expensive but yield highly accurate results and data from large numbers of LF models which are computationally cheap but yield approximate results are utilized. The approach combines the accuracy of hi-fidelity models with the efficiency of LF models to predict nearly accurate results in a reasonably efficient manner.

5. Conducted a state-of-the art literature review of existing approaches to probabilistically predict permanent ground deformation due to fault rupture. This includes review of regression equation based methods to quantify fault rupture induced ground deformations as well as review of stochastic source modelling based method to predict fault rupture induced ground deformations. Additionally, literature review on existing methods to quantify seismic risk to buried pipelines due to fault rupture induced permanent ground deformations are also studied.

6. Probabilistically estimated ground deformation hazard at a given region and integrate it with pipeline structural performance to determine pipeline strain hazard. The integrated pipeline seismic risk assessment methodology is first established and illustrated with a case study for the city of Victoria gas pipelines.

The integrated seismic risk assessment approach utilizes seismological information of the regional fault to stochastically model the earthquake source and thereafter use Okada equations to analytically compute probabilistic regional ground deformations. Additionally, the method utilizes site specific soil information, pipeline orientation, pipeline structural and operating properties, computed probabilistic differential ground deformation in a multi-fidelity analysis framework to quantify uncertainty in pipeline response. The multi-fidelity Gaussian processes uncertainty quantification includes one of the variable input parameters as the site specific differential ground deformation derived from the computed probabilistic differential ground deformation, thereby integrating the two studies.

7.2 Conclusions

1. Nonlinear material model for sand provided a match with experimental results. An RMSE of 0.0036 is achieved with the current study instead of existing 0.0392 [68]. Additionally, the pipe-soil FE model is found to predict large scale tensile experimental results with high accuracy. At 300 mm displacement for the large scale test, an RMSE of 0.0017 is achieved in comparison to previous 0.0031 and 0.0035 for the 'coupled' and 'interface' model by [1]. At 600 mm displacement for the large scale test, an RMSE of 0.0041 is achieved in comparison to previous 0.0059 and 0.0076 for the 'coupled' and 'interface' model by [1]. At 900 mm displacement for the large scale test, an RMSE of 0.0044 is achieved in comparison to previous 0.0094 and 0.012 for the 'coupled' and 'interface' model by [1].

2. The nonlinear sand material model is found to have negligible dependence on mesh size and aspect ratio of the elements. Both the material model as well as the pipe-soil model is found to provide better results compared to available numerical results.

3. Coefficient of determinations of 0.897, 0.944 and 0.924 are achieved between HF observed values and multi-fidelity model predicted values during cross-evaluation of results, there by establishing the validity of the multi-fidelity model. A significant savings of computational effort is achieved where 15 minutes run are used instead of 48 hours run for a total of 500 analyses using 3.2GHz processor and 32 GB RAM.

4. Probabilistic regional ground deformation approach is subsequently linked with multi-fidelity uncertainty quantification model to derive seismic risk of pipelines. The practical implications of this is significant. The method allows for quantifying uncertainty in pipeline response due to permanent ground deformation hazard arising out of fault rupture over a wide region. Uncertainty is considered in pipe response as well as fault rupture.

5. A method employing Taguchi Design of Experiments is successfully used to design pipelines faced with the risk of permanent ground deformations. The method predicted peak tensile strains and peak compressive strains as a function of differential ground deformation between the two ends of the pipe for a varying set of input parameters. Additionally, the most influential parameters are identified. The pipe-fault crossing angle is identified as the most influential factor affecting the variance in pipeline strains generated. The method has significant computational benefits as only 18 analyses are carried out instead of a full factorial 2916 possible combinations to arrive at the peak strain demands with increasing differential ground deformations.

Bibliography

[1] D. J. Robert, , K. Soga, T. D. O'Rourke, Pipelines subjected to fault movement in dry and unsaturated soils, International Journal of Geomechanics 16 (5) (2016) 1–16. → pages xii, 10, 11, 12, 26, 41, 49, 86, 105, 106, 125

[2] X. Xie, Numerical analysis and evaluation of buried pipeline response to earthquake-induced ground fault rupture, Rensselaer Polytechnic Institute, 2008. → pages xiii, 26, 41, 42, 44, 105

[3] K. Morell, C. Regalla, C. Amos, S. Bennett, L. Leonard, A. Graham, T. Reedy, V. Levson, A. Telka, Holocene surface rupture history of an active forearc fault redefines seismic hazard in southwestern british columbia, canada, Geophysical Research Letters 45 (21) (2018) 11–605. → pages xiv, 85, 94

[4] American Lifelines Alliance - Guidelines for the Deign of Buried Steel Pipe (2005). → pages xv, 52, 82, 88, 91, 92, 103

[5] O. Roueke, J. Michael, X. Liu, Response of buried pipelines subjected to earthquake effects, Multidisciplinary Centre for Earthquake Engineering Research, Monograph Series 13 (3) (1999). → pages 1

[6] M. O'Rourke, G. Ayala, Pipeline damage due to wave propagation, Journal of Geotechnical Engineering 119 (9) (1993) 1490–1498. → pages 2

[7] T. O'ROURKE, Effect of lateral spreading on buried pipelines during the 1971 san fernando earthquake, earthquake behavior and safety of oil gas strage facilities, Buried Pipelines and Equipment, PVP 77 (1983) 124–132. → pages 2

[8] T. Datta, Seismic response of buried pipelines: a state-of-the-art review, Nuclear engineering and design 192 (2-3) (1999) 271–284. → pages 2

[9] G. Taleb-Agha, Seismic risk analysis of lifeline networks, Bulletin of the Seismological Society of America 67 (6) (1977) 1625–1645. → pages 2

[10] B. Erel, G. M. Patelunas, J. E. Niece, I. J. Oppenheim, Measuring the earthquake performance of urban water systems, in: The current state of knowledge of lifeline earthquake engineering, ASCE, 1977, pp. 183–198. → pages

[11] I. J. Oppenheim, Vulnerability of transportation and water systems to seismic hazard methodology for hazard cost evaluation, in: The current state of knowledge of lifeline earthquake engineering, ASCE, 1977, pp. 394–409. → pages

[12] J. Mohammadi, A. H. Ang, Seismic hazard analysis of lifelines, Journal of the Structural Division 108 (6) (1982) 1232–1249. → pages

[13] H. Monzón-Despang, H. C. Shah, Seismic risk analysis of infrastructural systems, Journal of the Technical Councils of ASCE 108 (1) (1982) 10–23. → pages

[14] G. Atkinson, A. Davenport, M. Novak, Seismic risk to pipelines with application to northern canada, Canadian Journal of Civil Engineering 9 (2) (1982) 248–264. → pages

[15] M. Shinozuka, S. Takada, H. Ishikawa, Some aspects of seismic risk analysis of underground lifeline systems (1979). → pages

[16] R. V. Whitman, K. H. Hein, Damage probability for a water distribution system, in: The current state of knowledge of lifeline earthquake engineering, ASCE, 1977, pp. 410–423. → pages 2

[17] V. E. Melissianos, G. P. Korakitis, C. J. Gantes, G. D. Bouckovalas, Numerical evaluation of the effectiveness of flexible joints in buried pipelines subjected to strike-slip fault rupture, Soil Dynamics and Earthquake Engineering 90 (2016) 395–410. → pages 2, 10, 12, 23, 51, 106

[18] V. E. Melissianos, D. Vamvatsikos, C. J. Gantes, Performance Assessment of Buried Pipelines at Fault Crossings*, Earthquake Spectra 33 (1) (2017) 201–218. → pages 12, 23, 82, 86, 89

[19] → pages 2, 23, 82, 89

[20] G. Bridge, B. Özkaynak, E. Turhan, Energy infrastructure and the fate of the nation: Introduction to special issue, Energy research & social science 41 (2018) 1–11. → pages 8

[21] M. O'Rourke, X. Liu, Seismic design of buried and offshore pipelines: Monograph 4 (2012). → pages 8

[22] CAN/CSA-Z662-15, Oil and gas pipeline syatems, 2015. → pages 8, 50, 56, 106, 111

[23] Gas Transmission and Distribution Piping Systems, asme b31.8 Edition, The American Society of Mechanical Engineers, 2018. → pages 8

[24] Pipeline Transportation Systems for Liquids and Slurries, asme b31.4 Edition, The American Society of Mechanical Engineers, 2016. → pages 8

[25] Eurocode 8 - Design of Structures for Earthquake Resistance - Part 4: Silos, tanks and Pipelines, Tech. rep., European Committee for Standardization, Brussels, Belgium (2006). → pages 8

[26] C-CORE, I. , D.G. Honegger Consulting SSD, Guidelines for Constructing Natural Gas and Liquid Hydrocarbon Pipelines Through Areas Prone to Landslide and Subsidence Hazards., Tech. Rep. January, Pipeline Research Council International (2009). → pages 8, 10

[27] American Lifelines Alliance - Guidelines for the Deign of Buried Steel Pipe. → pages 8

[28] Newmark NM and Hall WJ, Pipeline design to resists large fault displacement, in: Proceedings of the US national conference on earthquake engineering, 1975, pp. 416–25. → pages 9, 12

[29] C. A. Kennedy RP, W. RA, Fault movement effects on buried oil pipeline., Journal of Transportation Engineering (ASCE 1977) (1977) 103:617–33. → pages 9, 12

[30] Wang LRL and Yeh YH, A refined seismic analysis and design of buried pipeline for fault movement., Earthquake Engineering and Structural Dynamics (1985) 13:75–96. → pages 10, 12

[31] D. K. Karamitros, G. D. Bouckovalas, G. P. Kouretzis, Stress analysis of buried steel pipelines at strike-slip fault crossings, Soil Dynamics

and Earthquake Engineering 27 (3) (2007) 200–211. → pages 10, 12, 106

[32] D. K. Karamitros, G. D. Bouckovalas, V. Kouretzis, G. P. and Gkesouli, An analytical method for strength verification of buried steel pipelines at normal fault crossings, Soil Dynamics and Earthquake Engineering 31 (11) (2011) 1452–1464. → pages 10, 12

[33] O. V. Trifonov, V. P. Cherniy, A semi-analytical approach to a nonlinear stress-strain analysis of buried steel pipelines crossing active faults, Soil Dynamics and Earthquake Engineering 30 (11) (2010) 1298–1308. → pages 10, 12

[34] G. C. Sarvanis, S. A. Karamanos, Analytical model for the strain analysis of continuous buried pipelines in geohazard areas, Engineering Structures 152 (1 December 2017) (2017) 57–69. → pages 10, 12, 49, 51, 86

[35] T. H. Abdoun, D. Ha, M. J. O'Rourke, M. D. Symans, T. D. O'Rourke, , M. C. Palmer, H. E. Stewart, Factors influencing the behavior of buried pipelines subjected to earthquake faulting, Soil Dynamics and Earthquake Engineering 29 (3) (2009) 415–427. → pages 10, 12

[36] D. Ha, T. H. Abdoun, M. J. O'Rourke, M. D. Symans, T. D. O'Rourke, M. C. Palmer, H. E. Stewart, Centrifuge modeling of earthquake effects on buried high-density polyethylene (HDPE) pipelines crossing fault zones, Journal of Geotechnical and Geoenvironmental Engineering 134 (10) (2008) 1501–1515. → pages 10, 12

[37] D. Ha, T. H. Abdoun, M. J. O'Rourke, M. D. Symans, T. D. O'Rourke, , M. C. Palmer, H. E. Stewart, Earthquake faulting effects on buried pipelines - Case history and centrifuge study, Journal of Earthquake Engineering 14 (5) (2010) 646–669. → pages 10, 12

[38] M. Moradi, M. Rojhani, A. Galandarzadeh, S. Takada, Centrifuge modeling of buried continuous pipelines subjected to normal faulting, Earthquake Engineering and Engineering Vibration 12 (1) (2013) 155–164. → pages 10, 12, 106

[39] Cornell University- RPI, NEESR-SG Final Report (2009) 50. → pages 10, 12, 26

[40] T. D. O'Rourke, Geohazards and large, geographically distributed systems, Geotechnique 60 (7) (2010) 505–543. → pages 10, 12, 27, 38, 39, 105, 106

[41] H. H. Jalali, F. R. Rofooei, N. K. A. Attari, , S. Masoud, Experimental and finite element study of the reverse faulting effects on buried continuous steel gas pipelines, Soil Dynamics and Earthquake Engineering 86 (2016) 1–14. → pages 10, 12, 49, 86

[42] H. Hojat Jalali, F. R. Rofooei, N. Khajeh Ahmad Attari, Performance of Buried Gas Distribution Pipelines Subjected to Reverse Fault Movement, Journal of Earthquake Engineering 22 (6) (2018) 1068–1091. → pages 10, 12

[43] F. R. Rofooei, N. K. A. Attari, H. Hojat Jalali, New Method of Modeling the Behavior of Buried Steel Distribution Pipes Subjected to Reverse Faulting, Journal of Pipeline Systems Engineering and Practice 9 (1) (2018) 04017029. → pages 10, 12, 49, 86

[44] H. E. Demirci, S. Bhattacharya, D. Karamitros, N. Alexander, Experimental and numerical modelling of buried pipelines crossing reverse faults, Soil Dynamics and Earthquake Engineering 114 (January) (2018) 198–214. → pages 10, 12, 49, 86

[45] J. M. Eidinger, M. O'Rourke, J. Bachhuber, Performance of pipelines at fault crossings, in: Proceedings of the 7th US National Conference of Earthquake Engineering, Earthquake Engineering Research Institute (EERI), July, 2002, pp. 21–25. → pages 10, 12, 51, 86

[46] S. Joshi, A. Prashant, , A. Deb, S. K. Jain, Analysis of buried pipelines subjected to reverse fault motion, Soil Dynamics and Earthquake Engineering 31 (7) (2011) 930–940. → pages 10, 12, 51, 86, 106

[47] B. Dezhkam, A. Z. Nouri, Dynamic response of nanoparticle-water pipes buried in the soil subjected to far-fault earthquake using numerical method, Soil Dynamics and Earthquake Engineering 113 (October 2018) (2018) 174–179. → pages 10

[48] P. Vazouras, S. A. Karamanos, P. Dakoulas, Mechanical behavior of buried steel pipes crossing active strike-slip faults, Soil Dynamics and Earthquake Engineering 41 (2012) 164–180. → pages 10, 12, 49, 86, 106

[49] P. Vazouras, P. Dakoulas, K. A., Spyros, Pipe-soil interaction and pipeline performance under strike-slip fault movements, Soil Dynamics and Earthquake Engineering 72 (2015) 48–65. → pages 12

[50] P. Vazouras, , S. A. Karamanos, D. Panos, Finite element analysis of buried steel pipelines under strike-slip fault displacements, Soil Dynamics and Earthquake Engineering 30 (11) (2010) 1361–1376. → pages 12, 49, 86, 106

[51] N. K. Psyrras, A. G. Sextos, Safety of buried steel natural gas pipelines under earthquake-induced ground shaking: A review, Soil Dynamics and Earthquake Engineering 106 (March 2018) (2018) 254–277. → pages

[52] O. V. Trifonov, Numerical Stress-Strain Analysis of Buried Steel Pipelines Crossing Active Strike-Slip Faults with an Emphasis on Fault Modeling Aspects, Journal of Pipeline Systems Engineering and Practice 6 (1) (2015) 04014008. → pages 12, 49, 86, 106

[53] M. Fadaee, F. Farzaneganpour, I. Anastasopoulos, Response of buried pipeline subjected to reverse faulting, Soil Dynamics and Earthquake Engineering 132 (2020) 106090. → pages 11, 12, 49

[54] G. Banushi, N. Squeglia, K. Thiele, Innovative analysis of a buried operating pipeline subjected to strike-slip fault movement, Soil Dynamics and Earthquake Engineering 107 (2018) 234–249. → pages 12

[55] A. Tsatsis, M. Loli, G. Gazetas, Pipeline in dense sand subjected to tectonic deformation from normal or reverse faulting, Soil Dynamics and Earthquake Engineering 127 (2019) 105780. → pages 10, 11, 12, 49, 86, 106

[56] K. Mitchell, J.K. and Soga, Fundamentals of soil behavior, 3rd Edition, John Wiley & Sons, Hoboken, 2005. → pages 11, 31, 38, 51, 88

[57] P. A. and Vermeer, R. De Borst, Non-Associated Plasticity for Soils, Concrete and Rock., Heron 29 (3) (1984) 29(3):164. → pages 11, 31, 50

[58] S. T. and Hsu, H. J. Liao, Uplift behaviour of cylindrical anchors in sand, Canadian Geotechnical Journal 35 (1) (1998) 70–80. → pages 11, 31, 32, 51, 88

[59] D. Guo, P., and Stolle, Lateral pipe-soil interaction in sand with reference to scale effect, J. of Geotech. & Geoenviron. Eng., ASCE (2005) 131(3), 338349. → pages 11, 31

[60] N. Daiyan, S. Kenny, , R. Phillips, R. Popescu, Investigating pipeline-soil interaction under axial-lateral relative movements in sand, Canadian Geotechnical Journal 48 (11) (2011) 1683–1695. → pages 11, 31

[61] M. D. Bolton, The strength and dilatancy of sands, Géotechnique 36 (1) (1986) 65–78. → pages 11, 31, 32, 38, 39, 88

[62] K. H. Roscoe, The Influence of Strains in Soil Mechanics, Géotechnique 20 (2) (1970) 129–170. → pages 11

[63] I. Vardoulakis, B. Graf, Calibration of constitutive models for granular materials using data from biaxial experiments, Géotechnique 35 (3) (1985) 299–317. → pages 11

[64] W. Huang, K. Nübel, E. Bauer, Polar extension of a hypoplastic model for granular materials with shear localization, Mechanics of Materials 34 (9) (2002) 563–576. → pages 11

[65] D. Loukidis, R. Salgado, Analysis of the shaft resistance of non-displacement piles in sand, Géotechnique 58 (4) (2008) 283–296. → pages 11, 30

[66] P. Guo, Critical length of force chains and shear band thickness in dense granular materials, Acta Geotechnica 7 (1) (2012) 41–55. → pages 11, 30

[67] I. Anastasopoulos, G. Gazetas, M. Asce, M. F. Bransby, , M. C. Davies, A. El Nahas, Fault rupture propagation through sand: Finite-element analysis and validation through centrifuge experiments, Journal of Geotechnical and Geoenvironmental Engineering 133 (8) (2007) 943–958. → pages 11, 30, 50

[68] Kshama Roy, Numerical modelling of pipe-soil and anchor-soil interactions in dense sand, Ph.D. thesis, Memorial University of Newfoundland (2018). → pages 11, 30, 31, 37, 43, 49, 88, 105, 125

[69] S. L. Babu, A. Srivastava, Reliability analysis of buried flexible pipe-soil systems, Journal of Pipeline Systems Engineering and Practice 1 (1) (2010) 33–41. → pages 12, 88, 89

[70] Y. Chai, T. Zhao, Y. Chai, T. Zhao, Probability of upheaval buckling for subsea pipeline considering uncertainty factors, Ships and Offshore Structures 0 (0) (2018) 1–7. → pages 12

[71] Z. J. Westgate, W. Haneberg, D. J. White, Modelling spatial variability in as-laid embedment for high pressure and high temperature (HPHT) pipeline design 1 1865 (April) (2016) 1853–1865. → pages 12, 88, 89

[72] Z. S. Xi, W. Ying, Reliability analysis of buried polyethylene pipeline subject to traffic loads 11 (8) (2019) 1–11. → pages 12

[73] A. Nazari, P. Rajeev, J. G. Sanjayan, Offshore pipeline performance evaluation by different artificial neural networks approaches, Measurement: Journal of the International Measurement Confederation 76 (2015) 117–128. → pages 12, 13, 88, 89

[74] J. M. Oswell, J. Hart, N. Zulfiqar, Effect of Geotechnical Parameter Variability on Soil-Pipeline Interaction, Journal of Pipeline Systems Engineering and Practice 10 (4) (2019) 1–9. → pages 12

[75] H. Wijaya, P. Rajeev, E. Gad, Effect of seismic and soil parameter uncertainties on seismic damage of buried segmented pipeline, Transportation Geotechnics 21 (April) (2019) 100274. → pages 12

[76] S. Imanzadeh, A. Marache, A. Denis, Influence of soil spatial variability on possible dysfunction and failure of buried pipe, case study in Pessac city, France, Environmental Earth Sciences 76 (5) (2017) 1–17. → pages 12, 88, 89

[77] A. Nobahar, S. Kenny, T. King, R. McKenna, R. Phillips, Analysis and design of buried pipelines for ice gouging hazard: A probabilistic approach, Journal of Offshore Mechanics and Arctic Engineering 129 (3) (2007) 219–228. → pages 12

[78] K. F. Tee, L. R. Khan, H. P. Chen, Probabilistic failure analysis of underground flexible pipes, Structural Engineering and Mechanics 47 (2) (2013) 167–183. → pages 12, 88, 89

[79] W. O. McCarron, Subsea flowline buckle capacity considering uncertainty in pipe-soil interaction, Computers and Geotechnics 68 (2015) 17–27. → pages 12

[80] S. Tesfamariam, B. Rajani, Possibilistic approach for consideration of uncertainties to estimate ... (2006). → pages 12, 88, 89

[81] J. Ji, D. J. Robert, C. Zhang, D. Zhang, J. Kodikara, Probabilistic physical modelling of corroded cast iron pipes for lifetime prediction Probabilistic physical modelling of corroded cast iron pipes for lifetime prediction, Structural Safety 64 (October 2017) (2016) 62–75. → pages 12

[82] J. D. Arregui-Mena, L. Margetts, P. M. Mummery, Practical Application of the Stochastic Finite Element Method, Archives of Computational Methods in Engineering 23 (1) (2016) 171–190. → pages 13, 88

[83] D. Rubinstein, R Y and Kroese, Simulation an the Monte Carlo method, Ne York, 1981. → pages 13, 88

[84] W. A. Ericson, Optimum Stratified Sampling using Prior Information, Journal of the American Statistical Association 60 (311) (1965) 750. → pages 13

[85] I. Draper, N.R. and Guttman, Some Bayesian Stratified 2-Stage Sampling Results, Biometrika 55 (1967) 131–139. → pages 13

[86] V. Bayer, C. Bucher, Importance sampling for ® rst passage problems of nonlinear structures 14 (1999) 27–32. → pages 13

[87] X. Yuan, Z. Lu, C. Zhou, Z. Yue, A novel adaptive importance sampling algorithm based on Markov chain and low-discrepancy sequence, Aerospace Science and Technology 29 (1) (2013) 253–261. → pages 13

[88] S. K. Au, J. L. Beck, A new adaptive importance sampling scheme for reliability calculations, Structural Safety 21 (2) (1999) 135–158. → pages 13

[89] G. E. Xiu, D. and Karniaakis, The Wiener-Askey polynomial chaos for stochastic differential equations, SIAM Journal on Scientific Computing 24 (2) (2002) 619–644. → pages 13, 89

[90] B. S. Ã, Global sensitivity analysis using polynomial chaos expansions 93 (2008) 964–979. → pages 13, 89

[91] S. Goswami, C. Anitescu, S. Chakraborty, T. Rabczuk, Transfer learning enhanced physics informed neural network for phase-field modeling

of fracture, Theoretical and Applied Fracture Mechanics 106 (November 2019) (2020) 102447. → pages 13, 89

[92] M. D. Buhmann, Radial basis functions, Acta Numerica 9 (2000) 1–38. → pages 13, 89

[93] I. Kaymaz, Application of kriging method to structural reliability problems 27 (2005) 133–151. → pages 13, 89

[94] R. Chakraborty, S. and Chowdhury, Polynomial correlated function expansion, Modelling an Simulation Techniques in Structural Engineering, IGI Global (2017) 348–373. → pages 13

[95] L. G. Yang, X., Choi M., K. G. E., Adaptive ANOVA decomposition of stochastic incompressible and compressible flows, Journal of Computational Physics 231 (4) (2012) 1587–1614. → pages 13

[96] A. Saha, S. Chakraborty, S. Chandra, I. Ghosh, Kriging based saturation fl ow models for tra ffi c conditions in Indian cities 118 (September 2017) (2018) 38–51. → pages 13, 89

[97] M. Mousavi, M. Hesari, A. Azarbakht, Seismic risk assessment of the 3rd Azerbaijan gas pipeline in Iran, Natural Hazards 74 (3) (2014) 1327–1348. → pages 13, 24

[98] A. Tamaro, S. Grimaz, M. Santulin, D. Slejko, Characterization of the expected seismic damage for a critical infrastructure: the case of the oil pipeline in Friuli Venezia Giulia (NE Italy), Bulletin of Earthquake Engineering 16 (3) (2018) 1425–1445. → pages

[99] A. Urlainis, I. M. Shohet, R. Levy, Probabilistic Risk Assessment of Oil and Gas Infrastructures for Seismic Extreme Events, Procedia Engineering 123 (2015) 590–598. → pages

[100] G. Tsinidis, L. Di Sarno, A. Sextos, P. Furtner, A critical review on the vulnerability assessment of natural gas pipelines subjected to seismic wave propagation. Part 1: Fragility relations and implemented seismic intensity measures 86 (January) (2019) 279–296. → pages

[101] G. Tsinidis, L. Di Sarno, A. Sextos, P. Furtner, Seismic fragility of buried steel natural gas pipelines due to axial compression at geotechnical discontinuities, Vol. 18, Springer Netherlands, 2020. → pages

[102] P. Ni, S. Mangalathu, Y. Yi, Fragility analysis of continuous pipelines subjected to transverse permanent ground deformation, Soils and Foundations 58 (6) (2018) 1400–1413. → pages 14

[103] O. Shabarchin, S. Tesfamariam, Risk assessment of oil and gas pipelines with consideration of induced seismicity and internal corrosion, Journal of Loss Prevention in the Process Industries 47 (2017) 85–94. → pages

[104] K. Pitilakis, H. Crowley, A. Kaynia, SYNER-G: Typology Definition and Fragility Functions for Physical Elements at Seismic Risk, Vol. 27, 2014. → pages 14

[105] V. Jahangiri, H. Shakib, Seismic risk assessment of buried steel gas pipelines under seismic wave propagation based on fragility analysis, Vol. 16, Springer Netherlands, 2018. → pages 13

[106] Ranjit K. Roy, A Primer on the Taguchi Method, second edi Edition, Society of Manufacturing Engineers, Dearborn, Michigan 48121, 2010. → pages 14, 107, 111

[107] Taguchi G., Orthogonal Arrays and Linear Graphs., Tech. rep., American Supplier Institute, Inc., Dearborn, MI (1986). → pages 14

[108] Bose R. C., Mathematical Theory of the Symmetrical Factorial Designs, Sankhya 8 (1947) 107–166. → pages 14

[109] Bose R.C. and Bush K.A., Orthogonal Arrays of Strength Two and Three, Annals of Mathematical Statistics (23) (1952) 508–524. → pages 14, 108

[110] B. Peherstorfer, K. Willcox, M. Gunzburger, Optimal Model Management for Multifidelity Monte Carlo Estimation, SIAM Journal on Scientific Computing 38 (5) (2016) A3163–A3194. → pages 14, 15

[111] M. G. Fernández-Godino, C. Park, N.-H. Kim, R. T. Haftka, Review of multi-fidelity models (2016). `arXiv:1609.07196`. → pages 14

[112] L. W. Ng, K. E. Willcox, Multifidelity approaches for optimization under uncertainty, International Journal for numerical methods in Engineering 100 (10) (2014) 746–772. → pages 15

[113] L. W. T. Ng, K. E. Willcox, Multifidelity approaches for optimization under uncertainty, International Journal for Numerical Methods in Engineering 100 (10) (2014) 746–772. → pages 16

[114] A. I. Forrester, A. Sóbester, A. J. Keane, Multi-fidelity optimization via surrogate modelling, Proceedings of the Royal Society A: Mathematical, Physical and Engineering Sciences 463 (2088) (2007) 3251–3269. → pages 17, 18

[115] D. R. Jones, A Taxonomy of Global Optimization Methods Based on Response Surfaces, Journal of Global Optimization 21 (4) (2001) 345–383. → pages 17

[116] A. I. Forrester, A. J. Keane, N. W. Bressloff, Design and analysis of "noisy" computer experiments, AIAA Journal 44 (10) (2006) 2331–2339. → pages 17

[117] S. T. Stepp, J. C., Wong I., Whitney J., Quittmeyer R., Abrahamson N., Toro G., Youngs R., Coppersmith K., Savy J., Y. M. P. P. Members, Probabilistic Seismic Hazard Analyses for Groun Motions and Fault Displacement at Yucca Mountain, Nevada, Earthquake Spectra (17) (2001) 113–150. → pages 21

[118] T. G. R. Youngs R. R., Arabasz W. J., Anderson R. E., Ramelli A. R., Ake J. P., Slemmons D. B., McCalpin J. P., Doser D. I., Fridrich C. J., Swan F. H., Rogers A. M., Yount J. C., Anderson L. W., Smith K. D., Bruhn R. L., Knuepfer P. L. K., Smith R. B., dePolo C., A Methodology for Probabilistic Fault Displacement Hazard Analysis (PFDHA), Earthquake Spectra 19 (1) (2003) 191–219. → pages 21

[119] R. Budnitz, G. Apostolakis, D. M. Boore, Recommendations for probabilistic seismic hazard analysis: guidance on uncertainty and use of experts, Tech. rep., Nuclear Regulatory Commission, Washington, DC (United States). Div. of ... (1997). → pages 21

[120] M. D. Petersen, T. E. Dawson, R. Chen, T. Cao, C. J. Wills, D. P. Schwartz, A. D. Frankel, Fault displacement hazard for strike-slip faults, Bulletin of the Seismological Society of America 101 (2) (2011) 805–825. → pages 21

[121] K. Goda, Probabilistic characterization of seismic ground deformation due to tectonic fault movements, Soil Dynamics and Earthquake Engineering 100 (March) (2017) 316–329. → pages 22, 82, 84, 85

[122] B. Y. Y. O. S. H. I. M. I. T. S. U. Okada, Surface deformation due to shear and tensile faults in a half-space 75 (4) (1985) 1135–1154. → pages 22, 84, 86

[123] K. Goda, T. Yasuda, N. Mori, T. Maruyama, New scaling relationships of earthquake source parameters for stochastic tsunami simulation, Coastal Engineering Journal 58 (3) (2016) 1650010–1. → pages 22, 84, 85

[124] K. K. S. Thingbaijam, P. Martin Mai, K. Goda, New empirical earthquake source-scaling laws, Bulletin of the Seismological Society of America 107 (5) (2017) 2225–2246. → pages 22

[125] M. Leonard, Earthquake fault scaling: Self-consistent relating of rupture length, width, average displacement, and moment release, Bulletin of the Seismological Society of America 100 (5A) (2010) 1971–1988. → pages

[126] L. Blaser, F. Krüger, M. Ohrnberger, F. Scherbaum, Scaling relations of earthquake source parameter estimates with special focus on subduction environment, Bulletin of the Seismological Society of America 100 (6) (2010) 2914–2926. → pages

[127] D. L. Wells, K. J. Coppersmith, New empirical relationships among magnitude, rupture length, rupture width, rupture area, and surface displacement, Bulletin of the seismological Society of America 84 (4) (1994) 974–1002. → pages

[128] P. Somerville, K. Irikura, R. Graves, S. Sawada, D. Wald, N. Abrahamson, Y. Iwasaki, T. Kagawa, N. Smith, A. Kowada, Characterizing crustal earthquake slip models for the prediction of strong ground motion, Seismological Research Letters 70 (1) (1999) 59–80. → pages

[129] F. O. Strasser, M. Arango, J. J. Bommer, Scaling of the source dimensions of interface and intraslab subduction-zone earthquakes with moment magnitude, Seismological Research Letters 81 (6) (2010) 941–950. → pages 22

[130] B. Y. Y. Okada, Internal deformation due to shear and tensile faults in a half-space 82 (2) (1992) 1018–1040. → pages 22

[131] K. D. Morell, C. Regalla, L. J. Leonard, C. Amos, V. Levson, Quaternary rupture of a crustal fault beneath victoria, british columbia, canada, GSA Today 27 (3) (2017) 4–10. → pages 22, 84

[132] G. Li, Y. Liu, C. Regalla, K. D. Morell, Seismicity relocation and fault structure near the leech river fault zone, southern vancouver island,

Journal of Geophysical Research: Solid Earth 123 (4) (2018) 2841–2855. → pages 22, 84

[133] J. V. Barrie, H. G. Greene, The devils mountain fault zone: An active cascadia upper plate zone of deformation, pacific northwest of north america, Sedimentary Geology 364 (2018) 228–241. → pages 23, 84

[134] S. Halchuk, T. Allen, J. Adams, T. Onur, Contribution of the leech river valley-devil's mountain fault system to seismic hazard for victoria bc 12th can. conf, Earthquake Engineering (2019). → pages 23, 84, 85

[135] J. Kukovica, H. Ghofrani, S. Molnar, K. Assatourians, Probabilistic seismic hazard analysis of victoria, british columbia: Considering an active fault zone in the nearby leech river valleyprobabilistic seismic hazard analysis of victoria, british columbia, Bulletin of the Seismological Society of America 109 (5) (2019) 2050–2062. → pages 23, 84

[136] K. Goda, A. Sharipov, Fault-source-based probabilistic seismic hazard and risk analysis for victoria, british columbia, canada: A case of the leech river valley fault and devil's mountain fault system, Sustainability 13 (3) (2021) 1440. → pages 23, 85

[137] S. Esposito, I. Iervolino, A. D'Onofrio, A. Santo, F. Cavalieri, P. Franchin, Simulation-Based Seismic Risk Assessment of Gas Distribution Networks, Computer-Aided Civil and Infrastructure Engineering 30 (7) (2015) 508–523. → pages 24

[138] R. De Risi, F. De Luca, O. S. Kwon, A. Sextos, Scenario-based seismic risk assessment for buried transmission gas pipelines at regional scale, Journal of Pipeline Systems Engineering and Practice 9 (4) (2018) 1–12. → pages 24

[139] N. Olson, Soil performance for large scale soil-pipeline tests (2009). → pages 27, 38, 39

[140] Abaqus documentation, dassault systemes (2013). → pages 28, 29, 35, 50, 86

[141] K. L. Lee, H. B. Seed, Drained strength characteristics of sands, Journal of Soil Mechanics & Foundations Div (1967). → pages 31, 88

[142] D. Kolymbas, W. Wu, Recent results of triaxial tests with granular materials, Powder Technology 60 (2) (1990) 99–119. → pages

[143] L. Lancelot, I. Shahrour, M. Al Mahmoud, Failure and dilatancy properties of sand at relatively low stresses, Journal of Engineering Mechanics 132 (12) (2006) 1396–1399. → pages 31, 88

[144] B. O. Hardin, W. L. Black, Sand stiffness under various triaxial stresses, Journal of the Soil Mechanics and Foundations Division 92 (2) (1966) 27–42. → pages 31

[145] T. O'Rourke, Neesr annual report, Rensselaer Polytechnic Institute, Sciencenter Discovery Center, and Cornell Univ., Ithaca, NY (2006). → pages 34

[146] J. Turner, F. H. Kulhawy, Experimental analysis of drilled shaft foundations subjected to repeated axial loads under drained conditions, Tech. rep., Cornell Univ., Ithaca, NY (USA). Geotechnial Engineering Group; Electric ... (1987). → pages 37

[147] A. Bishop, Discussion on soil properties and their measurement, in: Proceedings of the 5th International Conference on Soil mechanics and Foundation Engineering, Vol. 3, 1961, pp. 92–100. → pages 38

[148] F. Tatsuoka, M. Sakamoto, T. Kawamura, S. Fukushima, Strength and deformation characteristics of sand in plane strain compression at extremely low pressures, Soils and Foundations 26 (1) (1986) 65–84. → pages 39

[149] T. B. Pradhan, F. Tatsuoka, N. Horii, Strength and deformation characteristics of sand in torsional simple shear, Soils and Foundations 28 (3) (1988) 131–148. → pages

[150] M. Yoshimine, Archives–soil mechanics laboratory, Tokyo Metropolitan Univ. Accessed April 4 (2005) 2015. → pages 39

[151] M. Singh, T. Markeset, Hybrid models for handling variability and uncertainty in probabilistic and possibilistic failure analysis of corroded pipes, International Journal of Systems Assurance Engineering and Management 5 (1) (2014) 43–54. → pages 48

[152] P. E. Hess, D. Bruchman, I. A. Assakkaf, B. M. Ayyub, Uncertainties in material and geometric strength and load variables, Naval Engineers Journal 114 (2) (2002) 139–166. → pages 48

[153] L. Wang, S. C. Narasimman, S. R. Ravula, A. Ukil, Water Ingress Detection in Low-Pressure Gas Pipelines Using Distributed Temperature Sensing System, IEEE Sensors Journal 17 (10) (2017) 3165–3173. → pages 48

[154] S. Dey, S. Chakraborty, S. Tesfamariam, Structural performance of buried pipeline undergoing strike-slip fault rupture in 3D using a non-linear sand model, Soil Dynamics and Earthquake Engineering 135 (November 2019) (2020) 106180. → pages 49, 82, 86, 105, 111

[155] M. Sabagh, A. Ghalandarzadeh, Numerical modelings of continuous shallow tunnels subject to reverse faulting and its verification through a centrifuge, Computers and Geotechnics 128 (2020) 103813. → pages 51

[156] G. P. Kouretzis, D. Sheng, S. W. Sloan, Sand–pipeline–trench lateral interaction effects for shallow buried pipelines, Computers and Geotechnics 54 (2013) 53–59. → pages

[157] Y. K. Chaloulos, G. D. Bouckovalas, S. D. Zervos, A. L. Zampas, Lateral soil–pipeline interaction in sand backfill: effect of trench dimensions, Computers and Geotechnics 69 (2015) 442–451. → pages

[158] Q. Cai, J. Peng, C. W. Ng, J. Shi, X. Chen, Centrifuge and numerical modelling of tunnel intersected by normal fault rupture in sand, Computers and Geotechnics 111 (2019) 137–146. → pages

[159] H. Mroueh, I. Shahrour, A full 3-d finite element analysis of tunneling–adjacent structures interaction, Computers and Geotechnics 30 (3) (2003) 245–253. → pages 51

[160] M. C. Kennedy, A. O'Hagan, Predicting the output from a complex computer code when fast approximations are available, Biometrika 87 (1) (2000) 1–13. → pages 54

[161] A. I. Forrester, A. Sóbester, A. J. Keane, Multi-fidelity optimization via surrogate modelling, Proceedings of the royal society a: mathematical, physical and engineering sciences 463 (2088) (2007) 3251–3269. → pages 54, 55

[162] R. Nayek, S. Chakraborty, S. Narasimhan, A Gaussian process latent force model for joint input-state estimation in linear structural systems, Mechanical Systems and Signal Processing 128 (2019) 497–530. → pages 55

[163] S. Chakraborty, R. Chowdhury, Graph-theoretic-approach-assisted Gaussian process for nonlinear stochastic dynamic analysis under generalized loading, Journal of Engineering Mechanics 145 (12) (2019) 04019105. → pages 55

[164] J. W. Baker, Efficient analytical fragility function fitting using dynamic structural analysis, Earthquake Spectra 31 (1) (2015) 579–599. → pages 56, 91

[165] S. Dey, S. Chakraborty, S. Tesfamariam, Multi-fidelity approach for uncertainty quantification of buried pipeline response undergoing fault rupture displacements in sand, Computers and Geotechnics 136 (2021) 104197. → pages 82, 85, 86, 89

[166] R. R. Youngs, K. J. Coppersmith, Implications of fault slip rates and earthquake recurrence models to probabilistic seismic hazard estimates, Bulletin of the Seismological society of America 75 (4) (1985) 939–964. → pages 85

[167] V. Convertito, A. Emolo, A. Zollo, Seismic-hazard assessment for a characteristic earthquake scenario: an integrated probabilistic–deterministic method, Bulletin of the Seismological Society of America 96 (2) (2006) 377–391. → pages 85

[168] S. Y. Johnson, S. V. Dadisman, D. C. Mosher, R. J. Blakely, J. R. Childs, Active tectonics of the devils mountain fault and related structures, northern puget lowland and eastern strait of juan de fuca region, pacific northwest, Tech. rep. (2001). → pages 85

[169] S. Halchuk, T. I. Allen, J. Adams, G. C. Rogers, Fifth generation seismic hazard model input files as proposed to produce values for the 2015 national building code of canada, Geological Survey of Canada Open File 7576 (2014) 15. → pages 85

[170] K. G. E. Perdikaris, P., Venturi, D., Royset, J. O., Multi-fiddelity modelling via. recursive co-krigging and Gaussian-Markov random fields, in: Proceedings. Mathematical, physical, and engineering sciences/ the Royal Society, 2015, p. 471 (2179) (2015) 20150018. → pages 89

[171] M. C. Kennedy, A. O. Hagan, Bayesian Calibration of Computer Models Author (s): Marc C . Kennedy and Anthony O ' Hagan Source :

Journal of the Royal Statistical Society . Series B (Statistical Methodology), Vol . 63 , Published by : Wiley for the Royal Statistical Society Stable 63 (3) (2020) 425–464. → pages 89

[172] F. R. Rofooei, H. H. Jalali, N. K. A. Attari, H. Kenarangi, M. Samadian, Parametric study of buried steel and high density polyethylene gas pipelines due to oblique-reverse faulting, Canadian Journal of Civil Engineering 42 (3) (2015) 178–189. → pages 106

[173] K. Gawande, R. Kiran, H. Cherukuri, A numerical study of the response of buried steel pipelines undergoing strike-slip fault, Engineering Failure Analysis 102 (102) (2019) 203–218. → pages 106